UNIVERSIDAD POLITÉCNICA DE MADRID
Escuela Técnica Superior de Ingenieros de Caminos, Canales y Puertos

Flame-retardant Fiber-reinforced Thermoset Composites: Preparation, Characterization, and Fire Behavior

DOCTORAL THESIS

Submitted for the degree of Doctor by:

Xiang Ao
Ingeniero de Materiales

Madrid, 2024

UNIVERSIDAD POLITÉCNICA DE MADRID
Escuela Técnica Superior de Ingenieros de Caminos, Canales y Puertos

Doctoral Degree in Engineering of Structures, Foundations and Materials

Flame-retardant Fiber-reinforced Thermoset Composites: Preparation, Characterization, and Fire Behavior

DOCTORAL THESIS

Submitted for the degree of Doctor by:

Xiang Ao
Ingeniero de Materiales

Under the supervision of:
Dr. De-Yi Wang
Dr. Carlos González

Madrid, 2024

Title: Flame-retardant Fiber-reinforced Thermoset Composites: Preparation, Characterization and Fire behavior

Author: Xiang Ao

Doctoral Programme: Engineering of Structures, Foundations and Materials

Thesis Supervision:

Dr. De-Yi Wang, senior researcher, IMDEA Materials Institute, Madrid, Spain (Supervisor)

Dr. Carlos González, full professor, Technical University of Madrid, Madrid, Spain (Supervisor)

External Reviewers:

Thesis Defense Committee:

Thesis Defense Date:

Dedicated this thesis to my family

Acknowledgment

Looking back on the almost four years of life I had here in Spain, this PhD study and the lovely friends I met have really inspired me in every aspect of my life. It is said that life is like a movie; we write our own endings. I am sincerely grateful to everyone who has helped me write this part about the end of my life.

First, I would like to extend my greatest acknowledgment and appreciation to my supervisors, Dr. De-Yi Wang and Dr. Carlos González, for giving me the opportunity to carry out this doctoral thesis under their supervision. Over the past few years, they have never stopped providing me with constant advice and guidance, and they have shared their extensive knowledge and instructive ideas. They always strived to cultivate my ability to design ideas and experiments, take care of experimental details, write scientific papers as well as posters, and deliver presentations either to a broad audience or experts. From them, I have expanded my knowledge of composite materials and deepened my understanding of fire safety materials research in that field.

Secondly, I would like to thank all my colleagues from IMDEA Materials Institute, who have created such a friendly and comfortable working environment. Thanks to Rosa, Mariana, Ainhoa, Eduardo, and Alejandro for their administrative support. Also, I want to thank all the technicians: Vanesa, José Luis, Jimena, Mónica, Miguel, Manuel, Javier, Victor, and Sergio for their countless help and guidance. I am also grateful to all the members of High Performance Polymer Nanocomposite Group and Composite Materials Group for all their contributions to this research and for their support and company during these years. My sincere gratitude to Jing Zhang, Guangzhong Yin, Antonio Vázquez, José Sánchez, Davide Mocerino, Raquel, Arnab, Monsur, Sunan, Juan Pedro, and Yanyan, etc. for their helpful discussion and efforts during collaboration. I would also like to thank David Aviega, Junchen, Xiaolu, Keayvan, Moisés,Biaobiao, Mingyang, Chunxiang, Jie Xu, Jose Hobson, Juan, Wei Tang, Yunhuan, Meihui, Qi Chen, Jun Hu etc, which we helped each other and spend an unforgettable time in both work and life.

Finally, I would like to extend my gratefulness to my parents and close relatives, who give me endless support and consistent encouragement to pursue my life goals and career path.

Abstract

Fiber-reinforced polymer composites (FRPs) with thermoset matrices are valued for their high specific stiffness, strength, and lightweight properties. However, their vulnerability to fire, along with the release of heat, smoke, and toxicity, limits their broader application. Thermoset FRPs soften, decompose, and collapse under combustion, making it critical to develop flame-retardant versions with lower fire hazards, improved fire insulation, and delayed mechanical integrity loss.

Despite progress in flame-retardant materials, efforts to boost heat/fire insulation and maintain mechanical integrity during fire are still limited. Besides, current testing methods for fireproofing FRPs are time-consuming and require significant materials. To tackle these challenges, this thesis aims to: (a) develop flame-retardant FRPs with lower fire hazards like heat and smoke; (b) create composites with better insulation; (c) design a bench-scale device for easier validation of these materials.

(1) In Chapter 3, bilayer epoxy resin-based coating layers were designed, formulated, and blade-coated onto the substrate of fiberglass thermoset composites. The peak heat release rate (PHRR) and total smoke release (TSP) were lowered by 50% and 65% respectively when added bilayer coating layers. The heat/fire insulation properties for the bilayer-coated sample were enhanced, with backside temperatures kept at less than 300℃ with no fire burn-through.

(2) In Chapter 4, a cobalt-based nanohybrid was ingeniously designed, synthesized, and employed as a highly efficient synergist for commercial ammonium polyphosphate-filled bio-epoxy resin and its fiberglass composites. The filled resin showed a 74% reduction of PHRR due to its enhanced intumescent effect. Nevertheless, the intumescent effect was significantly retarded in fiberglass composite, showing only a 36% reduction of PHRR. Besides, the heat/fire insulation properties were only slightly improved after adding the synergist.

(3) In Chapter 5, a bench scale mechanical testing machine was designed, manufactured, and mounted on a widely used cone calorimeter aiming to validate of fire protective effects of the composites designed in Chapters 3 and 4 in a facile, material-saving manner. The machine was produced and calibrated. The fire protective coating showed higher efficacy in delaying in-plane axial mechanical loss under static force and fire damage compared to flame retardants added into the polymer matrix. Besides, protective effects were also found in postponing the

loss of off-axial mechanical properties. The usage of the derived heat release information was also discussed.

(4) In Chapter 6, a facile, chitosan/phytic acid-based polyelectrolyte coating was synthesized, and dip-coated on the surface of flax fabrics. The treated flax fabric showed self-extinguishing properties with low burnt length. The modified plant fiber/epoxy composite showed a reduction of PHRR by 36% and slowed mass decomposition. Heat/fire insulation tests also showed more than a 200% increase in resist-to-burn through time.

In conclusion, the above research findings highlight the benefits and limitations of different flame-retardant strategies, providing insights for advancing FRP designs from coupon to component levels.

Resumen

Los compuestos poliméricos reforzados con fibras (FRPs) con matrices termoestables son valorados por su elevada rigidez específica, resistencia y ligereza. Sin embargo, su vulnerabilidad al fuego, junto con la liberación de calor, humo y toxicidad, limita su aplicación más amplia. Los FRP termoestables se ablandan, descomponen y colapsan con la combustión, por lo que es fundamental desarrollar versiones ignífugas con menor riesgo de incendio, mejor aislamiento contra el fuego y pérdida retardada de la integridad mecánica.

A pesar de los avances en los materiales ignífugos, los esfuerzos para mejorar el aislamiento térmico y mantener la integridad mecánica durante el incendio siguen siendo limitados. Los métodos de ensayo actuales para la ignifugación de los FRPs llevan mucho tiempo y requieren una gran cantidad de materiales. Para hacer frente a estos retos, esta tesis pretende: (a) desarrollar FRP ignífugos con menores riesgos de incendio como el calor y el humo; (b) crear composites con mejor aislamiento; (c) diseñar un dispositivo a escala de banco para facilitar la validación de estos materiales.

(1) En el capítulo 3, se diseñaron, formularon y aplicaron capas de revestimiento bicapa a base de resina epoxi sobre el sustrato de compuestos termoestables de fibra de vidrio. La tasa máxima de liberación de calor (PHRR) y la liberación total de humo (TSP) se redujeron en un 50% y un 65% respectivamente cuando se añadieron capas de revestimiento bicapa. Se mejoraron las propiedades de aislamiento térmico y contra incendios de la muestra recubierta con bicapa, y las temperaturas de la cara posterior se mantuvieron por debajo de 300℃ sin que se produjeran quemaduras por incendio.

(2) En el capítulo 4, se diseñó, sintetizó y empleó ingeniosamente un nanohíbrido a base de cobalto como sinergista altamente eficaz para la resina bio-epoxi comercial rellena de polifosfato de amonio y sus compuestos de fibra de vidrio. La resina rellena mostró una reducción del 74% de PHRR debido a su efecto intumescente mejorado. Sin embargo, el efecto intumescente fue significativamente retardado en el compuesto de fibra de vidrio, mostrando sólo una reducción del 36% de PHRR. Además, las propiedades de aislamiento térmico mejoraron sólo ligeramente tras la adición del sinergista.

(3) En el capítulo 5, se diseñó, fabricó y montó una máquina de ensayos mecánicos a escala de banco en un calorímetro de cono ampliamente utilizado con el objetivo

de validar los efectos protectores contra el fuego de los materiales compuestos diseñados en los capítulos 3 y 4 de una manera sencilla y con ahorro de material. La máquina fue fabricada y calibrada. El recubrimiento protector contra el fuego mostró una mayor eficacia en el retraso de la pérdida mecánica axial en el plano bajo fuerza estática y daño por fuego en comparación con los retardantes de llama añadidos en la matriz polimérica. Además, también se observaron efectos protectores en el aplazamiento de la pérdida de propiedades mecánicas fuera del eje. También se discutió el uso de la información derivada de la liberación de calor.

(4) En el capítulo 6, se sintetizó un recubrimiento polielectrolítico fácil a base de quitosano/ácido fítico y se aplicó por inmersión sobre la superficie de tejidos de lino. El tejido de lino tratado mostró propiedades autoextinguibles con baja longitud de quemado. El compuesto modificado de fibra vegetal y epoxi mostró una reducción de la PHRR del 36% y una descomposición más lenta de la masa. Las pruebas de aislamiento del calor/fuego también mostraron un aumento de más del 200% en la resistencia a la combustión a lo largo del tiempo.

En conclusión, los resultados de esta investigación ponen de relieve las ventajas y limitaciones de las diferentes estrategias de retardancia de llama, y proporcionan información para avanzar en los diseños de FRP desde el nivel de cupón hasta el de componente.

Table of Contents

List of Figures

List of Tables

Abbreviations and Acronyms

AlPi	Aluminum Diethyl Phosphinate
APP	Ammonium Polyphosphate
ATH	Aluminum Trihydrate
CF	Carbon Fibers
CFRP	Carbon Fiber-reinforced Polymer Composite
CH	Chitosan
CNH	Cobalt-based Nanohybrid
DOPO	9,10-dihydro-9-oxa-10-phosphaphenan-threne-10-oxide
DMA	Dynamic Mechanical Analyzer
EDS	Energy Dispersive X-ray Spectroscopy
EG	Expandable Graphite
EP	Epoxy
FIGRA	Fire Growth Rate Index
FR	Flame Retardant
FRP	Fiber-reinforced Polymer Composite
FTIR	Fourier Transform Infrared Spectroscopy
GF	Glass Fiber
GFRP	Glass Fiber-reinforced Polymer Composite
HGM	Hollow Glass Microsphere
HRC	Heat Release Capacity
ISU	Insulation Layer
ITM	Intumescent Layer
LCM	Liquid Composite Molding
LOI	Limited Oxygen Index
MARHE	Maximum of Average Rate of Heat Emission

MCC	Micro Combustion Calorimeter
MOF	Metal-organic-framework
OOA	Out-of-Autoclave
PA	Phytic Acid
PAN	Polyacrylonitrile
PEC	Polyelectrolyte Complex
PEI	Polyethyleneimine)
PF	Phenolic Formaldehyde
PHRR	Peak Heat Release Rate
RDP	Resorcinol Bis(diphenyl Phosphate)
RTM	Resin Transfer Molding
SEM	Scanning Electron Microscopy
SPR	Smoke Production Rate
T_B	Backside Temperature
TGA	Thermogravimetric Analysis
THR	Total Heat Release
t_{ig}	Time-to-ignition
T_g	Glass Transition Temperature
TSP	Total Smoke Production
T_p	Temperature of Peak Heat Release
UP	Unsaturated Polyester
VARI	Vacuum Assisted Resin Infusion
VBT	Vertical Burning Test
VE	Vinyl Ester
VPA	Vinyl Phosphonic Acid
XPS	X-ray Photoelectron Spectroscopy
XRD	X-ray Diffraction

ZHO	Zirconium Hydroxide

1. Introduction

1.1. Fiber-reinforced polymer composites (FRPs)

A composite material is formed by the combination of two or more distinct materials to produce a new material with enhanced properties compared to its constituents. Fiber-reinforced polymer composites (FRPs), as one type of composite material, use polymer as a matrix and fiber for properties enhancement. Compared to the bulk form, the fiber form of the material demonstrated much stronger mechanical properties, which were mainly attributed to the sharp reduction in the number of defects. When continuous fiber was used as reinforcement with polymer matrix acting like glue, the FRPs demonstrated high specific strength and modulus with low-density value compared to most traditional metal materials or its alloys, thereby gaining great attractiveness toward weight reduction applications. With additional advantages of corrosion resistance and part-count reduction, FRPs have been widely used in various applications ranging from aeronautics to rolling stocks, marine, wind, automotive industries, etc.[1]

1.1.1. Polymer matrix and fiber reinforcement materials for FRPs

The great tailorability and design freedom provide FRPs versatility in mechanical, thermal, and other functional properties to meet requirements according to specific applications. As shown in Figure 1.1, the design and development of thermoset FRPs require a holistic view and consideration of raw materials, manufacturing methods, and final applications. The main components of FRPs are the polymer matrix as the continuous phase and the fiber reinforcement. The reinforcement fiber acts mainly as loading-bearing media alongside the fiber direction, providing most of the strength and stiffness. In comparison, the polymer matrix acts as load transfer media and protects the fiber from environmental attack.

1.1.1.1. Polymers used as matrix materials for FRPs

According to the physiochemical properties of polymers, the matrix materials used in FRPs can be mainly categorized into thermoset polymers and thermoplastic materials, which poses great influence on their processing methods and in-service performance.

Thermoset polymers are formed by the reaction of monomers with curing agents or catalysts into highly cross-linked networks with irreversible bonds. In general, thermoset resins have low viscosity under room or slightly higher temperatures, offering excellent impregnation of fiber reinforcement and high process speed. They are the most used polymer matrix systems mainly due to their ease of processing and wide range of properties, long shelf life, and ease of storage. During the curing process, the mixture releases or absorbs heat, gelates, solidifies, and shrinks. Depending on the choice of curing agents or initiators, catalysts, the reactivity of thermoset resins, the curing cycles, and the gelation time of thermoset resins can range from minutes to hours. According to the chemical composition, thermoset resins used in FRPs include polyesters, vinyl ester, epoxy, phenolic, bismaleimide resin, cyanate ester resins, etc.

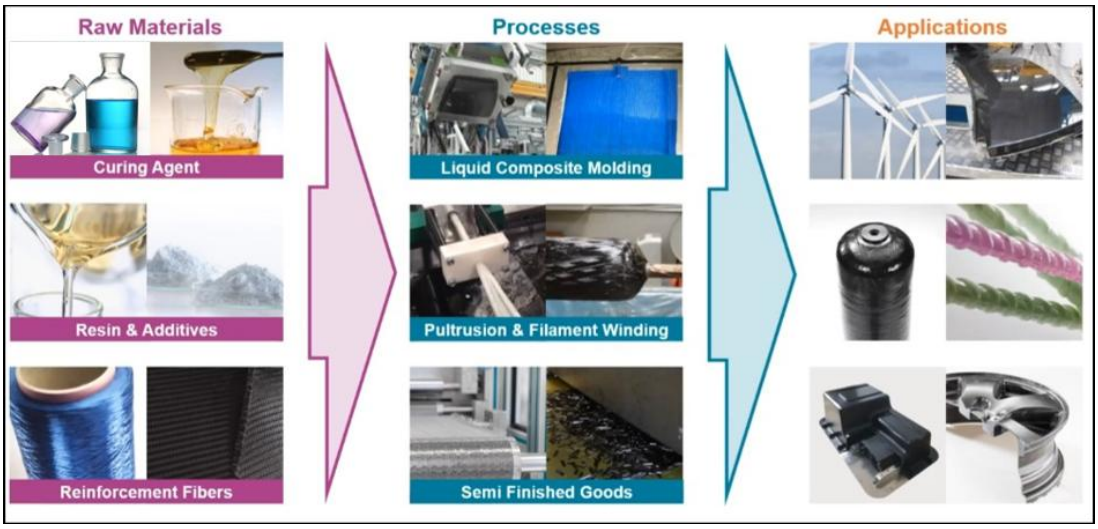

Figure 1.1: A holistic view of the development and application of thermoset FRPs. (Image credit: Evonik)

Epoxy (EP) resins are mainly composed of molecular structures that contain oxirane rings situated terminally, cyclically, or internally in a molecular chain. One of its symbolic synthetic routes from bisphenol A can be seen in Figure 1.2 (a). The oxirane ring reacts with either amine, anhydride, phenolic hydroxyl, thiol, or imidazole functional group-based curing agents through ring-opening polymerization and crosslinking reactions to form a cross-linked three-dimensional thermoset resin. It is widely used because of its versatility, high mechanical properties, and high corrosion properties. Epoxy resins are considered high-performance resins in the sense that their elongation to failure and higher service temperature is superior to that of most other commonly used thermoset resins. Hence, one of their main fields is application in the aircraft industry.[2]

Unsaturated polyester (UP) resins are long, chainlike, multiple-unit polyester molecules linked by an ester group while containing carbon-carbon doubles capable of undergoing future polymerization, as shown in Figure 1.2 (b). UP resin tends to dissolve in a reactive monomer, styrene vinyl toluene, etc., to form a low-viscosity, clear liquid. The addition of a free radical initiator and applied heat results in a free radical polymerization reaction between the unsaturated polyester and reactive solvent monomers to form a three-dimensional cross-linked network. The curing process of polyester resin at room temperature can be tailored using various types of initiators, suitable accelerators, and promoters. Polyester has a wide range of properties that can be matched to different applications and processing equipment. They tend to have moderate physical properties in terms of strength and modulus as well as chemical resistance but are very cost-effective due to their low initial cost and conversion cost.

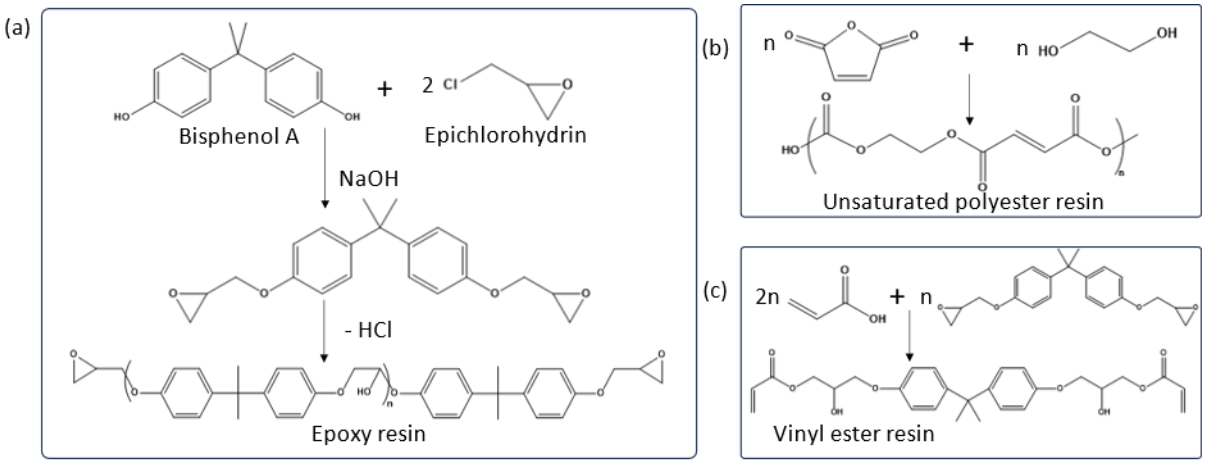

Figure 1.2: Typical reaction scheme for the synthesis of (a) epoxy resin, (b) unsaturated polyester, and (c) vinyl ester resins.[2]

Vinyl ester (VR) resins are the reaction products of epoxy resin with unsaturated carboxylic acids, as shown in Figure 1.2 (c). Hence, compared to UP resins, VR resins typically have terminal unsaturation except for some special types. Due to the localization of the terminal unsaturated double bond, the cross-linking density was lower than UPR resin, conferring better impact strength and higher elongation at break. In the meantime, the epoxy backbone used in making VR resin has better chemical resistance than UP resin, partly due to the absence of ester linkages in the formed network. Hence, VR resin provides a transition in properties and cost to high-performance epoxy resins while maintaining the processing versatility of polyesters.[3]

Phenolic Formaldehyde (PF) resins, considered the first truly synthetic commercial thermoset polymers, are made by polymerizing phenol and aldehyde under the influence of an acid catalyst or alkaline catalyst. PF resins have low flammability, high char yield, excellent ablative resistance, and low heat/smoke production under combustion. Hence, they are widely used in scenarios where fire must be extremely low, such as aircraft interiors or ablation resistance material for re-entry space vehicles. However, void formation during the curing process is a major drawback that hinders the processing of void-free composite products from phenolic resins, imparting complexity for processing and brittleness for FRPs. Hence, nowadays, new high-performance thermoset resins such as *Polybenzoxazine resin, Bismaleimide resin, and Cyanate Ester resin* are also being developed to overcome these disadvantages while maintaining high thermo-mechanical properties and low foamabilities.

In addition, to effectively address climate change and the global issue of polymer pollution, there is an increasingly popular shift from relying on fossil-based materials and energy to promoting the bio-based materials economy, particularly within key industries such as construction and building sectors.[4, 5] By extracting compounds from biomass feedstocks and converting them into bio-based polymers[6], vigorous efforts are being conducted to explore their full potential to replace petroleum-derived thermoset polymers such as in engineering materials application of thermoset FRPs.[7]

For **thermoplastic polymer**, it does not undergo chemical transformation during processing. Instead, the polymer is softened from the solid state to be processed, and it returns to a solid after processing is completed. Thermoplastics have high viscosity at processing temperatures, which makes them more difficult to process, which is partly the reason why they are not popular in the early stage of FRPs industry development. The high shear stresses needed to make thermoplastics flow cause damage to the fibers, resulting in a reduction of fiber length in the order of 10 to 100 times. Hence, up to now, the main types of thermoplastic polymer used for FRPs industries are high-performance polymers like Polyether ether ketone, Polyphenylene sulfide, Polyetherimide, etc., which have high thermomechanical properties to justify the cost-effective concerns. Thermoplastics do not require refrigerated storage, and they have virtually unlimited shelf and pot life. Also, thermoplastic composites can be repaired because the transition to the softened stage can be accomplished any number of times by application of heat. Hence, the development of high-performance thermoplastic polymer matrix-based FRPs has

recently gained great interest in aeronautic industries. Due to the focus on thermoset polymer matrix in this thesis, this.

Besides the polymer itself in the FRPs matrix, various additive fillers can be added to enhance and modify the processing ability and properties of the matrix and, thereafter, prepare composites. For instance, additives such as accelerators and retarders can be added to just the processing window of thermoset resin. Additives like reactive or non-reactive diluent, solvent, etc., can be added to adjust the viscosity to fulfill the requirements of different manufacture methods of FRPs. Filler particles, such as calcium carbonate, can be mixed with the matrix for weight and/or cost reduction. What's more, due to the intrinsic flammability of the polymer matrix, the addition of flame retardants into the polymer matrix was widely employed to lower the fire hazards and issues related to the fire safety of FRPs.

1.1.1.2. Type of fibers used as reinforcement of FRPs

A variety of fiber reinforcements were widely used in different applications, mainly according to their mechanical and physicochemical properties. When classified by raw material and chemical compositions, the reinforcement fiber can be mainly classified into organic, inorganic, carbon, and metallic fibers. Among them, carbon, glass, aramid, basalt, plant fiber, etc., are mostly used in the application of FRPs nowadays. As shown in Table 1.1, choosing the fiber type for the design of FRPs materials and structures mainly involves a trade-off between mechanical physiochemical properties and final cost.

Table 1.1: Typical properties of natural fibers and their comparison with traditional reinforcement fibers.[8]

Fiber	Density (g /cm^3)	Tensile Strength (MPa)	Young's modulus (GPa)	Specific modulus (GPa/(kg/m^3))	Elongation at break (%)
Flax	1.53	745-1145	44-61	35	2.07
Hemp	1.48	690	70	47	1.6
Jute	1.3	393-773	27	21	1.5-1.8
Ramie	1.5	560	25	17	2.5
Basalt	2.7	2130	93	47	2
Carbon (Hexcel AS4)	1.8	4330	231	129	1.8
E-glass	2.5-2.6	2000-3500	70-76	29	1.8-4.8
S-glass	2.5	4570	86	34	2.8

Glass fibers (GFs) are mainly composed of SiO_2, Al_2O_3, and a host of other oxides of boron, calcium, sodium, etc. The production of glass fiber can be broken down

into five basic steps: batching, melting, fiberization, coating, and drying/packing. Through the control of chemical composition and manufacturing process, the GFs demonstrated a variety of stiffness and chemical resistance. The tensile strength of GFs decreased with elevating temperature. As they are flexible, lightweight, and inexpensive, the use of glass fiber-reinforced polymer composites (GFRPs) is widely popular in low-cost weight-sensitive industries such as rolling stocks, marine, wind, automotive, etc.

Carbon fibers (CFs) are a high-performance reinforcement widely employed in composite materials due to their exceptional strength-to-weight ratio and stiffness. The raw materials for the fabrication of CFs are mainly from polyacrylonitrile (PAN), some of which are also made from rayon- or pitch-based precursors. Taking the manufacturing from PAN precursor as an example, the steps of making CFs mainly include: polymerization to make PAN precursor, wet spinning to from PAN fibers, oven oxidation to the crosslink polymer chain, carbonization at high temperatures and inert atmosphere, and finally, surface treatment and sizing. The mechanical properties of carbon fibers are determined by the atomic configuration of carbon chains and their connections, which are similar to the graphite crystal structure. The major limiting factor for the application of carbon fibers is the cost. The cost of carbon fibers can be justified when weight savings offer a large payoff, such as in aerospace applications.

Plant fibers are mainly harvested from the stems, leaves, stalks, or seeds of various plants. Fibers collected from the stem are called “bast” fibers, which are mainly used in FRPs applications. Examples of bast fibers used in FRPs are flax, hemp, ramie, and jute. Compared to leaf or seed fibers, the bast fiber is less coarse and has higher mechanical properties; therefore, it is used more in FRPs applications. The plant fibers possessed a hierarchical structure ranging from macroscopic scale to molecular scale[9], as shown in Figure 1.3 (a). Known as lignocellulosic fiber, most plant fibers are mainly composed of varied fractions of hemicellulose, cellulose, lignin, pectin, etc., as shown in Figure 1.3 (b). The common advantages of natural fibers, when considered alongside glass fibers, are good specific mechanical properties due to low density, renewable resource with low energy consumption, low cost, and low investment, easier handling and processing, recycling, and good thermal and acoustic insulation[10]. On the other hand, the disadvantages include low strength, variability in quality, higher moisture absorption, limited processing temperatures, lower durability, and inferior fire resistance.

Besides the above-mentioned fiber reinforcement materials, there are various types of fiber reinforcement that are also widely used in FRPs applications. For instance, poly para-phenyleneterephthalamide (commercial name Kevlar fibers) is one of the most used aromatic polyamide synthetic fibers. Aramid fibers have high energy absorption during failure, which makes them ideal for impact and ballistic protection. In terms of inorganic fibers, Basalt fibers are also used in some FRPs applications. Basalt fibers are made using volcanic basalt rock, melted, and extruded into fibers. Basalt fibers feature better mechanical properties than glass fibers and are less costly than carbon fibers. They display excellent thermal stability, good chemical stability, and good corrosion resistance.

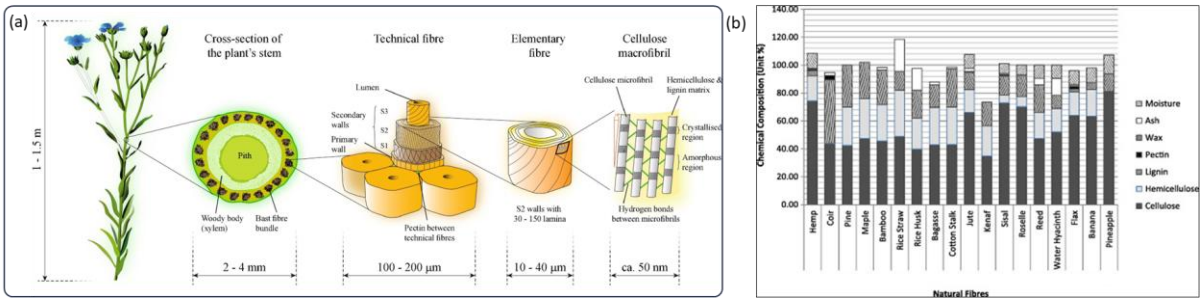

Figure 1.3: (a) Graphical illustration of a hierarchical structure of flax fiber, from macroscopic to molecular scale.[9] (b) Chemical composition of some selected natural fibers.[11]

Besides chemical compositions, fiber reinforcements may be obtained as continuous or discontinuous fibers, unidirectionally aligned fibers, or textile products. Among textile products, it is possible to use woven, knitted, and braided fabrics, to name a few. As fibers provide strength and stiffness while having low density, the reinforcement form is also a vital design parameter that affects both the quality and cost of the composite material.

1.1.2. Out-of-autoclave methods for fabrication of thermoset FRPs

Generally, the production steps of FRPs involve placement and compaction of fiber preform, impregnation of fiber by polymer matrix, degassing with consolidation, and solidification of polymer matrix. Autoclaves are pressure vessels that contain compressed gas during the processing of the composite. Autoclave processing of composites provides higher pressure than available with a vacuum and gives greater compression and void elimination. However, autoclave operations consume large amounts of energy and materials, such as industrial gases and bagging materials. Autoclave operations are also labor-intensive and time-consuming.

Hence, there is a popular trend in the FRPs industry to pursue manufacturing methods without the use of an autoclave, which is called the Out-of-Autoclave (OOA) method. Processes such as Resin Transfer Molding (RTM), Vacuum Assisted Resin Infusion molding (VARI), hand layup, compression molding techniques, vacuum bag molding, and filament winding offer cost-effective and scalable alternatives. These methods allow the produce high-quality composites with complex shapes and sizes without the need for high-pressure autoclaves, thereby reducing manufacturing costs and time. Due to the length limitation of this thesis, only the manufacturing methods used in this thesis will be elaborated.

The hand layup technique, also called wet layup, is the simplest and most widely used manufacturing process. Basically, it involves manual placement of the dry reinforcements in the mold and subsequent application of the resin, as shown in Figure 1.4 (a). Then, the wet composite is rolled using hand rollers to facilitate uniform resin distribution and removal of air pockets. This process is repeated until the desired thickness is reached. The layered structure is then cured either in an ambient atmosphere, vacuum bag, or positive pressure in a hot press machine. The hand layup process may be divided into four basic steps: mold preparation, gel coating (optional), layup, curing, demolding, and final trimming and finishing. The details of the manufacturing process are shown below.

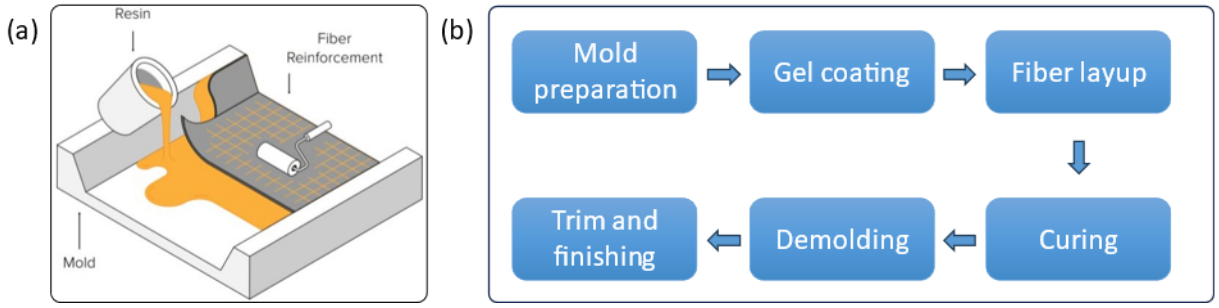

Figure 1.4: (a) scheme for wet layup process of FRPs production. (b) scheme for curing setup using a vacuum bag.[3]

First, a coating of release agent is applied to the mold to facilitate the removal of the finished part. The release agents in common use are wax, polyvinyl alcohol, silicones, and release papers. The choice of the release agent depends on the type of material to be molded and the degree of luster desired on the finished product. A gel coat is applied after the preparation of the mold to produce a good surface appearance of the part being molded. The coating is normally a thermoset resin, mineral-filled, pigmented, non-reinforced lamina. This resin lamina is applied to the mold before the reinforcement. Thus, the gel surface becomes the outer surface

of the laminate when molding is complete. This surface forms a protective lamina through which the fibrous reinforcements do not penetrate, and the product may require no subsequent finishing operations. The final steps involve material preparation, fiber placement, and curing. The fiber is applied either in the form of a chopped strand mat, cloth, or woven roving. Pre-measured resins and catalysts or curing agents are mixed together thoroughly. The resin mixture is then applied to the fibers. Serrated hand rollers are used to compact the material against the mold to ensure complete air removal. Curing is usually accomplished at room temperature, and the final molded part is removed by pulling it from the mold. However, curing under negative vacuum pressure or positive hot press is also used to increase fiber content and reduce defects, as shown in Figure 1.4 (b).

Vacuum Assisted Resin Infusion molding (VARI) is an open mold technique that employs a flexible plastic bag to enclose dry fibers that are put above a rigid mold, as shown in Figure 1.5 (a). A typical sequence of operation of the VARI process is as follows: (a) layup all laminae of dry fabric or perform in designated orientation on the surface treated tool. (b) cover with a highly permeability resin distribution medium on top of the dry fabric to help spread the resin quickly over the entire part. (c) place one or more resin inlet and outlet ports. (d) Cover it with a vacuum bag using pressure-sensitive sealant tape. (e) evacuate the entrapped air with a vacuum pump and compact the dry fiber reinforcement. (f) continue to apply a vacuum to draw liquid resin from an external reservoir into the layup. Being one of the methods in liquid composite molding (LCM), the VARI technique uses a pressure differential for the infiltration of the resin into a previously compacted dry fabric preform. Different numbers locations of inlet flow channels can be employed to design the liquid resin flow through the in-plane directions, as shown in Figure 1.5 (b). Besides, with the use of high permeability resin flow distribution media, the rapid flow of the resin through the distribution media is followed by the infiltration in the through-the-thickness direction, as shown in Figure 1.5 (c).

Faster layup can be achieved with lower labor costs because of the ease of layup of dry fabrics when compared with wet layup. The final parts made by this process have good dimension tolerances, which are comparable to RTM and prepreg manufacturing and better than those made by hand and wet layup. Typical applications of VARTM include large, complex parts such as boat hulls and so on.

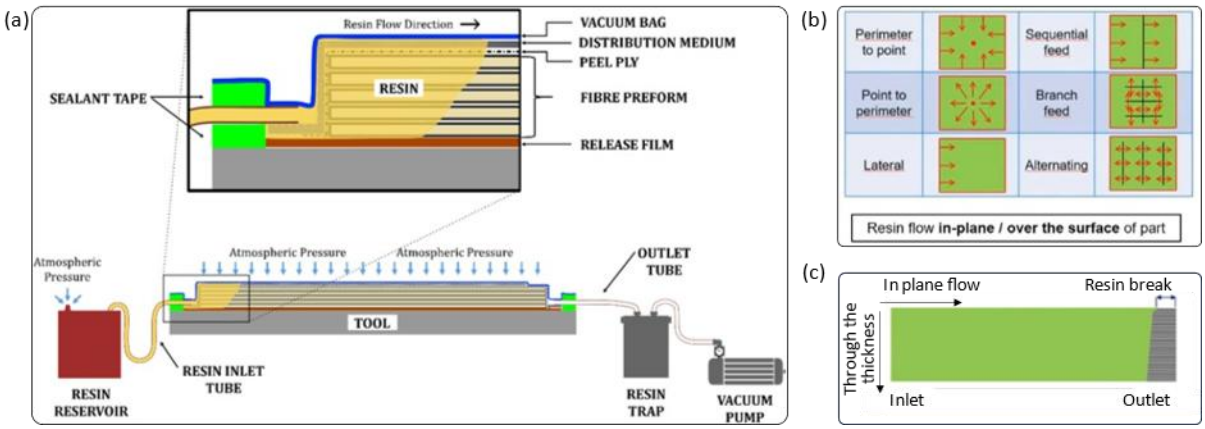

Figure 1.5: (a) scheme for VARI process set up. (b) Different designs of resin inlet and flow over the surface are used. (c) resin flows through the thickness and in-plane during the VARI process.[12]

1.2. Fire properties of thermoset FRPs

The inherent flammability of polymer matrix and organic fiber reinforcement has limited the broader application of FRPs in various industries. Hence, understanding the mechanism of combustions and mode of actions of flame retardants is of great importance for the development of flame-retarded thermoset FRPs. For many years, this complex process was simply understood as the fire triangle, but it has now been revised to a fire tetrahedron consisting of four key contributors: fuel, oxygen, heat and a chain reaction, which was shown in Figure 1.6.

For example, the common house fire begins with pyrolysis, an endothermic process that results from a flammable material experiencing heat from an ignition source, like a smoldering cigarette or a faulty electrical appliance. As the bulk material soften, decompose owing to thermal exposure, it releases unstable radicals and gaseous products into the gas phase. The volatile decomposition products act as fuel that, in the presence of an ignition source and enough oxygen from the air, ignite and lead to combustion.[13] This process means that the bulk material itself is not responsible for combustion but, rather, the decomposition products that evolve into the gas phase. The temperature for combustion to take place must be above the ignition temperature (or flash point) of the polymer, allowing for the transition into an exothermic process that releases toxic gases and smoke, while generating copious amounts of heat for further pyrolysis.[14] This thermal feedback, whether it is conductive, convective and/or radiative, continues to fuel the flame, resulting in a chain reaction that propagates the fire. It is for this reason that

surface treatments or creating a thermal/fire barrier at the interphase between gas phase and condense phase.

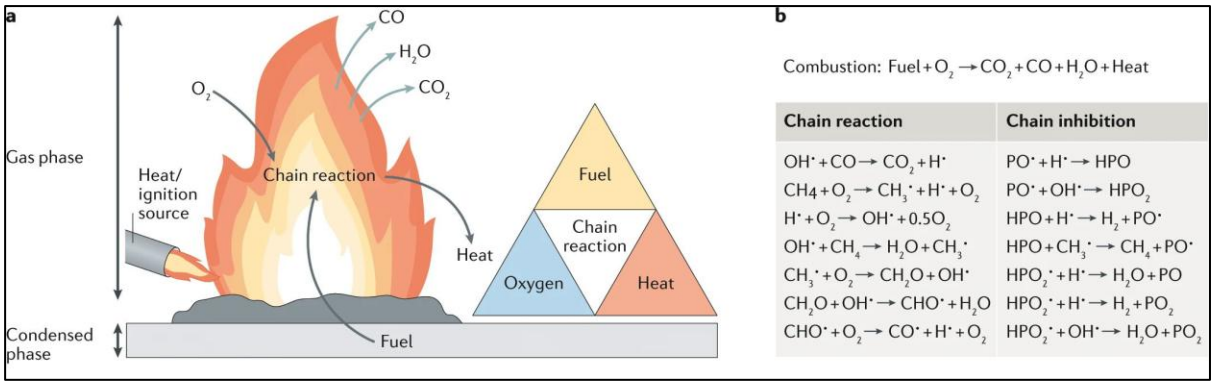

Figure 1.6: (a) A schematic representation of the mechanism of combustion and the associated fire tetrahedron. (b) The overall chemical reaction for combustion that leads to a series of chain reactions and examples of phosphorus-based radicals that can scavenge unstable radicals in the gas phase.[15]

During the combustion process of thermoset FRPs, the thermal decomposition process of FRPs is governed largely by the decomposition of the ***thermoset resin matrix*** in general. The weight ratio for the FRPs is 30~50wt% in most manufacturing methods. Unlike thermoplastics, which soften and melt upon heating, thermoset resins are cross-linked polymers that do not melt. Instead, they degrade or decompose when subjected to high temperatures. Most types of thermoset resins used in FRPs tend to decompose between 300~700℃. Generally, thermoset resins with more aromatic moieties in their cross-linked network tend to have more residues compared to the ones with mainly aliphatic and/or cycloaliphatic structures, showing stronger charring capabilities.

In terms of ***fiber reinforcement***, inorganic fibers such as glass fiber, carbon fiber, and basal fiber are non-combustible. The introduction of inorganic and carbon fiber imparts a dilution effect on the heat and mass generated from the combustion of FRPs. As is known, organic fibers are combustible and can decompose in a fire[16-18]. Hence, the combustion of organic fibers contributed to the release of flammable volatiles, heat, and smoke. As mentioned in section 1.1.1.2, most plant fibers are mainly composed of varied fractions of hemicellulose, cellulose, lignin, pectin, etc. Among them, hemicellulose is the least thermally stable and starts decomposing at 200 °C. Cellulose decomposes around 350 °C, while lignin decomposes in a wide range of temperatures from 200 to 600 °C.[19] The three main components of plant fiber have different abilities to char, and lignin generally has a high char tendency, mainly due to its polyaromatic structure.[20] In addition, the contribution of fiber

reinforcement to thermal degradation and combustion process is complicated since the type, thermal conductivity, orientation, content, size agent, and length of fibers can all influence the combustion behavior of the composite[21-26].

Flame retardants prevent one or more of the fire tetrahedron components from taking part in combustion. As pyrolysis is inevitable in extreme heat situations, it is not always realistic for flame retardants to completely negate ignition. The primary objectives of flame retardants is to impede pyrolysis and time to ignition (t_{ig}), prevent flame spread and suppress the production of toxic smoke, which provides time for people to safely evacuate the premises[13]. In the ***gas phase***, flame retardants can release free radicals to quench and scavenge the unstable OH· and H· radicals, thereby terminate or slowing down the chain reactions as shown in Figure 1.6 (b). Improved fire performance can also be physically achieved in the gas phase by attenuating the combustible gases through an endothermic release of non-flammable gases, such as N_2, H_2O and CO_2. In terms of ***condense phase***, mass and heat transfer in the condensed phase continually feed the flammable decom-position products that cause a fire to spread[14]. A protective layer on the surface of a flammable material reduces the amount of thermal feedback that contributes to the propagation of the fire. This protective layer is often an insulating, thermally stable physical barrier applied on the surface, but it can also be chemically formed at the interface during pyrolysis of the material[27]. This condensed-phase action prevents the polymeric fuel from taking part in combustion, further justifying the application of flame-retardant treatments at the interface where an ignition source meets a flammable material.

1.2.1. Combustion behavior and fire hazards of FRPs under fire

When a composite is exposed to a sufficiently large heat flux radiated from a fire, the polymer matrix (containing combustible fibers) will thermally decompose firstly, and the process is almost the same as that of virgin polymer. The detailed decomposition of virgin polymer has not been introduced, as numerous researchers have reported[13, 28-30].

Upon heat/fire damage, thermoset composite suffers softening and degradation char formation of the matrix, inter-ply delamination and matrix cracking, strength and stiffness depletion, and fiber/matrix debonding[31-33]. In detail, the surface of the composite exposed directly to one-side heating is the first region to be destroyed in a fire. Then heat conduction and heat diffusion occur. In terms of CFs as fiber

reinforcement, their rates in the through-thickness direction are much slower than the direction alongside the fibers because of the higher thermal conductivity of fiber than the polymer matrix. As a result, a temperature gradient through the composite is formed, and three regions in the through-thickness direction are divided, namely, the first region of the hot surface, the decomposition region below the first region, and the nearest to the rear face region.

With the increase of exposure time in the fire, the matrix in the hot surface of the first region can soften when the temperature reaches the glass transition temperature (T_g). At this time, fiber positions begin to reveal, and the composite begins to lose its strength. The heat conduction in the through-thickness direction proceeds progressively. When the temperature reaches thermally decomposition temperature, resin matrix cracks occur, and the matrix surrounding the fibers will begin to lose, and fibers become more visible, resulting in the further decrease of the mechanical properties of the composite. In this case, the reactive volatiles in the decomposition region and evaporated water in the nearest rear-face region of the composite flow through the char layer towards the hot surface. During the process, some of them can be trapped due to the low gas permeability of the composite, leading to a higher internal pressure and expansion of the composite. Therefore, delamination cracks between the plies and gas-filled pores occur, resulting in rapid creeping, buckling, collapse, or some other failure of the composite[18, 34-36]. The decomposed reaction continued until the matrix in the rear-face of the composite degraded to volatiles, smoke, and char completely. The fiber/matrix is almost de-bonding, and the composite is destroyed. At this stage, the decomposition process ceases unless the temperature is high enough to induce pyrolysis reactions between the fibers and char.

Unlike virgin polymers, there are ultra-small fragments of fibers in the dense smoke except for the toxic mix of combustion gases, soot particles, and heat. These fragments of fibers from burning composites are warped by organic compounds and can deposit toxins in the respiratory system, which may cause types of health problems not only for people experienced in the fire but also for the firemen and accident investigators[37-40].

1.2.2. Fire-induced mechanical failure under loading for FRPs

Furthermore, FRPs are known to be employed in structural loading scenarios mainly due to their high specific strength-to-weight ratio. Hence, the concept of

fire safety cannot be constrained within the hazards related to the combustion of flammable substances. Upon heat and fire damage, polymer matrix and some reinforcement fiber will soften, melt/decompose, and eventually decompose and be ignited; this will lead to structural failure of polymer composites, which pose an even greater risk due to structural collapse[41-43].

Due to the low thermal stability and glass transition temperatures of hemicellulose, cellulose, and lignin, plant fiber generally undergoes a quick reduction of mechanical properties during high temperatures and fire, which eventually leads to structural collapse[44, 45]. Hence, the low fire structural stability of plant fiber limits its usage for applications involving structural loading. Meanwhile, basalt fibers bring more interest in high-temperature applications due to their high softening temperature and non-combustibility. Basalt fiber reflects in the preservation of good mechanical properties at high temperatures thanks to their high thermal stability in the range of from 200℃ to 700℃. The softening temperature for basalt fibers is in the order of 960℃, resulting in greater than that of E-glass fibers by about 15%.[46] Hence, the investigation and validation of protective effects imparted by fireproofing methods is of pivotal importance, too, during the materials design stage of flame-retardant thermoset FRPs development.

1.3. Flame-retardant strategy and mechanism for thermoset FRPs

In view of the unique challenges when it comes to imparting flame retardancy and fire safety to the thermoset FRPs, increasing efforts have been being made to solve these ever-changing problems by incorporating flame-retardant moieties in recent decades. There are abundant flame retardants in the industrial market, while newly designed and synthesized flame retardants (FRs) are being proposed each year.[47-49] According to their chemical composition, FRs can be mainly categorized into halogen-containing substances, phosphorus-containing compounds (red phosphorus, phosphates, phosphinates, phosphites, phosphonates, phosphazene, etc.)[50], metal hydroxides (aluminum, magnesium, calcium, zirconium, etc.), silicon-based FRs (silicon oxide, silicate-based minerals, organic silicon-based FRs, etc.) nitrogen-based flame retardants, boron-containing FRs, metal hydroxides) based FRs, as well as intumescent flame retardants based on multicomponent FRs. What's more, hybrid or nano FRs[50-52], as well as biobased FRs, have gained

increasing interest, especially from researchers, mainly due to their high potential in both efficiency and environmental sustainability.

According to the methodologies by which FRs were introduced in thermoset FRPs, three categories can be classified as modification of resin either by additive or reactive FRs, surface treatment of the reinforcing fibers, and applying fire protective coating on the surface of FRPs, as shown in Figure 1.7.

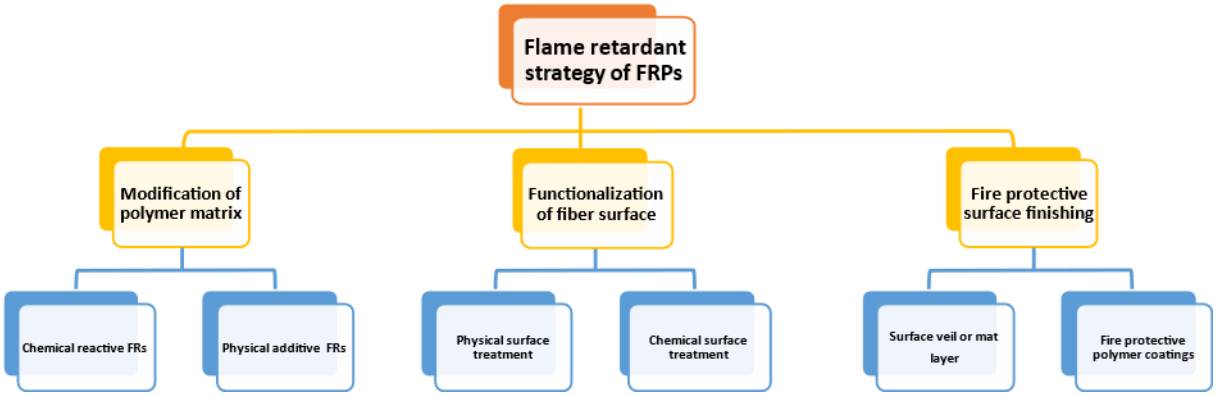

Figure 1.7: Flame-retardant strategies for introducing FRs in FRPs.[53]

1.3.1. Fire-protective surface finishing

Being one of the most widely popular methods in both industry and academia, fire-protective surface finishing has a minimum influence on the manufacturing of FRPs, leaving mechanical performance almost unchanged. Two main approaches were used depending on how FRs are introduced onto the surface of laminates. The first one is by premixing the FRs with a polymer matrix (mainly thermoset types) before applying them onto the substrate of laminates by either brush or spray coating methods. This method provides flexibility and tailorability on FRs formulations but requires additional steps. FRs containing polymer-based coating can also be applied either on the mold surface before the fabrication of the laminate or onto the surface of the composite after the laminate is manufactured. Another method is to utilize nonwoven fabric, such as a surface veil or mat, which contains FRs, short fibers, and organic binders. This method can be seemingly merged into the lamination process.[54] Numerous papers were found to apply fire protective coating on thermoset FRPs, and results are summarized in Table 1.2.

According to the flame-retardant mechanism, intumescent polymeric coatings are often used on the composites. The intumescent effect is a phenomenon in which polymer/FRs composite react to heat/fire by chemically or physically forming a highly porous, thick, and thermally stable char layer to substantially hinder

thermal and mass transfer, thereby protecting the underneath virgin polymer zone or to-be protected substrate. The equations demonstrate the sequential activation of the intumescent coating using ammonium poly phosphate (APP) as an example acid source, a polyol as an example carbon source and melamine as an example blowing agent as shown in Figure 1.8. Initially, intumescent coating was widely used in the protection of structural steel, which has expanded into wider applications.

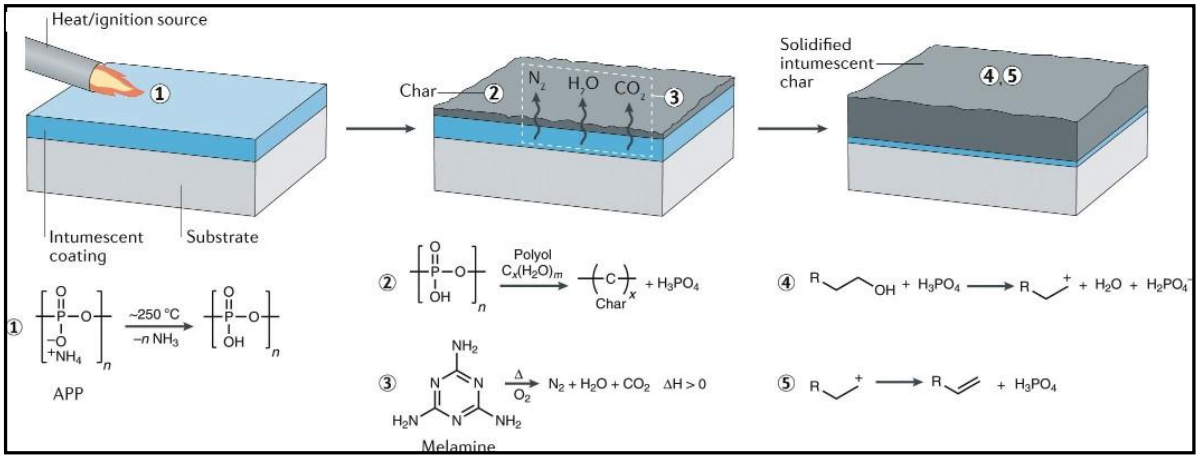

Figure 1.8: A schematic representation of the steps and components required for intumescent flame-retardant systems acting in the condensed phase.[15]

By premixing FRs into coating binders, Kandare[55] and Kandola[56]proposed to compare three commercial FRs containing polymeric coating: a non-intumescent but char-forming, a non-intumescent but halogenated and an intumescent coating, which all of them were coated on the surface of GFRPs independently. All of them demonstrated a reduction of peak heat release rate (PHRR) and delaying of time-to-ignition (t_{ig}), with the best one demonstrating a reduction of PHRR for 45% at 50 kW/m^2. Kandola et al.[57] tried to use a blend of UP resin with phenolic resin as a blended matrix for coating but found that FRs are still needed to improve flame retardancy. Recently, Pomázi et al.[58, 59] prepared an epoxy resin-based gel coat containing ammonium polyphosphate (APP) and resorcinol bis (diphenyl phosphate) (RDP) onto the substrate of carbon fiber-reinforced epoxy composites. APP mainly acted in the condensing phase, with RDP acting in the gas phase in terms of flame-retardant mechanism. The results demonstrated a synergy when employing both APP and RDP at an optimal ratio to yield best flame-retardant performance. Luangtriratana et al.[60] introduced four types of ceramic particles into the phenolic resin coating layer for protection of fiberglass UP resin composite. It was found that the introduction of ceramic particles improved the thermal

barrier effect but not a highly efficient improvement in terms of flame retardancy, showing the functionalities of ceramic particles.

Employing low flammability type thermosets are also used for polymeric coating. For instance, Luangtriratana[61] and Kandola[62] developed a vinyl phosphonic acid (VPA) based flame-retardant coating and employed on the surface of fiberglass composite using a UV polymerization technique. The high flame-retardant efficiency of VPA-based polymeric coating also displayed a great intumescent effect. The composite exhibited a delayed TTI by more than 300% and a reduction of PHRR by 85%. However, the coatings were hydrophilic, displaying considerable mass loss in a water soak test. Bourbigot et al.[63] introduced silicon resin-based coating containing EF, calcium carbonate, and clay onto the surface of carbon fiber-reinforced epoxy composite. Results showed coating with 1mm thickness demonstrated backside temperature can be contained within 300℃ for more than 10 minutes.

Table 1.2: Recent results for the development of flame-retardant thermoset FRPs using fire protective surface finishing method.

Fiber types	Strategy	FRs	Matrix	CCT results	References
GFs	Polymeric coating	EG	Epoxy	TTI: +56%; PHRR: -45% THR: +45%	[55, 56]
CFs	Polymeric coating	APP, RDP	Epoxy	TTI: +7%; PHRR: -57% THR: -28%	[58, 59]
GFs	Polymeric coating	P-rich polymer	Epoxy	TTI: +225%; PHRR: -85% THR: +110%	[61, 62]
GFs	Intumescent mat	EG	Epoxy	TTI: -43%; PHRR: -71% THR: +110%	[64]
Flax	Intumescent mat	APP	Epoxy	TTI: -9%; PHRR: -56% THR: -9%	[65]
CFs	Intumescent mat	EG	Epoxy	TTI: +1%; PHRR: -46% THR: -9%	[66]

Besides premix FRs with coating polymer, FRs containing nonwoven mats were used and investigated. The advantage of using this nonwoven mat is its seemingly ease of integration into the fiber perform layup process of FRPs manufacturing. Kandare[64] investigated the protective performance of 7 types of intumescent mats containing expandable graphite (EG) on fiberglass UP resin composite. The PHRR

of laminate with surface mat decreased PHRR by a maximum of 71% but increased total heat release (THR) by 110%. The thermal barrier effect was improved greatly. Researchers also prepared flame-retarded composites flax/epoxy composite with an additional surface glass fiber veils impregnated with APP[65]. The PHRR of the protected laminate was remarkably reduced, and a thermally stable and highly consolidated char layer remained after incorporating the flame-retarded glass fiber veil. The rigid and high char networks containing glass fibers increased the fire resistance. Li et al.[66] also explored the effect of EG-containing intumescent mat on protecting carbon fiber reinforced composites, and it showed a 46% reduction of PHRR with slightly decreased mechanical properties.

Although fire protective coating introduced the least detrimental effects on mechanical properties, it also possesses its own disadvantages. In terms of reaction to fire properties, fire protective coating usually brings up THR due to the increase of flammable substances. In addition, total strength-to-weight properties were also decreased due to the additional weight of fire protective coating or layers.

1.3.2. Modification of thermoset polymer matrix

Modification of the thermoset resin matrices mainly includes two strategies: one being adding FRs into uncured resins, another being chemically modifying the monomer and/or curing agent to incorporate FRs moieties into cross-linked networks. For the first one, abundant research concerning flame-retardant bulky polymer and traditional fiber-filled or reinforced polymer composites[67-69] can be drawn to inspire the research of fire-proofing thermoset FRPs. Due to the focus of the thesis, research using only traditional UP, VR, and EP resins will be discussed as shown in Table 1.3.

Various types of phosphorus FRs are widely used in flame retardant thermoset FRPs, which demonstrated tailored flame retardant mechanisms by varying chemical environments of phosphorus atom and FRs design.[70] By mainly acting in the gas phase, the 9,10-dihydro-9-oxa-10-phosphaphenan-threne-10-oxide (DOPO) and its derivatives chemically reactive dissolved in epoxy resin and showed good efficacy for imparting flame retardancy even when adding only 2–3 wt. % in some resin systems[71]. Early research from Schartel, Döring, and co-workers [72-74] reported a series of halogen-free and DOPO-based flame retardants and showed its efficacy in improving the flame retardancy of CFRPs. Recently, Campana et al. [75] introduced DOPO and aluminum diethyl phosphinate (AlPi)

separately into the unidirectional flax fiber-reinforced epoxy composites with a fiber volume ratio of 30vol%. By keeping phosphorus content at 2wt% with respect to the polymer, the content of AlPi and DOPO were 9.5wt% and 13.9wt%. The laminate with AlPi showed a better reduction of PHRR and higher char yield value compared to that of composite with DOPO, with similar THR value output collected. However, DOPO showed a better performance in terms of longitudinal modulus and tensile strength.

Table 1.3: Recent results for the development of flame-retardant thermoset FRPs using modification of thermoset polymer matrix.

Fiber types	Strategy	FRs	Matrix	CCT results	References
Flax	Additive FRs	DOPO	Epoxy	TTI: -16%; PHRR: -9% THR: -16%	[75]
Flax	Additive FRs	AlPi	Epoxy	TTI: +3%; PHRR: -13% THR: -15%	[75]
Flax	Additive FRs	Nano FRs	Epoxy	TTI: +34%; PHRR: -26% THR: -12%	[76]
GFs	FRs in molecular chain	DOPO based FRs	Epoxy	TTI: -18%; PHRR: -31% THR: -21%	[67]
GFs	Aromatic-rich molecular chain	None	Vinyl ester	TTI: +6%; PHRR: -37% THR: -3%	[77]

Phosphorus-nitrogen compounds have been proved to improve the fire performance of thermoset FRPs due to their roles in both the condense and gas phase. APP, an inorganic salt consisting of polyphosphoric acid and ammonia, has been a promising candidate as an acid source and fuel dilution agent in flame retarded polymers with ease of processability, low cost, and toxicity. For instance, Thiyagu et al.[78] prepared glass/ramie hybrid fabric reinforced epoxy composite with varying content of APP (10, 15, 20wt%). With over 10wt% APP, both vertical and horizontal burning achieved the highest rating in terms of flammability. Bachtiar et al.[79] investigated the effects of either melamine resin micro-encapsulated APP or aluminum trihydrate (ATH) for the plain-woven flax fabric-reinforced epoxy composites. It was found that APP and ATH alone showed limited improvement in terms of limited oxygen index (LOI) and UL 94 test results even if FRs content was more than 30wt%.

Nano FRs as additives have gained increasing popularity recently. Wei et al.[76] synthesized a novel polydopamine (PDA) coated silicon oxide nanosized FR named SiO_2@PDA and investigated its influence in both fire safety and mechanical properties of epoxy composite reinforced by 60wt% of flax fabric. The PDA-based nanocoating on SiO_2 provided a better dispersion of nanosized FR, which in turn generated a more compact and graphitized char layer there by showing higher LOI value with lower PHRR and THR results compared to those for laminate with only pristine SiO_2 fillers. Ejaz et al. [80] employed nanosized FRs (ATH with zirconium hydroxide (ZHO) nanoparticles) and explored their synergistic effect in 40wt% jute woven fabric reinforced UPR composite. With 4wt% of ATH or ZHO, PHRR decreased by around 15%, and similar results were achieved in the formulation in which 1.5wt% of both ATH and ZHO were used.

However, there are still several challenges when adding FRs into the polymer matrix. The charring behavior may be suppressed when using FRs that mainly work in the condensed phase in the polymer matrix. Manufacturing methods also play a vital role in the selection of FRs and the processing of FRPs. The functional temperature or decomposition temperature of additive FRs needs to be evaluated before processing, especially for thermoplastic polymers. In terms of the LCM process for composite manufacturing, it has been reported that oversized solid FRs may be filtered by fiber preform, especially short fiber mats or woven fabric.[81-83]

Incorporating FR moieties into polymer networks by molecular design and synthesis has had wider popularity recently, especially when it comes to combining features like recyclability or high biobased contents.[84, 85] For instance, Tian et al.[86, 87] designed two types of hydroxyl terminal groups containing DOPO-based derivatives and used them as co-curing agents with biobased dynamic bond containing curing agent and epoxy to prepare flame-retardant recyclable fiberglass/epoxy composites. Although no CCT was done for composites, the modified laminate coupons showed self-extinguishing properties under the vertical burning test. Zhang et al.[67] designed DOPO-containing 1-vinyl imidazole salts as a co-curing agent to cure with vinyl ester resin for GFRPs. CCT results showed a reduction of PHRR and THR by 31% and 21%. By incorporating more aromatic content, thermosets may show higher intrinsic flame-retardant properties, as shown in another work of Zhang et al.[77] It showed the design and synthesis of vanillin-based dynamic bonds containing vinyl ester resin. Due to its rich aromatic structure, the PHRR and THR were reduced by 37% and 23%, respectively.

It is worth noting that the addition of reactive or additive FRs may alter the curing kinetics during the solidification of the thermoset, which may pose a negative influence on certain parameters like mixed viscosity, gel time, and permeability, thereby influencing the processability and final mechanical properties of thermoset FRPs.

1.3.3. Surface functionalization of fiber reinforcement

Having higher surface area compared to other forms of materials, various efforts have been implemented by surface functionalization of fiber reinforcement to enhance the performance of thermoset FRPs. Fiber surface sizing, such as alkaline, silane, enzymatic, acetylation, etc., treatments, has been widely used to improve compatibility and stress transfer between reinforced fiber and polymer matrix in industries[88]. However, using alkali or silane treatments tends to provide little enhancement to overall fireproofing efficiency unless flame-retardant moieties are introduced, which can be categorized into surface chemical modification and surface physical modification. The abundant functional groups and hierarchical porous structure[9] of plant fiber make the introduction of FRs on plant fiber surfaces one of the promising solutions for fire-safe PFRPs. However, for inorganic or carbon fiber, due to their inert surface and relatively few polar groups, it remains harder to be surface functionalized compared to plant fibers.

For surface chemical modification, Zhang et al.[89] managed to introduce DOPO onto the surface of CFs by pretreating the cleaned CFs surface with an amine functional silane coupling agent, as shown in Figure 1.9 (a). By promoting the interfacial charring on the CFs, the modified composites showed a reduction of PHRR and smoke production rate (SPR) by 26% and 31%. It is envisaged that if a higher amount of FRs can be grafted on the surface of CFs, the flame retardancy will be better. For plant fiber, Chu et al.[90] synthesized phosphorus and nitrogen-containing silane coupling agent by reaction of silane agent with Dimethyl phosphate and paraformaldehyde. After the sol-gel treatment on ramie fabric by silane agent, ramie/UP composites were fabricated with fabric content of around 50wt%. While showing no rating for the UL 94 test, the treated ramie/UP laminate showed a reduction of PHRR and THR by 27% and 20% compared to those properties for untreated composite when exposed to 35 kW/m^2 heat flux.

Irradiation grafting of FR provided another approach to chemically treat such as plant fiber without involving the hydroxyl group, which was demonstrated by

Sonnier[91, 92] early by grafting dimethylvinyl phosphonates and dimethyl (methacryloxy) methyl phosphonate on the flax fabric by more than 3wt% and 0.5wt% phosphorus respectively as shown in Figure 1.9 (b). The grafting process gave a self-extinguishing fabric with only slight improvement when treated flax fabric was used in UPR composite. While grafting FR treatment promoted charring capabilities, it was suggested that low fiber content (30wt%) might lead to a limited reduction of flammability for composites.[20]

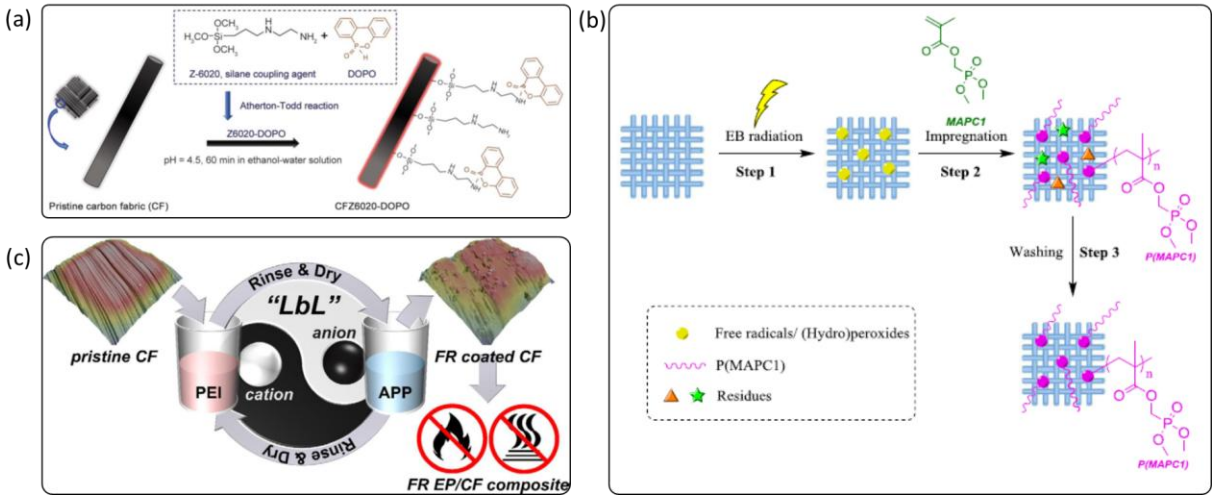

Figure 1.9: (a) Scheme showing chemical modification of CFs surface. [89] (b) The scheme shows irradiation grafting FRs on the flax fabric surface. [91, 92] (c) scheme showing LbL process to introduce FRs on CFs surface.[93]

For surface physical modification, impregnation and absorption of FRs is a straightforward approach and promising method, especially for plant fibers due to their hierarchical and porous structure. Jiang et al.[94] immersed ramie fabric into alkali-treated APP containing aqueous solution and pad-dried to get APP-absorbed ramie fabric. The treated ramie fabric was later hand-layup with epoxy resin with compression consolidation to get flame retarded NCFs. When the APP ratio reached 9wt%, the composite achieved a V0 rating in the UL 94 test and an increase from 23.0% to 33.8% in terms of LOI value. The CCT results showed a 26% reduction in PHRR and a more than 40% reduction in both THR and Total smoke production (TSP). Guo et al.[95] treated the dignified bamboo directly with boric acid under an alkaline aqueous solution and used vacuum-assisted infusion to prepare bamboo/epoxy composite. The treated bamboo/epoxy composites displayed a 36% reduction of PHRR and a 15% increase of LOI value compared to that for bamboo/epoxy composite without any treatment. Khalili et al.[96] treated plain woven jute fabric with an organic phosphonate ester or graphene nanoplates separately and thereafter fabricate jute/ polyacrylic composite with fiber volume

around 40%. The laminate with phosphorus-treated jute fabric (0.72wt% phosphorus content) demonstrated a 26% reduction of PHRR at a constant external heat flux of 35kW/m^2.

The layer-by-layer (LbL) strategy has raised immense interest in the flame retardant field, especially in flame retardant surface treatment, mainly due to its ease of combination of different types of FR, adaptability on different surfaces, and ambient processing conditions.[15] Shi et al.[93] introduced branched polyethyleneimine (PEI) and APP via LbL technology on the surface of CFs to fabricated carbon fiber-reinforced polymer composites (CFRPs), as shown in Figure 1.9 (c). After modification, the as-prepared laminates get a reduction of PHRR and THR for 33% and 22% in CCT results. For plant fiber, Song et al.[97] employed LbL strategies to deploy cationic polyethyleneimine (PEI) and anionic APP dispersed in an aqueous solution to functionalize the surface of continuous ramie fabric. With more than 8wt% of FR on fabric, the composite after CCT at 35 kW/m^2 also demonstrated a reduction of more than 50% in PHRR and a more intact char layer, exemplifying the condensed phase behavior.

Another promising method consisted of treating the fiber surface with polyelectrolyte complex (PEC), which forms between oppositely charged macromolecules.[98, 99] Shi et al.[100, 101] prepared two types of PEC solutions by using APP with either PEI or chitosan (CH) to surface functionalize the surface of CFs to prepare CFRPs. With phosphorus-nitrogen-containing FRs introduced, the CCT results showed a reduction of PHRR and SPR by 47-50% and 28-30%.

Fiber surface treatment brought the above-mentioned opportunities as well as challenges. While flame-retardant moieties were introduced on fiber surfaces, the efficacy of this method needs more comprehensive research, with many scattering reports published. What's more, natural fiber, especially plant fiber-reinforced polymer composites, tends to have lower fiber contents when produced by the LCM process, which will bring more challenges compared to traditional fiber-reinforced polymer composites.

1.4. Enhancement of fire mechanical properties of flame-retardant thermoset FRPs

As mentioned in section 1.1.2, the vulnerability of polymer matrix against fire imparts thermoset FRPs with low performance upon heat/fire damage, eventually leading to mechanical failure. Hence, academic communities are looking into the

enhancement of fire mechanical properties of laminates when developing new materials for flame-retardant thermoset FRPs. Several aspects of fire mechanical properties are being studied. According to stages of fire incident, post-fire mechanical properties and in situ mechanical response are studied to demonstrate the protective effects. Besides, various types of mechanical properties are studied, such as fiber-dominated mechanical properties or matrix-dominated properties, such as flexural in-plane axial tensile properties. Due to Kodur[102] published a review of the mechanical characterization and properties of FRP composite at elevated temperatures, hence only mechanical properties of FRPs influenced by fire damages will be elaborated in this thesis. In addition, the comparison of thermal stability between plant-based fibers and conventional fibers showed a pronounced disadvantage in terms of fire structural response, behavior, and survivability[103]. Hence, in this thesis the fire mechanical properties of plant fiber-based thermoset FRPs will not be elaborated in detail.

1.4.1. Protection of matrix-dominated post-fire mechanical properties

For matrix-dominated properties, Kandare et al.[55, 64, 104] investigated the influence of several flame-retardant approaches on thermal barrier effects as well as post-fire flexural properties of the thermoset fiberglass composites. Surface protective methods like commercial intumescent mat or surface polymeric coating with and without flame retardant additives in the polymer matrix were investigated under different heat flux values. The specimens are exposed to elevated temperatures for a certain time duration and subsequently cooled to ambient temperatures to measure their post-fire flexural properties. The general trend was found that the surface protective methods prolonged the temperature rising and thermal transfer through the thickness direction and prevented the fast loss of flexural modulus by fire damage. Later, Krishnan et al.[105] and Luangtriratana et al.[60] investigated the influence of novel flame retardant formulations in surface coating and polymer matrix for the post-fire impact and flexural modulus on glass fiber-reinforced thermoset composites. Results also showed a loss of slowed mechanical properties and better stiffness retention over time. Zhu et al.[106] also studied the post-fire flexural properties of sandwich composite with intumescent mat surface finishing and found that it also helped retain posit-fire mechanical properties.

1.4.2. Protection of fiber-dominated post-fire mechanical properties

To the best of my knowledge, few works have investigated the influence of flame-retardant approaches on the fiber-dominated mechanical properties of FRPs under fire. So far, the current research on post-fire fiber-dominated mechanical properties has centered on pristine FRPs with no fireproofing properties. For instance, Mouritz et al.[107, 108] showed that the post-fire tension properties of glass fiber laminates (with no fireproofing properties) were severely reduced (more than 80%) once the polymer matrix decomposed to char. Anjang et al.[109] also studied the post-fire tensile mechanical properties of sandwich composites without fire protective methods and found the severe degradation of tensile properties under fire. Decomposition of the polymer results in the loss in stress transfer between the matrix and glass fibers, resulting in large reductions in the tension stiffness and strength of the laminate.

Hence, it is envisaged that the addition of fireproofing methods would contribute to the prolonging of mechanical properties of thermoset FRPs under fire, even when it comes to fiber-dominated mechanical properties. However, the post-fire mechanical properties cannot fully demonstrate the influence of fire protective methods on mechanical integrity loss of laminate due to samples being usually cooled down after fire damage and tested at ambient temperature.

1.4.3. Postponing of mechanical failure of FRPs in fire

A composite that has good fire reaction properties, such as low heat release rate and smoke yield, may not necessarily have good fire-resistive properties, especially in fire. Hence, several pioneers like Mouritz and Gibson et al.[31] have designed various experiments and proposed models to predict the mechanical failure of pristine FRPs in fire, demonstrating the influence of fiber types, ply orientation[110], stacking sequence[25], and external heat flux influences.

As shown in Figure 1.10 (a, b), the coupons were generally tested in the universal testing frame with specially designed sample grips, jigs, and an external heating source. Various types of heat sources were used, such as propane burners. Lately, a cone heater has been used due to its creation of an evenly distributed heat flux over the sample surface. For instance, Bhat et al.[45] demonstrated basalt fiber composite has lower tensile fire resistance than an equivalent glass fiber laminate when exposed to the same heat flux representative of a possible fire scenario as shown in Figure 1.10 (c, d). However, basalt fiber possessed lower thermal

conductivity, high oxidation resistance, and higher softening and melting temperatures than E-glass fiber. It is found that the higher emissivity of basalt fiber composite caused it to heat faster and reach higher temperatures. This caused the basalt composite to undergo softening and decomposition of the polymer matrix and weakening of the fibers at a faster rate, resulting in inferior fire resistance compared to the glass fiber composite under combined tensile loading and one-sided radiant heating.

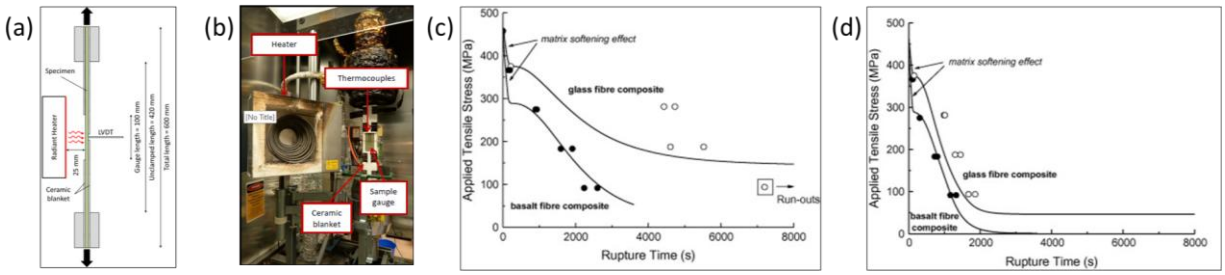

Figure 1.10: (a) schematic illustration and (b) digital photos for the setting of the tensile stress rupture test.[111] Effect of constant tensile stress on the rupture times of the basalt and glass fiber composites when exposed to heat fluxes of (c) 25 and (d) 50 kW/m^2.[45]

Surface fire protective finishing has shown great potential in the retention of post- Nevertheless, this method mentioned above is cumbersome and time/material consuming since it requires a large specimen and a universal tensile testing machine with special protection. In terms of the fire scenario, autoignition was employed, as well as the potential existence of upward fire/thermal damage on the upper part of the coupons, which leaves room for future improvements of the experimental method.

fire mechanical properties, as discussed in sections 1.4.1 and 1.4.2. However, few works have explored the protection effect of fireproof coating on the postponing of mechanical failure of FRPs in fire. For instance, Kandare et al.[112] A fire structural model for laminate with intumescent coating was proposed to predict the failure time of these coupons under tension and fire at the same time. However, the results were found to be approximate due to simplified assumptions in the analysis.

1.5. Motivation and objectives

Based on the introduction and stated-of-the-art discussed in the above sections, the development of flame-retardants thermoset FRPs requires not only enhancing its flame retardancy and lowering fire hazards but also improving its heat/fire insulation and postponing the mechanical failure upon fire damage. In addition, there is an imperative necessity to design and develop a bench scale machine to

verify the protective effects of flame-retardant thermoset FRPs simply and less time/material consuming in the early material design stage. In view of these unique challenges for thermoset FRPs materials development, this thesis tried to pursue the following objectives:

(a) to develop novel flame-retardant FRPs materials with low fire hazards like heat, smoke, etc.

(b) to develop novel flame-retardant composites with enhanced heat/fire insulation properties.

(c) to design and manufacture a bench-scale mechanical instrument that enables the facile validation of the protective effects of the above-developed materials.

2. Materials and characterization methods

2.1. Materials

Epoxy-modified vinyl ester resin (Derakane 8084, Ashland Inc.) was purchased from Resinas Castro S. L. Methyl ethyl ketone peroxide (MEKP) initiators, and Cobalt octoate (CoOct) promoters were purchased from Plastiform S.A. A bisphenol F-type epoxy (EP-Gel Coat) and an aliphatic and cycloaliphatic mixed amines type hardener (Hardener L) were purchased from R&G Faserverbundwerkstofffe GmbH, Germany. Epoxy resin (Resoltech 1800 ECO) and cycloaliphatic & aliphatic amine curing agent (Hardener 1804 ECO) were purchased from Resoltech, France, which has a ~36% biobased content after mixing.

Expandable graphite (type: GHL PX96) was provided by Georg H. LUH GmbH. Silicate-based inorganic fillers (ADINS Fireproof 20) were kindly provided by TOLSA S.A. Hollow glass sphere (HGM) with type code iM16K was supplied by 3M. Exolit AP 750 and Exolit IFR 36 with phase II type APP as the main component were kindly provided by Clariant. Glycerol triglycidyl ether (GTE) was purchased from Biosynth AG.

Aluminum trihydrate (SB-432) was provided by J.M. Huber Corporation. Cobalt (II) acetate tetrahydrate was purchased from Alfa Aesar. 2-Methylimidazole (2-MIM) was purchased from TCI. Phytic acid (50wt% water solution) was purchased from Sigma Aldrich, Spain. Chitosan (MW~1526kDa) was purchased from Fluorochem Ltd, UK. Hydrochloric acid and acetic acid were purchased from Sigma Aldrich, Spain, and used without purification. Type II water was produced by a water purification machine (Wasserlab Automatic plus).

Glass fabrics (GF) (area density: 275g/m^2, plain weave, UTE 275P) were purchased from Castro Composites SL. Flax fabric (area density: 220g/m^2, type code: FlaxDry BL200) was purchased from EchoTechnilin, France.

2.2. Characterization methods

Fourier transform infrared spectroscopy (FTIR)

The FTIR spectrums of tested samples in this thesis were conducted on the Fourier transform infrared spectrometer (Nicolet iS50) with the attenuated total reflection (ATR) module.

X-ray photoelectron spectroscopy (XPS)

The XPS analysis was carried out in a Thermo Scientific Multilab 2000 spectrometer fitted with a dual-anode X-Ray source (Mg K alpha and Al K alpha with photon energies 1253.6 and 1486.7 eV, respectively) and a 110 mm hemispherical sector analyzer.

X-ray diffraction (XRD)

XRD was recorded with a diffractometer (Empyrean, PANalytical) using Cu Kα (λ=0.154 nm) as the anode resource and Ni filter. The voltage and current were 45kV and 40mA, respectively, with a range from 5° to 50°.

Scanning electron microscopy (SEM) and energy-dispersive X-ray spectroscopy (EDS)

SEM analysis was carried out on field emission scanning electron microscopes (FEI Helios NanoLab 600i or Apero 2, Thermo Fisher). Powder samples were dispersed in acetone before being dropped on the conductive carbon double-sided tape and dried. The samples were gold sputtered to generate a thin gold layer on the sample surface. Various voltage, current, and scanning intervals were chosen according to the different samples tested. EDS Analysis provides elemental and chemical composition and distribution of a sample. The measurements were done using EDS detectors (Ultim® Max, Oxford instruments, UK) mounted in SEM.

Thermogravimetric analysis (TGA)

The thermal decomposition behavior of various fillers or filled epoxy composites was studied by TGA (TA Q50, USA) in a nitrogen atmosphere with a heating rate of 20 ℃/min. The sample gas purge flow rate was set as 90 mL/min. Samples weighing around 5 mg were used for the test at the temperature range between room temperature up to 800℃.

Thermogravimetric analysis-Fourier transform infrared spectroscopy (TG-FTIR) coupled analysis.

The evolved gaseous products from polymers under a degradation process were characterized by coupling techniques of TG-FTIR. The evolved volatiles from the specimen in the TGA analyzer (Q50) were directed to the gas chamber in an FTIR

spectrometer (Nicolet iS50) through a heated pipe at 300 °C. FTIR spectra were recorded in a range of 4000–500 cm^{-1} with a 4 cm^{-1} resolution. The invariable weight (15±0.2mg) sample underwent heating from ambient temperature to 800oC with a heating rate of 20 °C/min.

Ultrasonic C-scan

The ultrasonic C-scan is perhaps one of the most commonly used nondestructive testing methods. In this technique, the surface of an immersed sample is scanned, and a projection of the reflected and/or transmitted ultrasound is collected and analyzed. Therefore, it is a volumetric inspection method. The transmission C-scan gives an integrated view of the damage zone, while the reflection C-scan offers the details on the depth distribution of the damage zone. Typical frequencies are 1-10 MHz (low MHz range) for composite materials. In this thesis, C-scan (Tecnitest Triton 1500 USPC-3100 ultrasonic) was performed to determine the quality of the panel after manufacturing and to localize the possible defects.

In-plane static tensile mechanical tests

Following standard ASTM D3039/D3039M, the tensile strength of the composite coupons at ambient temperature was measured using a universal testing frame (3300 series, Instron) equipped with a suitable range load cell. Rectangular coupons of 250×25mm^2 were milled from the composite from the prepared laminate and subsequently tabbed with glass/epoxy laminates glued with epoxy adhesive to prevent damage in the grip area during testing. The extension rate was 2mm/min, with at least three samples being tested for each type of specimen. Vertical deformation was measured by a 12.5mm gauge length standard resistive extensometer.

In addition, a post-fire in-plane axial tensile strength test was employed to demonstrate the protective effects of bilayer coating in chapter 3. The two edge and back sides of composite coupons with standard tensile test size were protected by thermal insulative fabric, leaving an opening area with a length of 100mm. The coupons were then heated and fire-damaged for 120s under 35 kW/m^2 by using the horizontal CCT test set up with sparkle ignition. After that, samples were taken out from the heat zone, and the fire was extinguished. After cooling down to room temperature, the tensile properties of the damaged laminates were tested using the procedure mentioned above. In chapter 3, three batches of specimens were prepared for the three testing conditions: as produced GFRP and non-protected

and protected specimens with both no fire damage and damage by exposing to radiant heat for 120s.

Metallographic examination

After the failure of the test coupons, the areas close to the failure surface of the composite coupons were disc-cutted and cold-mounted in epoxy resin to prepare for examining failure mechanisms. The samples were subsequently grounded and polished to get a nearly scratch-free surface. Optical microscopy was carried out by using optical microscopes (SZX 10 and BX 51, Olympus). The polished samples are either directly inspected by optical microscope or gold-suspended for inspection under scanning electron microscopy.

Dynamic mechanical analysis (DMA) test

DMA test was measured with a dynamic mechanical analyzer named Q800 from TA Instrument using a single cantilever mode with a heat ramp of 3°C/min to 170°C at the amplitude of 30μm and frequency of 1Hz.

Vertical burning UL 94 test for bulk polymers

UL-94 vertical burning test was performed on samples of 127.0mm×12.7 mm×3.0mm according to ASTM D3801. The flaming times were recorded twice 10 seconds after flaming, which were assigned as afterflame time t1 and afterflame time t2, and afterglow time t_3 was defined. In terms of the dripping sample, the burner was tilted 45°, as shown in Figure 2.1 (a). It also records whether any debris or drips are sufficient to cause secondary ignition of an underlying surgical cotton wool sample. At least five sets of specimens were tested. The UL-94 vertical burning ratings were assessed in Table 2.1. The flame moved upward, which directly heated the undamaged polymers. The fire intensity was enhanced.

Table 2.1: Materials classification of UL 94 test.

Criteria Conditions	V-0	V-1	V-2
Afterflame time, t_1 or t_2 for each specimen	≤10s	≤30s	≤30s
Total afterflame time (t_1+t_2 for five specimens)	≤50s	≤250s	≤250s
Afterflame + afterglow time (t_2+t_3 for each specimen)	≤30s	≤60s	≤60s
Afterflame or afterglow of any specimen to holding clamp	No	No	No
Cotton ignited by flaming drops	No	No	Yes

Vertical burning test (VBT) test for fabric samples

Vertical burning for flax fabric was performed following standard ASTM D6413 with a sample width of 76mm and length of more than 200mm. A Bunsen burner

with a flame height of 38mm was applied on the lower edge of the fabric for 12 seconds only one time. Afterflame time and afterglow time are recorded. The burnt length and char length are recorded, too.

Limited oxygen index (LOI) test

LOI value was employed to assess the flammability of polymers, which was defined as the minimum oxygen concentration in mixed O_2/N_2 to permit persistent flaming. Herein, LOI measurement was carried out according to ASTM D2863 on the sample of 12.7mm×6.5mm×3.0 mm. The sample ignition occurs at the polymer sample top to give a vertically downward burning geometry, as shown in Figure 2.1 (b). Compared to vertical burning tests, this yields direct quantitative and fire science-related data, and it proves to be a very effective indicator of ease of ignition.

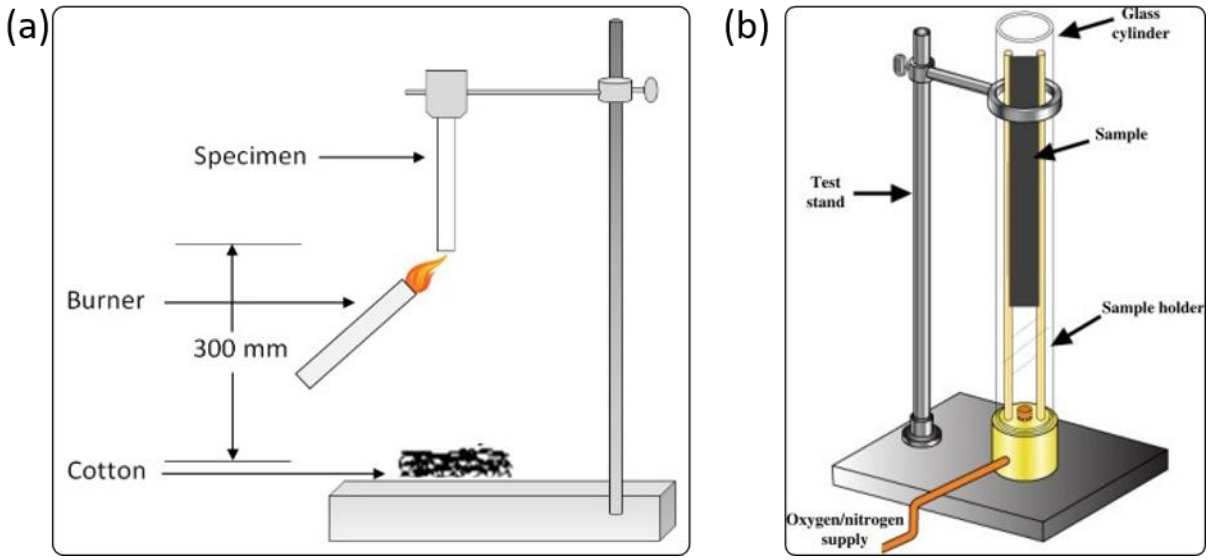

Figure 2.1: schematic illustration of UL 94 (a) and LOI tests (b).[113]

Microscale combustion calorimeter (MCC) test

MCC test, also called pyrolysis-combustion flow calorimetry, was developed to perform a huge number of analyses with only some milligrams of materials. The working mechanism is also based on the consumption of oxygen, such as a cone calorimeter test (CCT).

However, during PCFC tests, pyrolysis and combustion are monitored independently in two different chambers, as shown in Figure 2.2. Hence, there is no feedback from combustion to pyrolysis, contrary to fire tests such as cone calorimetry, for which the heat released by the flame goes back to the condensed phase and contributes to accelerating the pyrolysis. Indeed, there is no feedback from combustion to pyrolysis, contrary to fire tests such as cone calorimetry, for

which the heat released by the flame goes back to the condensed phase and contributes to accelerating pyrolysis. In this thesis, MCC results were recorded using MCC from the UK FTT company. Each specimen was tested three or four times under a nitrogen atmosphere. According to standard ASTM D7309, combustion parameters about samples, especially the peak heat release rate (peak HRR), heat release capacity (HRC), temperature of the peak heat release (T_p), and total heat release (Total HR), were obtained by the software.

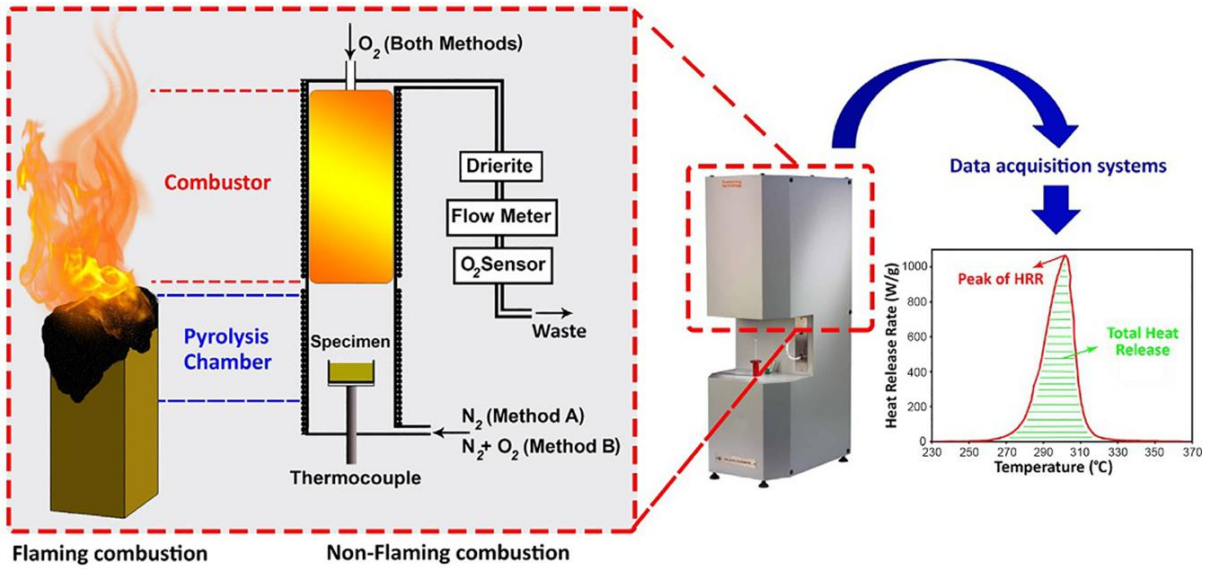

Figure 2.2: schematic presentation of the pyrolysis-combustion flow calorimeter.[114]

Cone calorimeter test (CCT)

The CCT is the most significant bench-scale test for evaluating fire hazards and combustion behaviors of polymeric materials under a real fire-like surface flaming condition.[114] The name cone calorimeter comes from the conical shape of the heating coil, which produces a relatively even distributed heat flux under a certain height and area, as shown in Figure 2.3 (a). This imposes a uniform heat flux across the surface of the tested sample. The cone heater is connected by a hinge and can be tested in a horizontal or vertical fashion. It has been widely used in research on fire-safe polymeric materials as well as in the regulatory standards of various industries.

According to the standard ISO 5660, the information toward heat release, like heat release rate (HRR), PHRR, and THR, is determined on the basis of the speed and volume of oxygen consumption during the combustion of the specimen as shown in Figure 2.3 (b). The information about the smoke release, such as SPR and TSP, is calculated from the measurement of the attenuation of a laser light beam by the

combustion smoke stream. Other parameters, e.g., the time to ignition, the specimen weight change during combustion, and the production of CO and CO_2, are also measured in this test. Among those, the value of PHRR is regarded as one of the most important parameters for evaluating the flame-retardant properties of materials. A Cone Calorimeter is so designed that the specimen sits on a precision weight cell, and its real-time mass loss record is thereby produced.

CCT carried out in this thesis uses a dual cone type cone calorimeter from Fire Testing Technology, UK. Different external heat fluxes were used, mainly 35kW/m^2 and 50 kW/m^2. The sample surface to the rear edge of the cone heater is 25mm. The surface size of the specimen was 100 mm × 100 mm with a thickness of around 2mm for all the works in this thesis. Each sample group was tested at least twice in the same conditions.

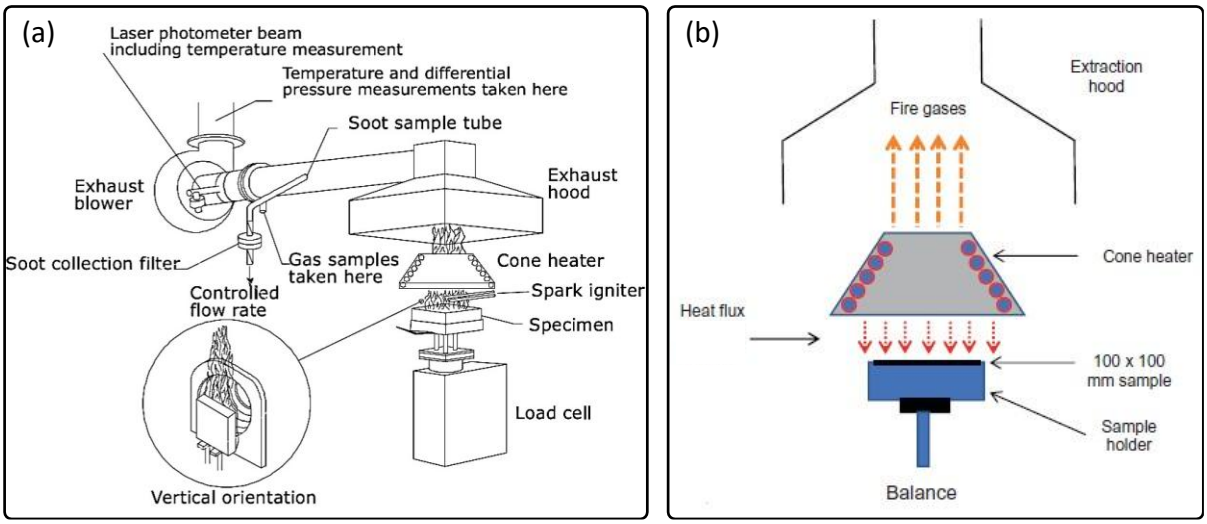

Figure 2.3: (a) a schematic drawing of the several parts of the cone calorimeter.[115] (b) core operation principle of cone calorimeter.[114]

Heat/fire insulation tests

The heat/fire insulation test was employed to evaluate the resistance of heat transfer and fire damage of polymer composite through the thickness direction. For the work in chapter 3, the test was done by placing laminates 60mm away from the cone heater in vertical mode. The heat flux of the cone heater was calibrated by a heat flux meter. No backside insulation was used in this scenario. Due to the device's limited size, an extra handheld electric arc lighter (JL872, Ronxs) was used to ignite the samples. Laminate samples were sandwiched between two calcium silicate-based insulation frames with a central cavity of 70× 700 mm^2 to prevent edge burning and flame propagation to the edge and then into the back face of the tested sample. For works in chapters 4 and 5, a torch-fire-induced fire

impingement burn-through test was performed. Except for this time, a torch fire burner (φ22mm) with an outer fire temperature of around 1400℃ was used as a direct fire impingement source, which provide a much server direct fire damage and ablation attack through the impulsive torch fire. The distance between the tip of the burner and the surface of the laminate was kept at 7cm.

The thermographic method was used to monitor the backside temperature of the one-side heat/fire-damaged sample in a non-contact manner. For chapter 3, a thermal camera (Ti401 PRO, Fluke) was used. For works in chapters 4 and 5, the backside temperature was recorded with a thermographic infrared camera named AT31UZ from InfiRay, China. The measurement was done either at a specific time or until the sample demonstrated burn-through failure. The average temperature in the central area was extracted to plot the temperature rising versus the time profile.

3. Bilayer coating on fiberglass laminate substrate

3.1. Introduction

According to Chapter 1, a few efforts mentioned above demonstrated both flame retardancy and avoiding loss of mechanical properties after fire. The ceramification effect is a phenomenon in which a filled polymer composite undergoes a eutectic reaction to form a porous and compact ceramic layer, providing better resistance to fire properties in the lateral stage of fire hazards.[116] Hence, in this chapter, we proposed a bilayer coating strategy to impart fire-protective properties for FRPs in this work. By introducing an intumescent effect on the top layer to bring down fire hazards and introducing a certification-induced insulative layer for enhancing thermal insulative performance in the later stage of burning, the bilayer strategy was proposed to bring enhanced comprehensive fire-safe performance to FRPs compared to that by traditional single-layer fire protective coating method. First, the multiple fillers-based epoxy coating layers were applied on the laminate's surface. Then, the reaction to fire properties and fire insulation properties were screened by using CCT tests. In addition, the post-fire tensile properties after 120s fire damage were screened to demonstrate the capabilities of protective coatings. Finally, the fire protective mechanism was investigated by multiple measurements, and a theory was proposed, which explained the mechanism of this fire protective coating on the variation of fire safety and post-fire mechanical properties.

3.2. Samples preparation

3.2.1. Preparation of fiberglass composite

Ten layers of dry glass fabric were stacked upon each other by the notation $[(0/90)_2]_T$ for GFRP. Derakane 8084 was employed as a resin matrix for composites, which was mixed with initiator MEKP and promoter CoOct evenly and degassed right before the vacuum infusion process. The details of the laminate fabrication process can be found in our previous publication.[117] After completing the infusion process, the resin was cured at 99 ℃ for 6 hours. The cured laminates were inspected by ultrasounds (C-scan) to ensure they were free of large internal

porosities and delamination prior to machining. The average cured thickness of the laminates was 2.4mm and a volume ratio around 45%.

3.2.2. Preparation of bilayer coating on laminate substrate

The formulation of each coating layer can be seen in Table 3.1. For the formulation of the EG layer, the fillers and additives were first added into Gel coat resin and mechanically mixed evenly before adding the curing agent Hardener L and then curing at room temperature overnight. For the HGM layer, the reactive diluent GTE was used to improve the dispersion of silicate fiber and adjust viscosity. The silicate fillers Fireproof were first introduced into the mixture of Gel coat and GTE with some extra acetone. The as-prepared mixture is then ultrasonicated, mechanically mixed, heated to evaporate acetone, and finally added with the stoichiometrically equal Hardener L to cure at room temperature overnight. For the bilayer sample EG/HGM/GFRP, the HGM layer was first applied to the GFRP surface. Then, the outer EG layer was applied above the EG layer. All the coating layers were applied onto the substrate by a doctor blade-based film applicator (BGD209/4, Biuged) to get a dry film thickness of around 1mm each.

Table 3.1: Formulation table for samples with different coatings.

Sample name	EG (wt%)	HGM (wt%)	Fireproof (wt%)	IFR 36 (wt%)	Gel coat (wt%)	GTE (wt%)	Hardener (wt%)
GFRP	0	0	0	0	0	0	0
Pure Coat/GFRP	0	0	0	0	72.4	0	27.6
ITM/GFRP	15	0	5	10	50.7	0	19.3
ISU/GFRP	0	15	11.3	5	36.0	10.0	23.0
ITM/ISU/GFRP	There are two layers, each layer having the same formulation as mentioned above.						

3.3. Coating preparation

As shown in Figure 3.1, The outer coating layer, named the ITM layer, was mainly based on the physical intumescent mode flame retardant expandable EG[118], with APP-based and silicate fiber fillers as synergists. The middle layer, named the ISU layer, applied directly on the substrate of GFRP laminate, is mainly based on a silicon dioxide-based hollow microglass sphere (HGM) with APP and silicate fibers (Silicate) as synergists. The detailed mass ratio of each filler in two coating layers is shown in Figure 3.1. The mass ratio of EG and APP in the ITM layer was chosen

according to the experience gained from former work[119]. The weight ratio of HGM and Silicate was selected as 4:3 according to reference[116, 120] to achieve idea creamification capacity. The total weight ratios of ternary fillers-based two coating layers were explored and determined with additional consideration of suitable viscosity and good processability to find the final coating formulations, as shown in Table 3.1.

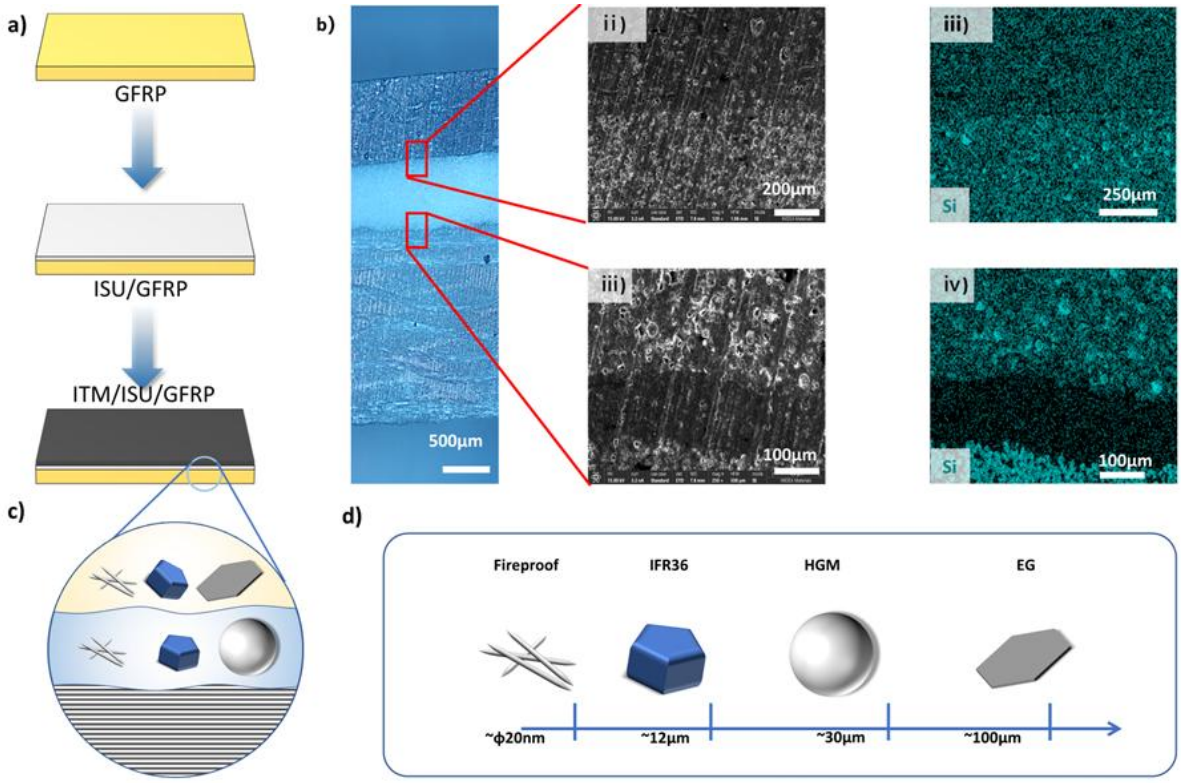

Figure 3.1: a), c) schematic illustration for the application of bilayer on the substrate of GFRP and b) optical image (i) for the cross-section of coated GFRP. SEM (ii) and EDS images (iii) for the boundary between the ITM layer and the ISU layer. SEM (v) and EDS images (vi) for the boundary between the ISU layer and GFRP matrix. d) Size comparison of different fillers used in the formulation.

As shown in the scheme of Figure 3.1 a), the ISU layer was first applied onto the substrate of GFRP laminate, while the ITM layer was then applied above the ISU layer. The fillers used to possess different types of shapes were introduced into the coating polymer matrix, as shown in Figure 3.2. According to the optical microscopy image in Figure 3.1 b), both two cured coating layers have a dry film thickness of nearly 1mm. EDS mapping also showed a clear boundary between each layer from the element distribution of silicon, validating the successful application of bilayer coating.

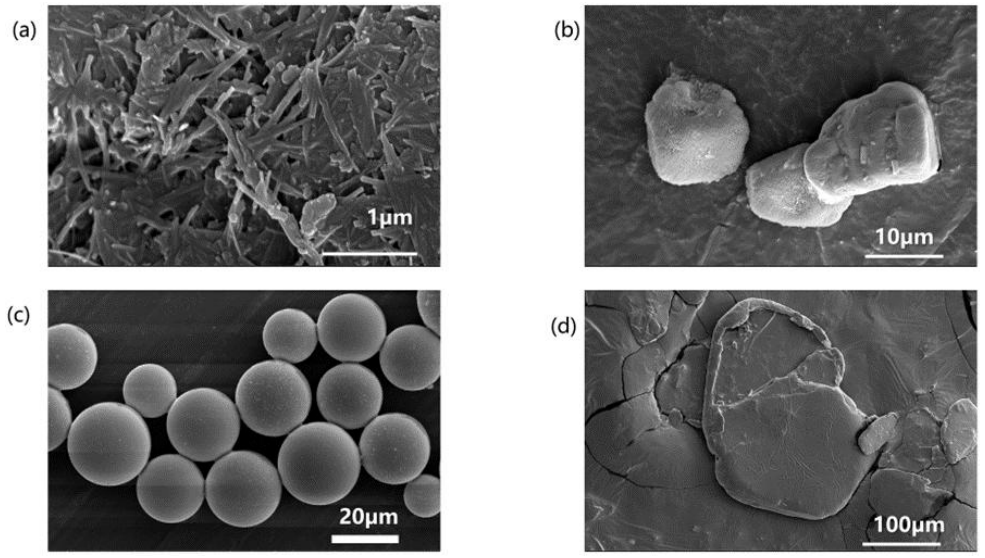

Figure 3.2: Morphology of filler for a) Fireproof, b) IFR 36, c) HGM, d) EG.

3.4. Combustion behavior of polymer composites

CCT tests were used to screen the fire reaction properties of composite panels under forced flaming scenarios. As shown in Figure 3.3 and Table 3.2, both laminates protected by either one or two coating layers significantly slow the combustion process, as exemplified by two times more combustion time than that of GFRP in Figure 3.3 (a).

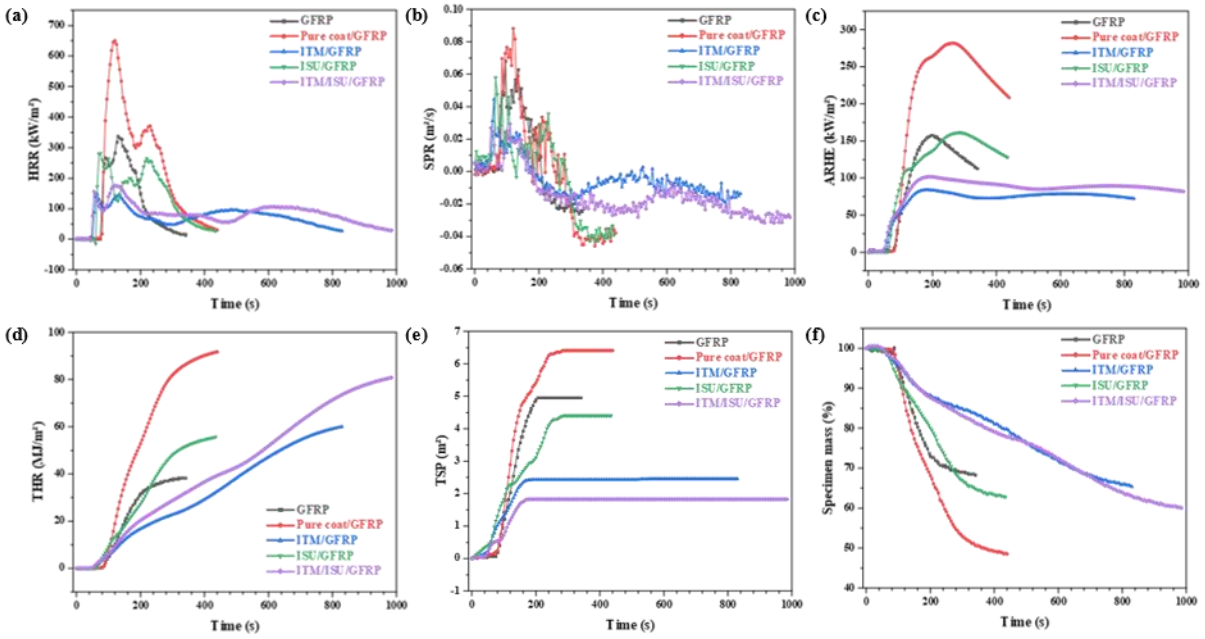

Figure 3.3: CCT result curves for (a) HRR, (b) SPR, (c) ARHE, (d) THR, (e) TSP, (f) mass versus time.

The 2mm thick pure gel coat (named Pure coat/GFRP) shows no PHRR lowering and prolonging burning time effects during the combustion process, which indicates pure coat resin even brings higher flammability if no FRs are added. Compared to heat release rate (HRR) curves of ITM/GFRP and ISU/GFRP with Pure Coat/GFRP, prolonged burning time indicates slower matrix decomposition and generation speed of combustible volatiles during the combustion process.

Table 3.2: CCT results for laminates with no coatings and three different coatings.

Samples	TTI (s)	PHRR (kW/m²)	THR (MJ/m²)	PSRR (m²/s)	TSP (m²)	MARHE (kW/m²)	Residue (wt%)
GFRP	73	349	38	0.07	4.9	157	68.3
Pure Coat/GFRP	77	669	92	0.09	6.2	282	48.5
ITM/GFRP	50	150	60	0.04	2.2	84	65.4
ISU/GFRP	60	286	56	0.06	3.9	161	60.0
ITM/ISU/ GFRP	46	179	81	0.03	1.7	102	60.0

It is noteworthy that by adding functional fillers into the coating layer, the PHRR and Maximum average rate of heat emission (MARHE) were significantly reduced by more than 50% and 35% for either laminate with one ITM layer or a bilayer of protective coatings, implying an impressive fire protective effect. In addition, in terms of the mass loss curve, the slope value decreased obviously for ITM/GFRP and ITM/ISU/GFRP, as shown in Figure 3.3 (f). In comparison, the slope value of Pure gel coat GFRP and ISU/GFRP showed nearly no difference compared to that of GFRP. The Pure coat GFRP showed a residue value of around 48%, which was mainly due to the increased mass ratio of combustible organic resin in the tested sample. The residue value of three coated samples was increased by more than 20% compared to that of Pure Coat/GFRP, indicating the strong char formation and reduction of gasification reaction due to interplay between the charring forming effect of APP[121, 122] and other fillers, as shown in Table 3.1.

Due to the incorporation of fillers lowering thermal stability parameters like DTGmax1, the t_{ig} of laminates with the coating layer was earlier than that of GFRP, as exemplified by the results and discussions of TGA tests in Table 3.3 and Figure 3.4. The THR increased as more organic layers were introduced onto the substrate, leading to a higher content of flammable organic substances. As shown in Figure 2 (e), the TSP of ITM/ISU/GFRP was lower by 65% and 22% compared to that of

GFRP and ITM/GFRP, indicating better fire safety in terms of smoke prevention for the bilayer coating system.

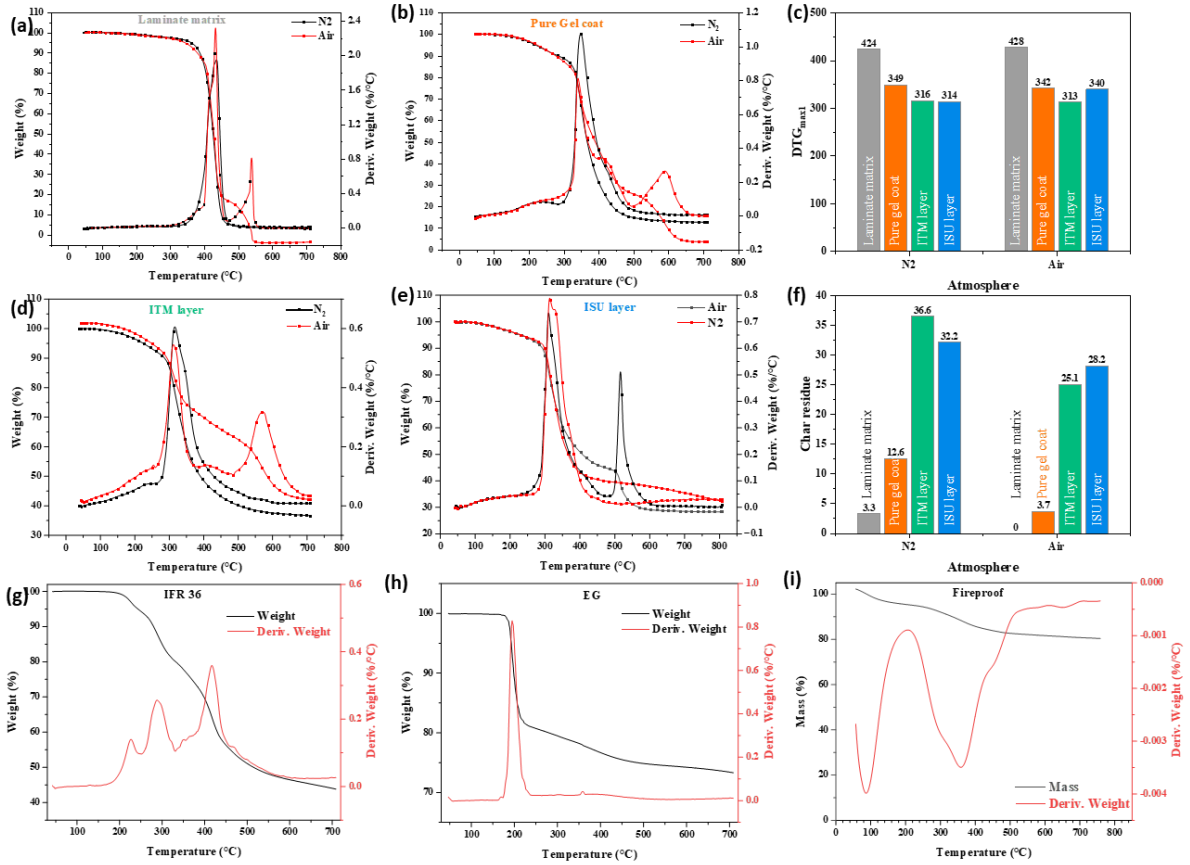

Figure 3.4: Mass loss curves for (a) Derakane resin, (b) Pure Gel coat layer, (d) ITM layer, (e) ISU layer under nitrogen and air. Bar chart for comparison of (c) DTGmax1 value and (f) Char residue value for samples in both nitrogen and air. TGA curves of g) IFR 36, h)EG, (i) Fireproof in the nitrogen atmosphere.

Table 3.3: Thermal stability data for laminate matrix, Pure Gel coat, ITM layer, and ISU layer.

Samples	$T_{5\%}$ (°C)		DTG_{max1} (%/°C)		DTG_{max2} (%/°C)		Residue (wt%)	
	N_2	Air	N_2	Air	N_2	Air	N_2	Air
Resin matrix	361	341	424	428	None	523	3.3	0
Pure Gel coat	219	220	349	342	None	592	12.6	3.7
ITM layer	224	206	316	313	None	547	36.6	25.1
ISU layer	232	228	314	310	None	516	32.2	28.2
Resin matrix	361	341	424	428	None	523	3.3	0

3.5. Heat/fire insulation of laminates

The in situ thermal imaging of backside temperature (T_B) for composite laminates was employed by using the cone heater in vertical mode as a heat resource, as shown in Figure 3.5 (a). The temperature distribution of the reverse face at different times is shown in Figure 3.5 (b). The fire quickly consumed all the flammable organic resin in sample GFRP, with burn-through failure occurring in less than 4 min for GFRP. The temperature spike for GFRP in Figure 3.5 (c) was due to the flame generation at the reverse face after burn-through failure.

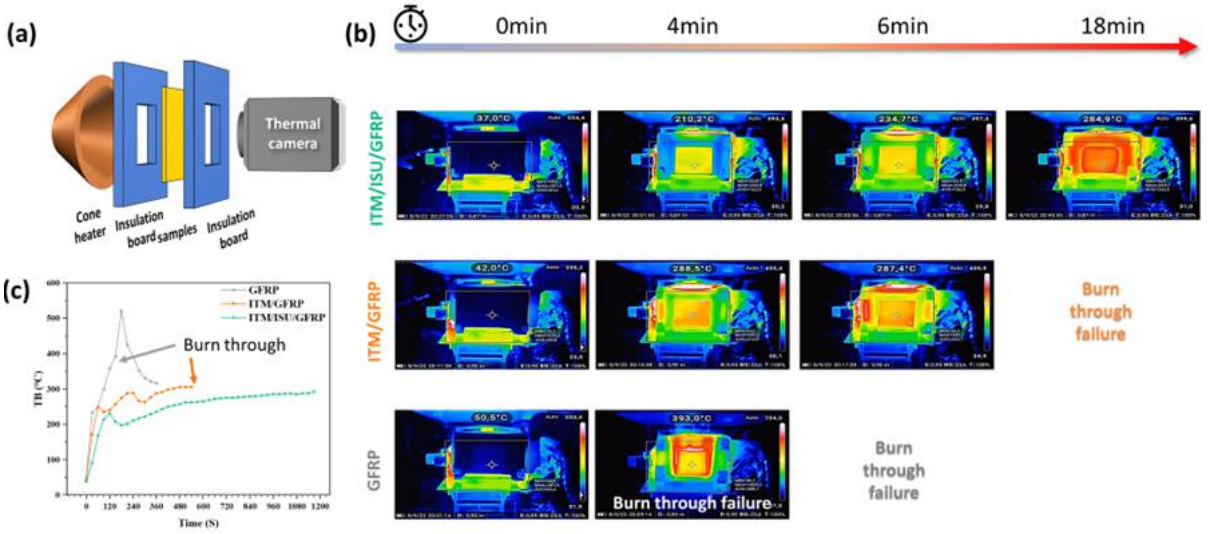

Figure 3.5: (a) Schematic illustration for the setup of TB detection by thermal camera. (b) Thermal images are taken at different times for GFRP, ITM/GFRP, and ITM/ISU/GFRP. (c) Center area temperature versus time curves for GFRP, ITM/GFRP, and ITM/ISU/GFRP.

The temperature profile of the central point of the reverse face showed that ITM/ISU/GFRP showed a value of 184℃ maximum difference compared to that of GFRP before burn-through failure. In terms of ITM/GFRP, the intumescent char layer provides good thermal insulation compared to GFRP without any coating protection. At the same time, the consistent irradiant heat provided by the cone heater still induced a burn-through failure after 9 mins of thermal attack, as shown in Figure 3.6. Nevertheless, the T_B of ITM/ISU/GFRP was kept lower than 300℃ for 20 minutes with no burn-through failure until the end of the test. The T_B of ITM/ISU/GFRP showed a maximum difference of almost 90℃ compared to that of ITM/GFRP. The digital photos of the tested sample after the vertical burning test are shown in Figure 3.6. In conclusion, the bilayer protective coating provided superior fire insulation properties in terms of T_B and avoidance of burn-through failure.

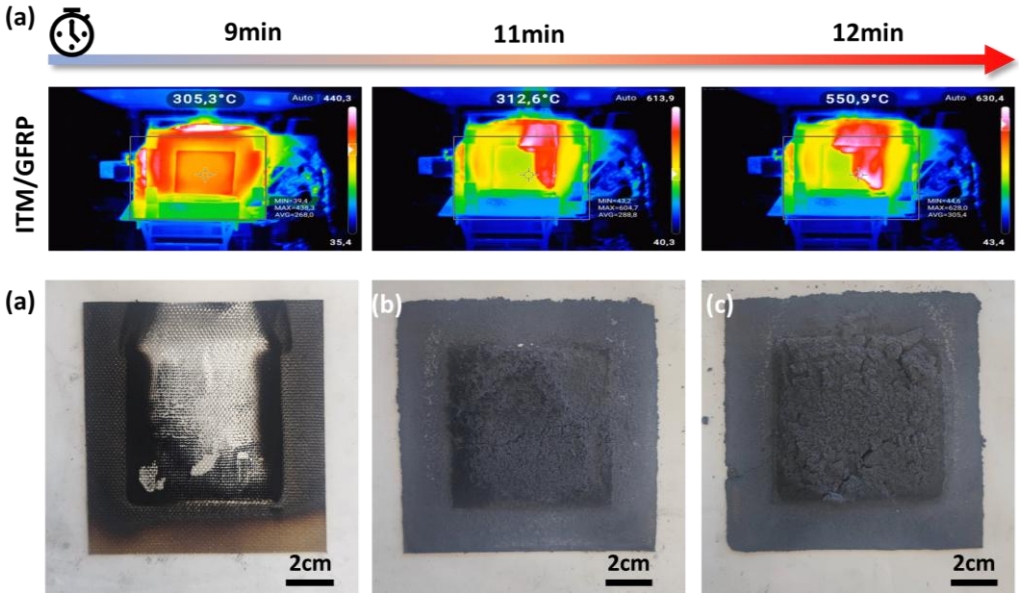

Figure 3.6: (a) Thermal image for ITM/GFRP after brun-through. Digital photos samples of GFRP a), ITM/GFRP b), ITM/ISU/GFRP c)after vertical burning tests.

3.6. Charring behavior and residue structure

The laminate with the coating layer after the CCT test displayed a sandwich char structure derived from the bilayer coatings in the schematic diagram Figure 3.8 (a). As shown in Figure 3.7, char from the ITM layer displayed a worm-like porous structure, providing typical insulation effects on heat and mass transfer at earlier stages[119, 123]. The middle char layer derived from the ISU layer after the CCT test was sampled for SEM measurement in Figure 3.8 b). The char morphology showed that the HGM sphere, which is linked by substances formed from reactions between silicate fiber and phosphorus agents, is distributed among the char residues. The EDS measurement in Figure 3.8 (c), (d) of ISU layer char demonstrated a large presence of oxygen and silicon elements, indicating the creamification process and formation of the inorganic insulating layer[116].

XRD and FTIR measurements were employed to explore the char composition and structure. As shown in Figure 3.8 (e), HGM is an amorphous inorganic filler that showed two broad peaks at 7° and 22°, which were still preserved inside of the two char residues due to its excellent thermal stability. After the combustion or thermal treatment of the ISU layer, the curves of char showed an obvious presence of HGM board peaks. In contrast to the XRD curves of fillers used in formulations, new peaks in char residues were generated after combustion or thermal treatment, implying a creamification reaction happening during combustion. The FTIR curves

of two char residues in Figure 3.8 (f) showed a strong absorption peak around 1050 cm^{-1} ascribed to the Si-O-Si asymmetric stretching vibration and another absorption peak around 450 cm^{-1} ascribed to the bending vibration of the O-Si-O bond. Due to the low content of two other inorganic fillers in the ISU layer, the new peaks for XRD and FTIR in both char residues were of relatively weak intensities, indicating the creamification process may only take place around the interface between the HGM surface and two inorganic fillers as like the interfacial charring from our previous work[124].

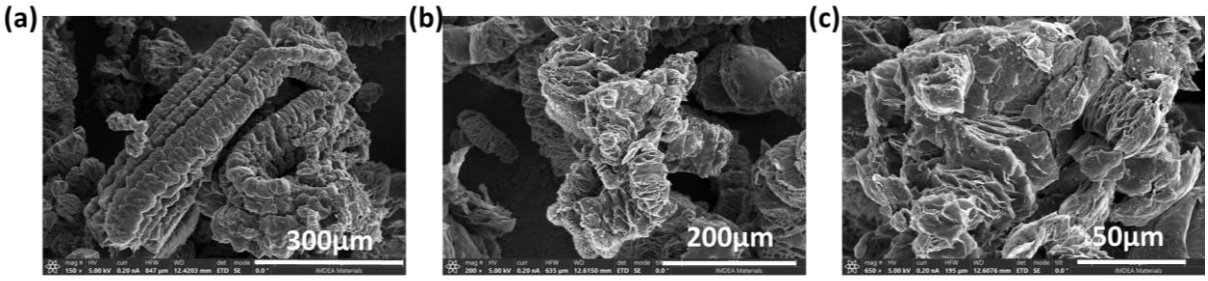

Figure 3.7: ITM layer derived char residue morphology by SEM test.

Based on the results and investigation above, a fire protective mechanism based on the synergistic effects of bilayers is proposed, as shown in Figure 3.8 (h). Under forced flaming conditions during fire hazard, composite panels with bilayer coatings first reacted to fire with the outer layer, turning into a highly porous structure by intumescent effects derived mainly from the interplay of fillers inside of top ITM layers. The EG in the top layer quickly reacted with volume expansion after being heated above the onset temperature. Shortly after the initiation of intumescent effects from the ITM layer, the interfacial creamification reactions were also happening between the surface of HGM and silicate fillers with the help of phosphorus fillers, forming a compact and insulative char structure inside of the ISU layer. The highly porous structure derived from the ITM layer limited thermal and mass transfer, thereby lowering PHRR and TSP and slowing matrix decomposition. However, a single ITM layer-based coating is not enough to limit thermal transfer at a higher temperature range and improve fire resistance properties, which are vital for FRPs. The compact char structure derived from the ISU coating layer showed a synergistic effect with the ITM layer by enhancing thermal insulation properties and avoiding the burn-through effect, which provides further protective capabilities against fire damage.

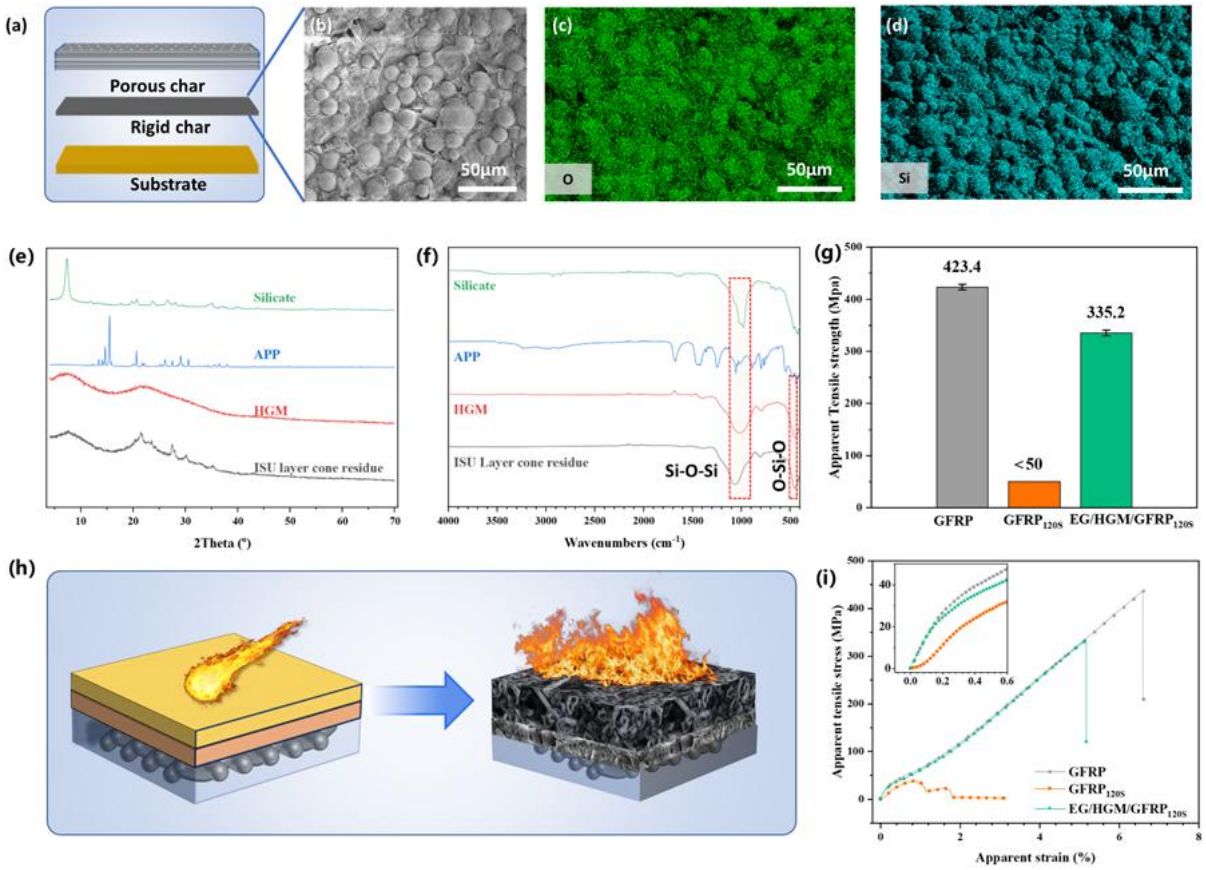

Figure 3.8: (a) schematic illustration of the sandwich structure of the char after the test. (b) SEM image and (c), (d) EDS images of ISU layer char after CCT. (e) XRD curves and (f) FTIR curves for fillers and char residues after the CCT test. (g) bar chart for tensile strength of GFRP, GFRP120s, and ITM/ISU/GFRP120s. (h) schematic illustration of the proposed fire protective mechanism. (i) apparent strain versus apparent tensile stress curves.

3.7. Post-fire in-plane axial tensile strength of composites

The *postmortem* mechanical properties were employed to measure the mechanical properties of FRPS after fire damage. As shown in Figure 3.8 (g), (i), for GFRP without any protective coating, the 120s heat flux and fire damage brought a hugely detrimental effect on the laminates, resulting in severe delamination between glass fiber layers as well as nearly full consumption of flammable organic resin. The pristine laminates, after the 120s heat attack, leave only non-combustible glass fabric due to rapid decomposition, gasification, and burning of volatiles evolved from resin matrix. Therefore, the tensile behavior of the $GFRP_{120s}$ displayed very similar behavior to that of a dry fabric exhibiting nonlinear deformations caused by yarn undulations during strain straightening. Under the tensile stress, each glass fabric played an individual role without collectively resisting deformation, leaving very low and highly scattered tensile strength

results for $GFRP_{120s}$ with a maximum tensile strength of less than 50 MPa. Compared to the tensile strength of pristine laminate, less than 12% of that can be retained after 120s of fire damage, which exemplifies the vulnerability of FRPs to fire without any protection.

The bilayer-coated laminate formed a rigid char residue with good adhesion derived from the ISU layer. The bilayer-coated laminate, after damage, preserved around 79% of the original apparent tensile strength, as shown in Figure 3.8 (g). In addition, the rigid char residue layer still maintained a good adhesion even under high tensile stress, as shown in Figure S8, indicating the capability of thermal insulation effects under structural loading. As shown in the inset of Figure 3.8 (i), the apparent stress-extension curve showed a nonlinear behavior in the traditional elastic region, which differs from the GFRP without fire damage. This may be attributed to the effects of fire protective coating. In this way, the $ITM/ISU/GFRP_{120s}$ can be treated as a non-symmetric sample with gradient strength in the through-the-thickness direction caused by the degradation and, therefore, showing nonlinear tensile behavior. The drastic strength difference between pristine laminates and protected laminates after 120s of fire damage indicated a highly protective capability derived from the synergistic effect of bilayer coating during the combustion process.

3.8. Conclusions

In this work, a bilayer strategy for fire-protective coating was designed and prepared for FRCs. An intumescent ITM coating layer with a ceramifiable ISU coating layer was deposited on the substrate of GFRP composite laminates. The CCT test showed this bilayer imparted a 50% reduction in PHRR and a 65% reduction of TSP compared to that of GFRP, indicating a lower contribution to fire propagation and poisoning effects under fire hazards. In addition, the postmortem tensile test after fire damage indicated strong protective effects on strength perseverance during fire hazards with good adhesion of protective layer even under high structural loadings. The investigations of char residue morphology and compositions by several tests indicated a strong protective role of the condensing phase contributed by the bilayer during CCT tests, which contributed to the superior post-fire mechanical properties. This bilayer strategy provides a novel perspective for fire safety engineering and the design of polymer composites aiming for the increasingly expanding application of structural loadings among several sectors.

4. Cobalt-based nanohybrid additive in fiberglass polymer matrix

4.1. Introduction

By controlling polymer chain length and branching, APP has been used as a popular candidate for tailoring the fire safety of a wide variety of thermoplastics and thermosets either by coating or physically blending compared with other P-containing flame retardants.[125, 126] However, APP generally needs to be improved either by surface modifications[127] and/or by blending with other synergists to improve its matrix compatibility, water solubility, and, most importantly, efficacy.

Metal-organic framework (MOF) and their derived nanohybrids have been proposed to enhance fire retardancy and smoke suppression through catalytic oxidation and char formations.[128, 129] The versatile compositions and abundant structures of MOF-derivatives offer great design flexibility for flame-retarded epoxy resin. Some works have been reported on short fiber-filled polymer composites. Lin et al.[130] introduced cobalt-based MOFs on the surface of short carbon fibers and introduced them into APP-filled epoxy resins. With 1wt% of novel filler substituting APP, the PHRR and THR were reduced by 30% and 16% for epoxy-based composites. Unnikrishnan et al.[131] melt blended Aluminum MOFs with short glass fiber in a polyamide matrix. With 10wt% of MOFs, the peak HRR was decreased by 10% in MCC tests. However, for GFRPs, especially continuous fiber-reinforced polymer composite, the mechanical integrity is of the same importance as flame retardancy, as suggested in chapter 1. Nevertheless, few previous efforts have demonstrated the incorporation of MOF-based derivates in epoxy resin-based polymer composites and evaluated their influence on fire retardants' efficacy and mechanical properties to the best of our knowledge.

ATH, as a widely used synthetic mineral FRs has shown potential as a host material for the synthesis of multi-metal-based nanohybrid for flame retardant coating or additive applications.[132, 133] Based on the afore mentioned modification of polymer matrix approaches for the development of flame retardant FRPs, in this chapter, we designed and synthesized a novel cobalt-based nanohybrid (CNH) by using a facile approach to in-situ grow cobalt-based MOF particles on the slab of micro-sized ATH. After verifying the successful synthesis of CNH, this new filler

was used as a novel, high-performance synergist with APP based FRs for filled biobased epoxy resin and GFRCs. The efficacy of FRs was screened in epoxy resin to select the optimized formulation for fabricating GFRPs. The flame-retardant mechanisms were investigated and proposed to explain the different behaviors between unreinforced resin composite and GFRCs. Finally, FRs' influence on composites' mechanical properties was investigated to explore the influence of nanohybrid on the mechanical properties.

4.2. Samples preparation

4.2.1. Synthesis of cobalt-based nanohybrid additive

As shown in Figure 4.1, a fully dissolved 2-MIM/water with a concentration of 0.224g/ml solution was prepared by magnetic stirring. After that, ATH was dispersed into a 2-MIM/ DI water solution under an ultrasonic probe (500W) with an ice bath to form a suspension. Meanwhile, Cobalt salt was fully dissolved in DI water with a concentration of 0.12g/ml by magnetic stirring. Then, the Cobalt salt/water solution was poured into ATH/2-MIM/water suspension under continuous ultrasonic probe dispersing for 10 mins. After that, the suspension was centrifuged several times under 3000 RPM for 5min, washed with methanol, and finally put in a vacuum oven at 70℃ overnight. The resulting solid purple product was crushed into a fine powder before use.

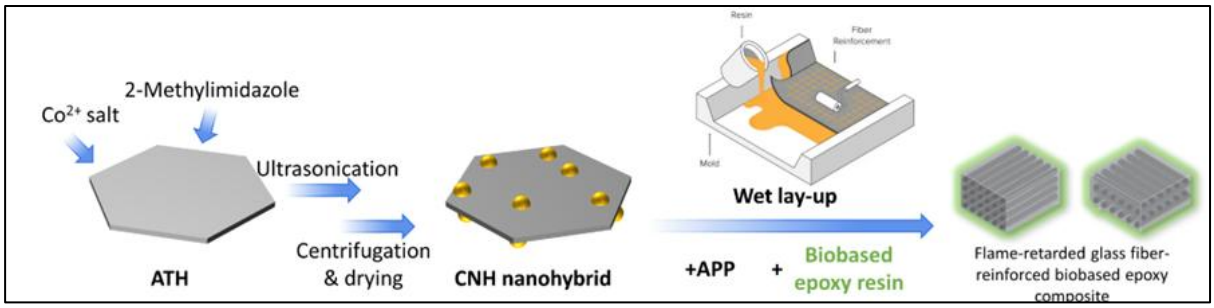

Figure 4.1: Facile synthesize CNH and its use in the fabrication of GFRP

4.2.2. Preparation of epoxy resin with APP and CNH

Different weight ratios of APP and CNH were added into the epoxy under 1300RPM for 10 minutes using an overhead stirrer with high-shear disperser blades. After that, a stoichiometric amount of amine hardener was added and mixed for at least 3 minutes. The resulting viscous liquid mixture was degassed in

a vacuum chamber at -0.9 bar for 10 minutes before being transferred and poured into a silicon resin-based flexible mold and heat-cured according to the temperature program recommended by the supplier in a conventional oven. Six FRs filled with epoxy resin were prepared: Pure EP, 20APP/EP,14APP-6CNH/EP,10APP/EP, 7APP-3CNH/EP, 5APP-5CNH/EP according to the details shown in Table 4.1.

Table 4.1: Formulations of epoxy resin with different ratios of FRs and their LOI value and UL 94 rating (3.2mm)

Sample	APP (wt%)	CNH (wt%)	Epoxy (wt%)	Hardener (wt%)	LOI (%)	UL 94
Pure EP	0	0	79.4	20.6	21.7	NR
20APP/EP	20	0	63.5	16.5	24.2	NR
14APP-6CNH/EP	14	6	63.5	16.5	39.7	V0
10APP/EP	10	0	71.5	18.5	22.9	NR
7APP-3CNHEP	7	3	71.5	18.5	28.9	V2
5APP-5CNH/EP	5	5	71.5	18.5	25.1	NR

4.2.3. Preparation of GFRP with APP and CNH

GFRP laminates were prepared using hand layup methods. The glass fiber-based fabric was applied and impregnated using the liquid mixture and hand rollers. Ten layers of glass fiber woven fabric were stacked $[0°/90°]_{5s}$. The stacked impregnated fabrics were then transferred to a hot press machine to cure at around 1.3 bar following a temperature program of 50℃ for three hours and 100℃ for three hours to obtain a quasi-isotropic laminate. The laminate was inspected for minimal defects by a nondestructive ultrasonic scan. The resulting laminate has a thickness of around 2.3mm and a fiber weight ratio of around 63% and volume ratio of around 47%. Finally, the laminates were machined to get the desired dimension testing. Three laminates were prepared: Pristine GFRP, 20APP/GFRP and 14APP-6CNH/GFRP.

4.3. Chemical composition and structure of CNH

The XRD test was employed to screen the crystal structure of CNH. As shown in Figure 4.2 (a), the cobalt-based MOF showed peaks similar to those of our previous works. The ATH filler displayed a distinctive high-intensity peak around 20°. After the in-situ growth of cobalt-based MOF on the slab of ATH fillers, the peaks around 7.4°, 10.4°, 12.7°, and 18° were present in both cobalt-based MOF and newly

synthesized CNH. In addition, the strong intensity of the peak at 18° peak in the CNH sample indicates that ATH is the primary component in the hybrid fillers.

The morphology and composition of CNH were screened by SEM and EDS. Figure 4.2b reveals the morphology of the newly formed micronized grain on the slab of ATH fillers, which is distinct from the pristine ATH. By comparing the EDS images of three different elements in Figure 4.2 (c), it is evident that the grown grain on the ATH slab consists of Cobalt elements. In conclusion, the successful synthesis of the MOF and ATH hybrid CNH can be verified from the test results mentioned above.

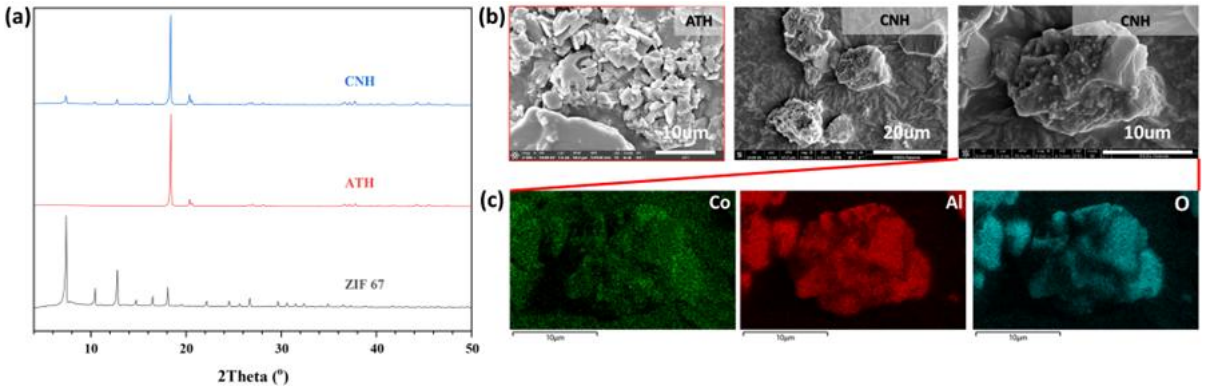

Figure 4.2: XRD curves, SEM, and EDS images of ATH and CNH.

4.4. Flammability of FR-filled biobased epoxy resin

The flammability of FR-filled biobased epoxy resin is measured by small fire tests such as the LOI and the UL 94 test. As mentioned in the previous section, the low charring pure epoxy resin exhibited a low LOI value of 21.7 and an NR rating in the vertical burning test, as shown in Table 4.1. The introduction of APP solely into the epoxy resin only slightly increased the LOI value to less than 25% and showed no improvement in the vertical burning performance, even with a filler content of 20wt%. This indicates that APP exhibited poor efficiency in this kind of biobased epoxy resin, which has low viscosity and low charring capabilities.

When the total amount of FR fillers was set as 10wt%, the optimized ratio between APP and CNH was explored. After replacing parts of APP with CNH synergists, the LOI value increased by 33% when the ratio of APP to CNH was 7:3. However, when the ratio of CNH was further increased, the LOI value decreased, indicating that insufficient APP will retard the intumescent effects. Hence, an optimized ratio of 7:3 between APP and CNH was found. Due to the V-0 rating not being reached with 10wt% of total loading, a higher 20wt% of total loading was tested, and it was

found that the LOI value increased by more than 80% to 39.7% with a V-0 rating for vertical burning tests. Hence, this formulation was selected for the further preparation of glass fiber-reinforced biobased epoxy composites.

4.5. Combustion behavior of flame retarded biobased epoxy resin

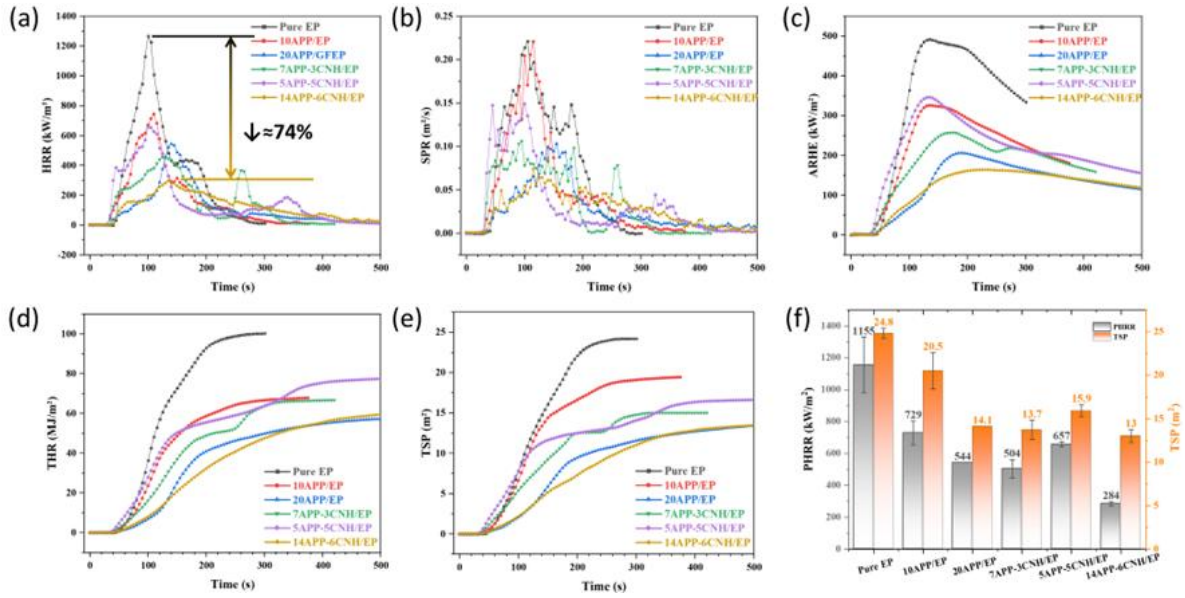

Figure 4.3: CCT results curve for heat release (a, c, d), smoke release (b, e), and bar chart (f) for comparing the PHRR and TSP values of Pure EP, 10APP/EP, 7APP-3CNH/EP, 5APP-5CNH/EP, 20APP/EP, and 14APP-6CNH/EP.

The influence of the filler ratio and content of APP and CNH on the heat and smoke release behavior of biobased epoxy resin was evaluated using a Cone calorimeter, as shown in Figure 4.3 and Table 4.2. As can be seen in Figure 4.3, the addition of APP alone reduced the PHRR and THR by more than 40% and 32%, respectively. In terms of smoke release, 10APP/EP showed minimal change in the peak smoke release rate (PSRR) but decreased the total smoke production (TSR) by 19.8%. The introduction of APP didn't drastically change the shape of the HRR curve compared with Pure EP. Both samples displayed a thermally thin type of heat release characterized by a main sharp peak, which can be attributed to the failed formation of protective char during the combustion process.[134]

Nevertheless, the introduction of cobalt-containing CNH led to significant changes in the heat release behavior, as observed in Figure 4.3 (a). Both CNH-containing samples showed two distinct peaks during the heat release profile and an even lower PHRR value compared to that of 20APP/EP. The maximum average rate of

heat emission (MARHE) of CNH-containing samples was lowered too. The formation of a two-peak heat release profile is usually derived from the formation of protective, compact char during the first peak range. During the early stage of combustion, the char formation hinders the heat and mass transfer and prolongs the bulk thermal decomposition, resulting in a lower PHRR. However, due to the thermal oxidation of char and continuous heat conduction from the cone heater, the char protection eventually fails, leading to a second heat release peak.

Table 4.2: CCT results of Pure GFRP, 20APP/GFRP, 14APP-6CNH/GFRP, 10APP/EP, 7APP-3CNH/EP, 5APP-5CNH/EP, Pure GFRP, 20APP/GFRP and 14APP-6CNH/GFRP

Sample	t_{ig} (s)	PHRR (kW/m^2)	THR (MJ/m^2)	TSR (m^2/m^2)	MARHE (kW/m^2)	Avg-EHC (MJ/m^2)
Pure EP	42	1266	100.2	24.2	491.4	25.0
20APP/EP	35	544	58.9	14.1	206.1	19.1
14APP-6CNH/EP	37	297	63.8	13.7	163.9	21.3
10APP/EP	30	743	67.7	19.4	325.8	21.7
7APP-3CNH/EP	32	456	66.6	15.0	257.2	19.3
5APP-5CNH/EP	32	659	78.1	16.7	346.4	24.1
Pure GFRP	41	484	31.3	7.8	230	24.5
20APP/GFRP	41	385	35.1	9.0	214	22.3
14APP-6CNH/GFRP	27	309	26.6	7.9	184	21.7

MOF, especially nickel-based MOF, has been suggested to contribute to the catalytic charring effect in the flame retarded polymeric system by several reviews[128, 129]. With this biobased epoxy resin possessing every limited charring capability by itself, the decomposition products of APP acted as an acid source, and the blowing source showed limited intumescent effects due to the lack of a carbonizing source. After adding CNH as a synergist, CNH was suggested to demonstrate a strong charring-promoting effect, producing more char formation for the intumescent swelling actions. With the release of gas source NH3 into the gas phase, the binary FRs flame retarded epoxy resin system showed a highly intumescent effect, as shown in Figure 4.7.

It is noteworthy that a lower ratio of APP in 5APP-5CNH/EP would bring higher PHRR, THR, and TSP values compared to that of 7APP-3CNH/EP, as shown in Figure 4.2 (f). It suggests that a lower amount of phosphorus acid source leads to an epoxy composite with lower charring capabilities. Since APP primarily functioned as an acid source and gas source in the intumescent system, having too

low of an APP ratio with an overloaded content of CNH synergists would lead to poor intumescent effects, thereby compromising fire protective effects. Hence, an optimized ratio of 7:3 between APP and CNH was determined when formulating FRs for biobased epoxy resin.

4.6. Combustion behavior of flame retarded GFRP

The burning behavior of the prepared laminates was evaluated under forced flaming conditions by CCT tests. As can be seen in Table 4.2 and Figure 4.4, the Pure GFRP exhibited a much lower heat and smoke release and a higher residue value compared to the pure biobased epoxy resin, which can be attributed to the dilution effects of the noncombustible glass fiber with a weight ratio of more than 60 wt%.[135] After the introduction of APP fillers, the PHRR value was reduced by 20%, a much lower reduction compared to the 40 % reduction in PHRR when only 10 wt% APP was added to the pure resin system.

Surprisingly, the THR and TSR values of 20APP/GFRP were higher than those of Pure GFRP. After adding CNH synergists to the laminates, the 14APP-6CNH/GFRP exhibited a smaller reduction in PHRR of 36% and in MARHE of 20%. What's more, the THR was lowered by 15%, and the TSR showed a similar value to that of Pure GFRP. The t_{ig} value was extended to 27s while the DTG_{max} value of 14APP-6CNH/GFRP was similar to that of 20APP/GFRP, as shown in Figure 4.4.

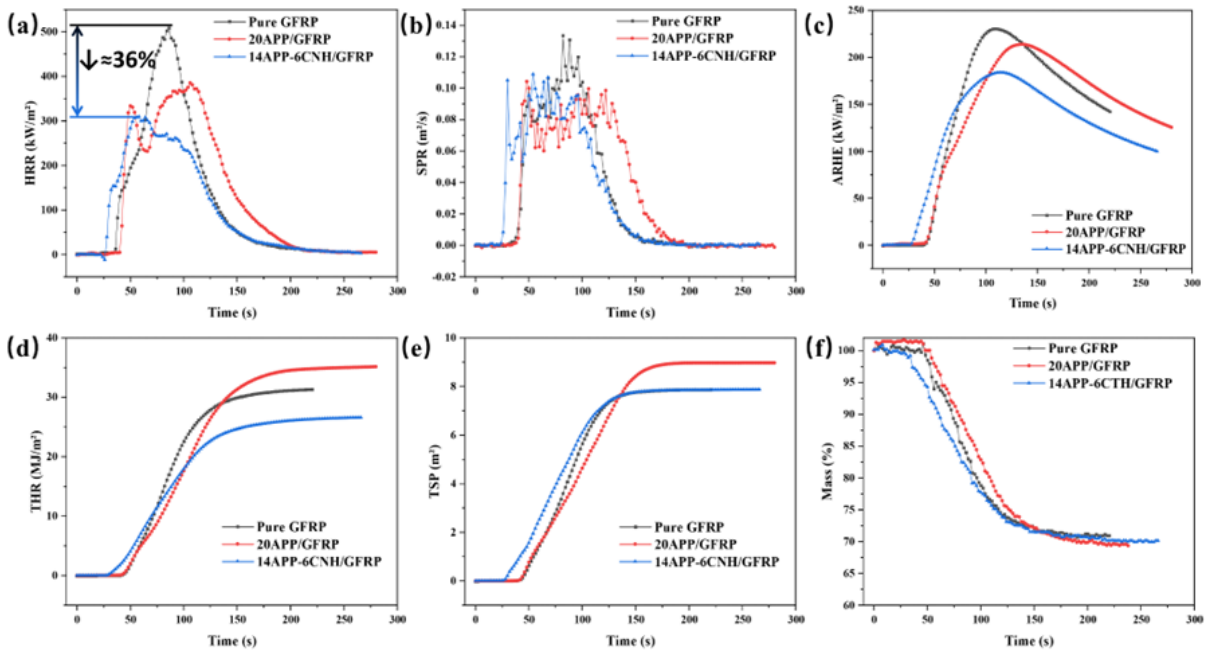

Figure 4.4: CCT results curve for heat release (a, c, d), smoke release (b, e), and mass loss (f) of Pure GFRP, 20APP/GFRP, and 14APP-6CNH/GFRP.

4.7. Thermal stability of FR-filled biobased epoxy resin

TGA investigated the thermal stability of CNH synergists and the FR-filled epoxy resin to understand the fire behavior. As shown in Table 4.3 and Figure 4.5, the Pure EP exemplified a DTG_{max1} at around 340℃ with a low residue value of around 3.7%, indicating the low charring capability of this biobased epoxy resin. After adding APP and CNH synergists, the residue value significantly increased compared to that of Pure EP, primarily due to the charring promotion provided by the phosphoric acid of APP. However, the DTG_{max} value decreased in both 20APP/EP and 14APP-6CNH/EP, which may be derived from the low thermal stability and the catalytic promotion of thermal decomposition of APP and CNH.

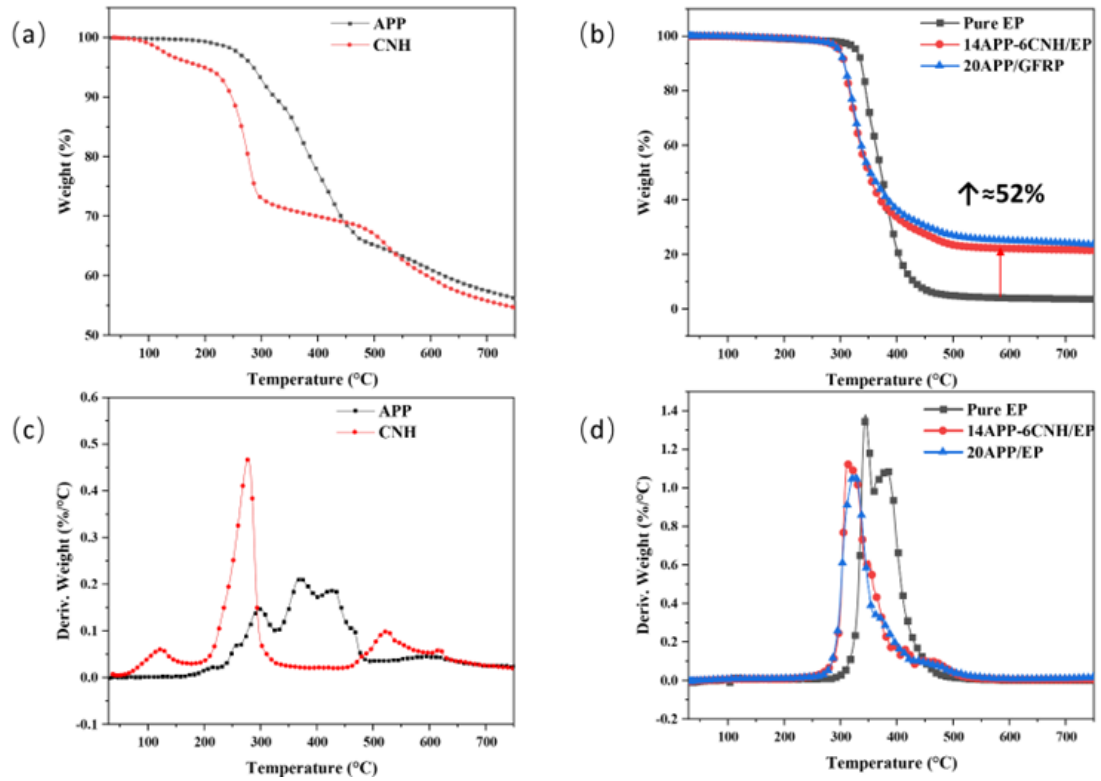

Figure 4.5: TGA and DTG curves of CNH and APP in air and N_2. TGA and DTG curves of Pure EP, 14APP-6CNH/EP, 20APP/EP in N_2.

Based on the assumption that no synergistic chemical reactions occurred between the FRs and the polymer matrix, the residue values of the 20APP/EP and 14APP-6CNH/EP were calculated to be 14.2% and 14.1%, respectively. The catalytic function of cobalt can be demonstrated by an increase of more than 50% in the measured residue value compared to the calculated values, suggesting the addition of APP and CNH induced a synergistic reaction with the resin matrix.

Table 4.3: Measured thermal stability values of APP, NMH, Pure EP, 20APP/EP, and 14APP-6NMH/EP.

Sample	$T_{5\%}$ (℃)	DTG_{max1} (℃)	Residue (wt%)
APP	285	298	56.0
CNH	205	278	54.6
Pure EP	327	343	3.7
20APP/EP	297	322	23.3

4.8. Transfers of FRs behavior from resin to composite

The char residues after the Cone test for different samples are displayed in Figure 4.6. Due to the very limited charring capabilities of pure biobased epoxy resin, there was almost no char residue, and the resin was consumed almost entirely during combustion. When 10 wt% APP was introduced into epoxy resin. The resin system exhibited an intermediate intumescent phenomenon with insufficient char integrity after the CCT test in Figure 4.7(c). However, after incorporating the CNH synergist, the char expansion was significantly enhanced, as observed in the cross-section digital images. When comparing the influence of different ratios of APP to CNH on the combustion behavior of resin, the 7APP-3CNH/EP exhibited a more porous inner structure compared to that of 5APP-5CNH/EP, as demonstrated in Figure 4.7 (a, b). The porous structure of the char layer plays a positive role in limiting the mass transfer of combustible volatiles and thermal feedback from the flaming zone into the underlying virgin zone.[136] Hence, the optimized ratio between APP and CNH can provide better fireproofing performance during forced flaming combustion, as shown in Table 4.2.

When glass fiber reinforcement was introduced into the resin matrix, significant changes were shown in combustion behavior and CCT results. Ideally, glass fiber, an incombustible substance, should hardly influence the chemical aspects of the combustion process. While a reduction of 74% in PHRR was observed when glass fiber was not introduced into the resin, the efficiency decreased to only a 36% reduction in PHRR for the laminates. In addition, a sharp contrast was observed in the char macro morphology between the bulky resin and polymer composites. The resin with FRs exhibited a distinct intumescent phenomenon, while the laminates after cone tests showed limited charring with a very limited intumescent phenomenon.

The change in combustion behavior from Cone results in this study was proposed to be partly attributed to the incorporation of glass fiber reinforcement, as shown in the schematic illustration of Figure 4.6 (b). The thermal expansion difference

between the glass fiber and polymer matrix tends to induce delamination, as seen by some research.[41, 137] Meanwhile, the dense, high-weight ratio of glass fabric may create a barrier effect that influences the macro thermal decomposition process, thereby limiting the reach of a critical mass of flammable, volatile concentrations. The interplay of the two abovementioned possible factors contributed to the complex ignition time variation among the flame retarded epoxy system with and without glass fiber with other parameters such as fire test set-up etc., as suggested by former reports [115].

As can be seen in Figure 4.6 (b) and Figure 4.7, the intumescent phenomenon is significantly retarded in the polymer composites of both 20APP/GFRP and 14APP-6CNH/GFRP. This can be attributed to two factors associated with glass fabric. First, the large surface area of glass fiber inhibits the formation of a compact insulation char layer. Second, the rigid and dense fiber layer restricts the physical expansion of the char layer induced by the release of nonflammable gas. The contribution of fiber reinforcement also weakens the reduction of THR and TSP. These two physiochemical factors retarded the intumescent behavior of the FRs in the GFRCs, thereby demonstrating a transfer of FRs behavior from the resin to the polymer composites, as also suggested by former researchers [72, 89, 138].

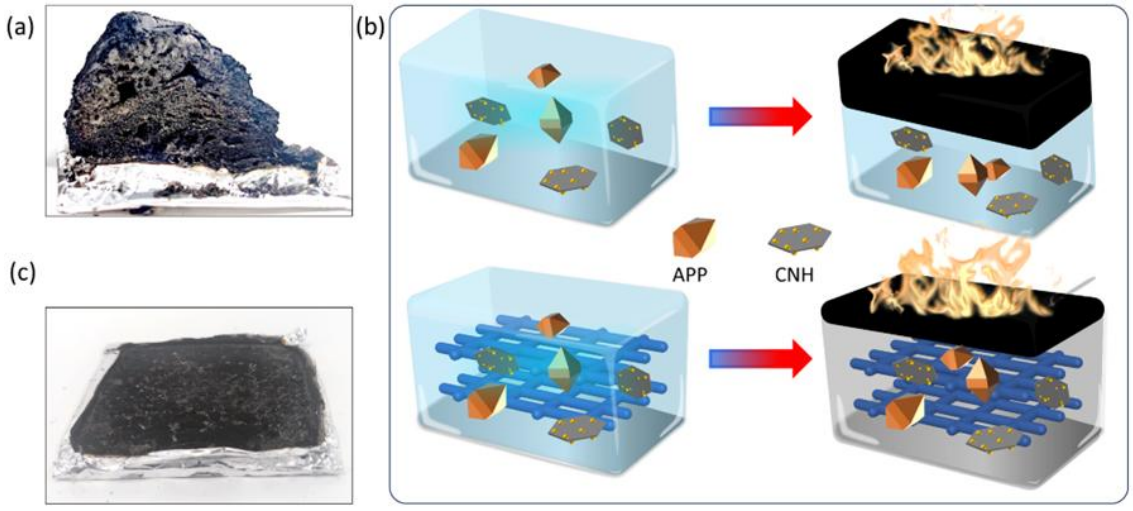

Figure 4.6: Cross-section digital images of 7APP-3CNH/EP (a) after cutting the char residue in half. Scheme illustration demonstrating the difference in charring behavior transfer from resin to GFRCs. (b) Digital images of char after CCT tests of 14APP-6CNH/GFRP (c).

In terms of composite laminates, the two flame retarded formulations showed almost close residue mass value at the end of the Cone test in Figure 3 (f) compared to Pure GFRP. Besides, the value of average effective heat of combustion (Avg-EHC) in Table 4.2 decreased by around 10% for flame retarded formulation

compared to that of Pure GFRP, which indicated a gas phase action. In addition, the release of ammonia may contribute to fuel dilution and heat removal when adding more than 10wt% of APP flame retardants. Hence, it is possible that this binary FRs formulation may also display a more prominent gas phase flame retardant mechanism in fiberglass composite compared to that of resin with only FRs. By comparing the digital images of Figure 4.7, the sample named 14APP-6CNH showed its glass fiber's surface blanked by char residue while Pure GFRP nearly burned out all resin, leaving a visible large area of dry glass fabric after combustion. These indicated that this APP-CNH composition also demonstrated some condensed phased action in terms of flame retardancy. Hence, the change of matrix system from epoxy resin to fiberglass composite may transfer the APP-CNH binary flame retardants system from a condensed phase-dominated intumescent mechanism into a bi-phase flame-retarding action.

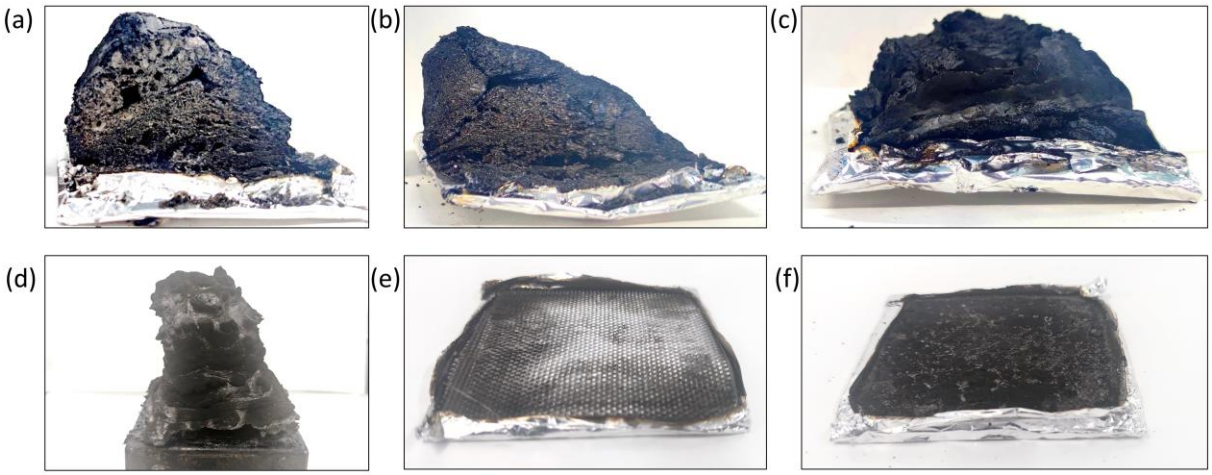

Figure 4.7: Cross-section digital images of 7APP-3CNH/EP (a) 5APP-5CNH/EP (b) after cutting the char residue in half. Digital images of char after CCT tests of 10APP/EP (c), 14APP/6CNH/EP (d), Pure GFRP (e) and 14APP-6CNH/GFEP (f).

4.9. In-plane axial tensile properties of Flame retarded GFRP

Table 4.4: Tensile test results of 20APP/GFEP and 14APP-6CNH/GFRP

Sample	Tensile modulus (GPa)	Tensile strength (MPa)	Elongation at break (%)
20APP/GFRP	20.7±0.7	284±11	1.9±0.1
14APP-6CNH/GFRP	20.3±0.7	354±11	2.4±0.2

The influence of FR fillers on the mechanical properties and stress transfer of the composite coupons was investigated under axial tensile loading on coupons extracted from the manufactured laminates, as observed in the side section of

digital photos of the two failed coupons in Figure 4.8 (b, e). The fracture of the 20APP/GFRP material, Figure 4.8 (b), is more localized around failure with reduced delamination between the piles. However, the damage is observed far from the fracture surface for the 14APP-6CNH/GFRP material in Figure 4.8 (e). This fact indicates a global redistribution mechanism opposing the local one observed in the 20APP/GFRP laminate.

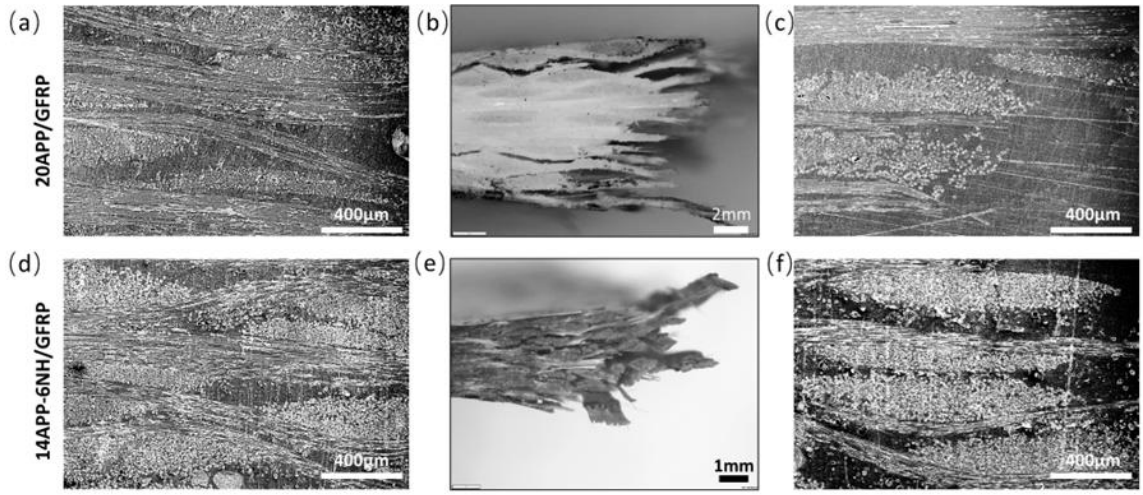

Figure 4.8: SEM images from locations away from the failed area of 20APP/GFRP (a) and 14APP-6CNH/GFRP (d). Optical microscope images for the side view of failed coupons of 20APP/GFRP (b) and 14APP-6CNH/GFRP (e). SEM images from locations close to the failed area of 20APP/GFRP (c) and 14APP-6CNH/GFRP (f). (h) Bar chart for comparing Young's modulus and tensile strength of 20APP/GFRP and 14APP-6CNH/GFRP.

To illustrate such mechanisms, metallography images of the failed coupons were captured by SEM from locations both close to and away from the failure area. Compared to 14APP-6CNH/GFRP, 20APP/GFRP exhibited less delamination and a more concentrated failure area, as shown in Figure 4.8 (a, c). On the other hand, 14APP-6CNH/GFRP exhibited a more globalized failure, indicating a failure process in which energy was dissipated between ply layers during the failure process, as demonstrated in Figure 4.8 (d, f). The measured tensile test results in Table 4.4 (modulus and strength) further supported that 14APP-6CNH/GFRP possessed greater tensile strength and elongation at break compared to 20APP/GFRP. In conclusion, the CNH resulted in additional improvement in mechanical properties by reducing the APP content and enhancing stress transfer during failure, leading to higher tensile properties.

4.10. Fire insulation properties

The ability to resist heat/fire transfer through the thickness direction is measured by direct torch fire impingement of 5 minutes for 3 types of laminates. The sudden jump is due to the switch of lenses in the thermal camera. As can be seen from Figure 4.9 (a, b, c), the digital photos of the Pure GFRP after torch fire tested showed a complete burnout of organic substances, leaving only dry fiber around the central area. In addition, due to the relatively low melting point of glass fabric, few surface glass fiber layers around the central area were melted upon consistent fire attacks. In contrast, the 20APP/GFRP showed better charring after flame attack with less melting phenomenon. When the CNH synergist was added, although the intumescent effect was severely constrained due to the impulsive fire attack, the sample demonstrated less glass fiber melting phenomenon.

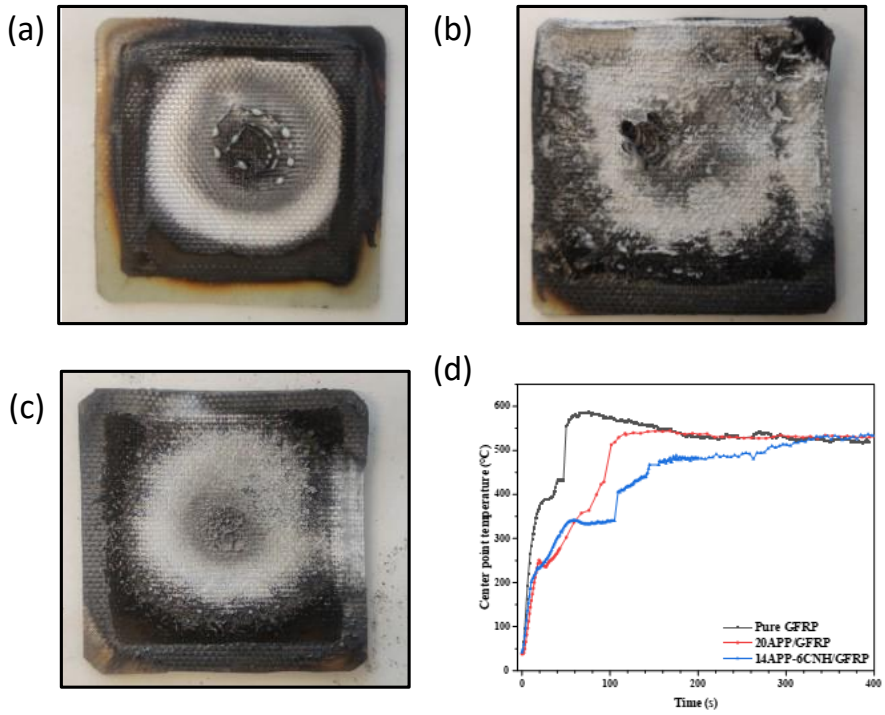

Figure 4.9: Digital photos of Pure GFRP (a), 20APP/GFRP (b), and (c) 14APP-6CNH/GFRP. (d) T_B back side central area temperature profile versus time.

As shown in Figure 4.9 (d), the T_B temperature variation with respect to the time showed a delaying effect of temperature rising after the addition of CNH into the polymer matrix of fiberglass composites. Hence, the heat/fire insulation properties were enhanced for 14APP-6CNH/GFRP, indicating better fire mechanical properties in the fire.

4.11. Conclusions

To tackle the challenge of the flammability of biobased epoxy resin systems, a novel cobalt-based nano-micro hybrid filler was proposed, designed, and prepared in this work. When the ratio of CNH to APP was 7:3 when added to epoxy, it demonstrated the best flame-retardant performance, as indicated by LOI, UL 94, and CCT results. It is worth noting that when the GFRCs, fabricated using the flame-retarded resin, were observed with suppressed intumescent effects compared to that of resin, which was proposed to be derived from the interference of glass fibers. In addition, the 14APP-6CNH/APP showed a better axial tensile strength due to the global failure redistribution mechanism opposing the local one observed in the 20APP/GFRP laminate. Heat/fire insulation properties were also enhanced after the addition of CNH synergist.

5. Design of Mechanical testing machine

5.1. Introduction

The cone calorimeter (CCT) is a widely used bench-scale heat release measurement apparatus that provides an even distribution of heat flux by using a radiative heater with a symbolic conical shape.[139, 140] Based on the cone heater, some novel accessories have been reported to provide additional material properties under the external influence of ignition and fire. Pan et al.[141] introduced gas collection and detection devices to check the release of hydrochloride gas when measuring the flame retardancy of PVC composite, which showed a promising function in measuring the suppression of toxic gas released by flame retardants. Chapple et al.[142, 143] designed and fabricated a lab-scale device that can collect aerosolized particles while the carbon fiber-reinforced polymer composites (CFRPs) are subjected to the effect of simultaneous heat/fire and impact. These studies demonstrated the development of novel equipment and methodology needed to provide the key data essential for future health and safety risk assessment in combination with particle toxicity data. Elmughrab et al.[144] designed and manufactured a loading frame with CCT to test composite materials under heat and fire. With a bolt-joint type connection between sample grips and coupons, they found out that the increasing stress promoted heat release and lowered the stress rupture times. These devices are of great help for the materials design and formulation as they provide useful key data and properties from materials that are vital and need to be validated later by the end industry using large samples. Up to now, few efforts have been being made to investigate the influence of the protective polymeric coating on the mechanical integrity of fire FRPs under simultaneously burning and mechanical load based on a bench scale cone calorimeter.

As mentioned in chapter 1, the prolonging of mechanical failure of FRPs under fire is of pivotal importance. Hence, the flame-retardant thermoset FRPs developed in chapters 3 and 4 should be demonstrated for their protection effects introduced by flame-retardant approaches. Hence, in this chapter, a bench scale device or accessory was designed and manufactured to be mounted on widely used fire testing equipment (CCT), which will enable fire hazard screening and fire mechanical testing under simultaneous heat and force, especially for structural polymer composite materials. Two types of FRPs materials were prepared. For the

first one, a fire-protective coating for the laminate coupons was chosen and prepared, as mentioned in Chapter 1. For the second one, the flame retardants used as additives in fiberglass composite, as shown in Chapter 4, were investigated. The composite coupons demonstrated either a fiber-dominated mechanical failure or a matrix-dominated mechanical failure when subjected to axial and off-axial loading. By employing this novel bench-scale device, the effects of protective coating on the structural survivability of polymer composites under fire hazards can be exemplified. The device was finally filed for patent and get approved with patent number as ES1308130U.

5.2. Design of mechanical testing devices

A bench scale device or accessory can be mounted on the CCT machines, as shown in Figure 5.1. The device is mainly composed of 5 sections: 1) a pneumatic transducer section, 2) an axial load sensing section, 3) a sample gripping section, 4) a guide pin-based structural section, and 5) a supporting frame section. The device can be optimized for the different types of commercial CCT. Several changes must be made for the traditional cone tests, which include discarding the mass measuring load cell and changing sample size and geometry. Overall, this device or accessory can be used to screen and investigate as well as to compare samples on their structural survivability under fire.

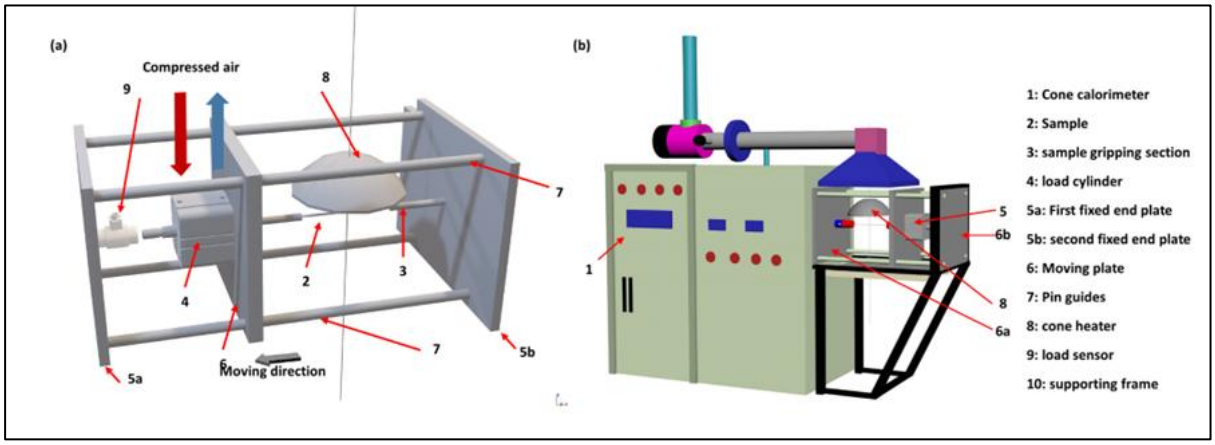

Figure 5.1: (a) Schematic illustration of design idea for the mechanical test instrument without supporting base frame. (b) The schematic illustration of the component used to build the machine mounted on CCT.

5.2.1. Instrument section design and optimizations

1. Pneumatic transducer sections are composed of a pneumatic or hydraulic cylinder, a compressed air control unit, a supply of compressed air, and other connection parts. The working range for compressed air is 0~6.5 bar. The pressure regulator can regulate the compressed air up to 10 bars.

2. Axial load sensing sections are composed of an in-line load cell and a computer equipped with a LabVIEW-based computer program that visualizes and records real-time load and other connection parts. The accuracy of the load sensor is ±0.2%.

3. Sample gripping sections are composed of miniature wedge-action types of tensile sample grips that create a self-tightening gripping force. Due to the moving grip bodies design, few preloads were applied to the coupon. This type of tensile grip is miniature and modular, which means they can be slightly changed and adapted to different sample sizes and space restrictions from various types of cone calorimeter. A thread to clevis adapter for connections between sample grips and device structural base with horizontal pin connection, facilitating quick connection, especially under high temperature. This shortened connection time also prevents sample softening before the test starts, thereby minimizing result errors. Details can be seen in the relevant picture section.

4. Guide pin-based structural sections are mainly a four guide-pin configuration composed of four guide pins and three structural base plates for supporting, mounting, and bearing connections for smooth load transfer. The design and geometry of this section can be adapted to different cone calorimeters.

5. A supporting frame section is composed of three structural supporting plates to support the main functional part of the device with threaded holes for connection with the cone calorimeter. This design and the geometry of this section can be adapted to different cone calorimeters.

The working mechanism of this bench scale instrument was based on the relative motion of the piston rod and cylinder barrel of the pneumatic cylinder. With the piston rod from the cylinder thread connected to the in-line load senor and structural base, its relative position remained stationary while the cylinder barrel was moving with respect to the piston rod due to the pressure difference of the two chambers. An in-line load sensor was threaded to the piston end of the cylinder to give real-time load feedback. A pneumatic pressure control unit supplied the pneumatic cylinder with filtered compressed air. The pressure control unit was

equipped with an IO link interface, which enabled its remote-control using LabVIEW-based software.

The fire structural survivability for the coupon was demonstrated as failure time vs different stress levels. By choosing certain types of samples, the results can be used to compare structural materials such as fiber-reinforced polymers with different orientations, protective coatings, and heat flux levels. The use of a pneumatic cylinder instead of a hydraulic cylinder provides much more feasibility for the manufacture of this instrument. Besides, the optimized grip design caused real failure for the composite at the coupon levels. Thus, this instrument may be much more adaptable and accessible for various types of CCT.

5.2.2. Equipment used in the instrument

- The cone calorimeter, from Fire Testing Technology, UK, is of dual-mode type.
- A calibrated piezoresistive-based load sensor used is from Applied Measurements Ltd, UK, and is of the type DBCL In-Line Column load cell. The sensor is also equipped with a cell amplifier ICA6H from the same company. The precision of the load cell is ±0.2%.
- A pneumatic cylinder-type actuator is used from a series of CMPC of Metal Work Iberica S.A. The cylinder has a bore diameter of 100 mm and a maximum stroke of 50mm.
- A proportional precision pressure regulator used is from the Regtronic series, Metal Work Iberica S.A. The regulator can be controlled via a cable or directly using the keys on the device.
- The manual sleeve valve used is from UNIVER Group with a type code of CM-9423E.

5.2.3. Grips design and optimizations

Initially, a bolt-joint connection between the sample and grips was proposed. However, by using this type of mechanically fastened joints in structural polymer composites, a kind of bearing tension was built upon the gripping region. Due to the geometry constraint required for the designed grip to be fitted into the CCT, the bolt-joint type of connection created a shear-out failure[145] within the gripping area, which demonstrated no real failure of the material under fire. Hence, a wedge

action tensile grip was proposed, designed, and manufactured to ensure an acceptable type of failure during this test.

As shown in Figure 5.2, the grip body has a truncated-cone-type cavity that coordinates movement with two jaws in relative motion. The jaws have a V-serrated face to promote a good transfer of load between sample coupons and the grip section. Between the threaded end of the adapter and jaws, there was a spacer to ensure the grip body moved toward the threaded adapter while the two jaws were maintained stationary in relative position. A thread-to-clevis adapter was used to connect the grip body to the female clevis fixture at the end of the structural base. With the horizontal insert and pull-out of the clevis pin, the grip, and adapter can be quickly mounted or removed from the female fixture end of the structural base, even under high temperatures. The fixture was kindly provided by Technology University of Madrid, while part 14 was redesigned to adapt to this specific machine so it can connect to part 16 by clevis pin 15.

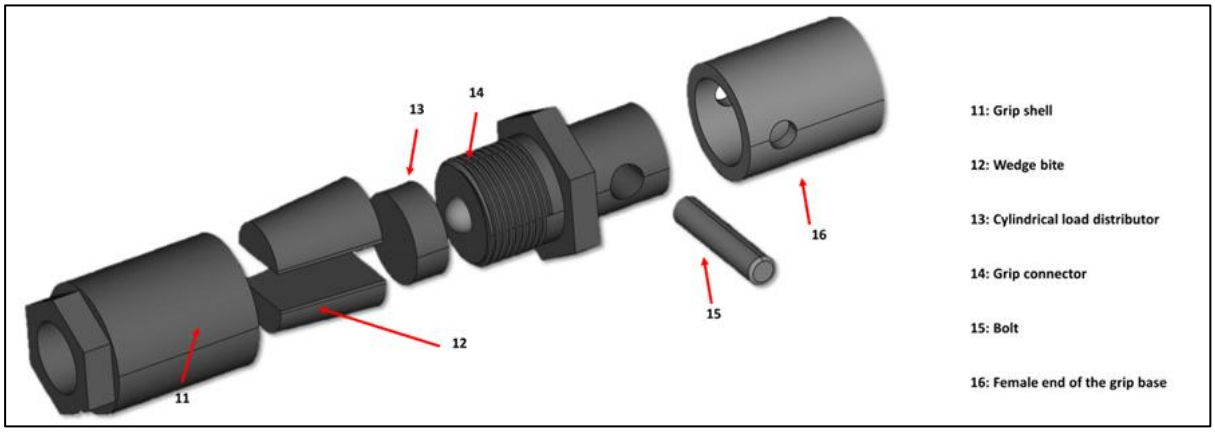

Figure 5.2: Schematic demonstration of the optimized grip section and its thread-to-clevis connector and pin.

5.2.4. Instrument load transfer design and calibration

Guide pins with bearings were chosen to ensure accurate horizontal motion of the middle moving plate while providing minimal friction and preventing loss of load. Four guide pins were chosen as they provide the most stable and accurate load transfer. Both ends of the guide pins were thread-connected to two structural base plates. The two structural base plates with the supporting frame were thread-connected to the cone calorimeter machine, which is shown in Figure 5.3, with an optimized grip design.

Instrument stress transfer between the transducer and sample was calibrated by applying known compressed air pressure to the pneumatic cylinder to produce a calculated static load while measuring the elastic strain of a high-modulus metal reference coupon using an extensometer. With the known elastic modulus and strain of the high-strength steel, the load applied onto the sample coupon can be calculated and compared with the input load derived from the pneumatic cylinder.

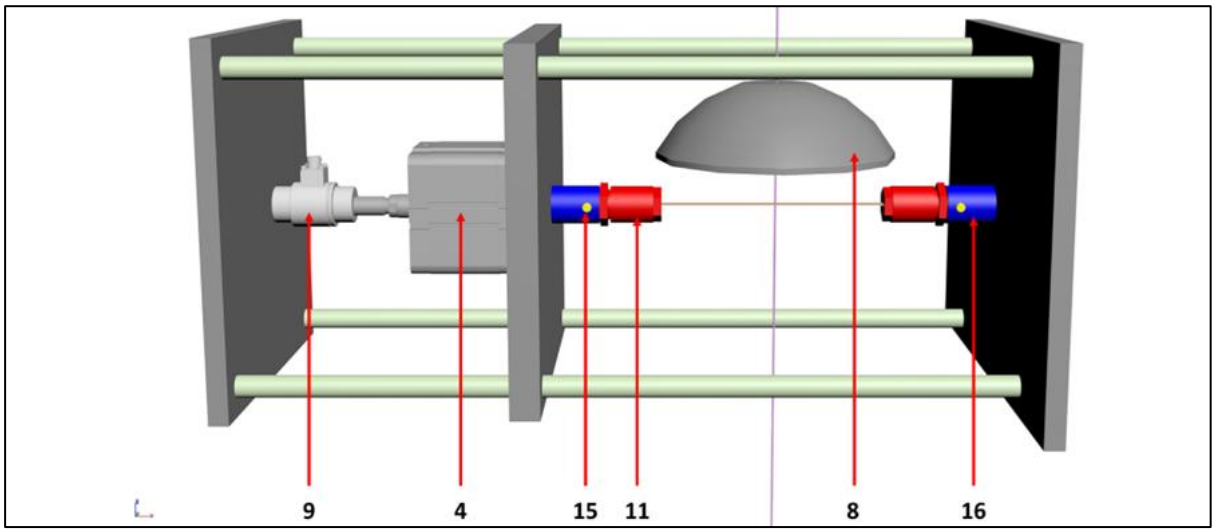

Figure 5.3: Schematic illustration of the bench scale machine with optimized grip sections.

Cone calorimeters have been widely employed to evaluate the combustion behavior of materials under forced surface flaming conditions. With this additional accessory, which can be easily mounted on or disassembled from the cone calorimeter, the material development scientist can quickly get an indication of the protective efficacy of fireproofing mitigation methods employed for fiber-reinforced polymer composites, especially with the thermoset matrix. The mounting structure can be easily redesigned to accommodate cone calorimeter machines from different suppliers, with core parts possibly intact due to the similar cone heater design and mounting scheme in different machines. In terms of practical applications, this accessory can be used to validate the different protective coatings on laminate substrates, for which this study provided a detailed case study. In addition, the protective efficacy of different fireproofing methods like FRs additives, FRs polymeric coating, and flame retarded polymer matrix by molecular design can be compared. In the meantime, by controlling the heat flux levels of cone heaters, this accessory can investigate materials' mechanical behavior under different fire hazard levels, thereby providing more information about their fire resistance properties.

5.3. Samples preparation and test procedures

5.3.1. Preparation of glass fabric-reinforced polymer composite

For the first type of FRPs, ten layers of dry glass fabric were stacked upon each other for GFRP to provide a laminate with a thickness of ca. 2.2mm. An epoxy-modified vinyl ester resin (type code: Derakane 8084, Ashland) was employed as a resin matrix for composites. The vacuum infusion process was chosen to manufacture the laminates. An isotropic composite laminate was manufactured with plain woven glass fabric using a ply layup being of $[(0°/90°)_2]_T$. Laminates were screened with an ultrasonic scan for quality check. Details can be found in section 3.2.1.

For the second type of FRPs, the same glass fiber reinforcement layup was used. The epoxy resin was well mixed with APP and CNH before adding a curing agent. After that, the glass fiber was impregnated by the degassed resin mixture by wet layup and compacted and consolidated by hot press. Details can be found in section 4.2.3.

5.3.2. Bilayer coating onto the laminate substrate

The formulation of each coating layer and detailed procedures to apply bilayer coating on GFRP can be found in our former work[146]. A total coating thickness of 2mm was used in our former study, which displayed great improvement in terms of flame retardancy and post-fire mechanical strength. The polymeric coating was applied by blade coating methods on a big laminate plate to get a uniform coating on the laminate. Then, the coated laminate was milled with a CNC machine to sample bars with dimensions of 130mm by 10mm. During the machining process of the laminate, the sample coupon was milled with a side length either parallel to or with 45° respect to the axial direction of the glass fiber. Hence, the composite coupon would demonstrate either fiber-dominated or matrix-dominated properties when subjected to in-plane axial force loading.

5.3.3. Testing procedures

The constant load under fire test was done by preloading sample coupons into the wedge action grip, which was fastened by the threaded section of the grip adapter. Insulating fabrics were applied to the sample's area, which is located close to the

jaw and back side, leaving an open area with a length of 10cm and a width of 1cm. The open area of sample coupons was wrapped with insulating fabric temporally until removed when the radiation shield of the cone heater was removed.

After the cone heater reached the desired heat flux of 50 kW/m^2, the sample coupon preloaded into the wedge grip was quickly inserted into the machine by inserting the pin into the clevis section of the adapter. Once the radiation shield fabric is opened, the warping of the sample's open area will be swiftly removed with the radiation shield opening. An electrical sparkle was inserted right above the middle point of the open area, and a compressed air supply was introduced into the pneumatic cylinder simultaneously.

After this, it commences the start of the test. The sample coupon will be heated, ignited, and burned while loaded with a constant force. The sample coupon will eventually mechanically fail under this extreme condition, and the time-to-failure value will be recorded. In the meantime, the heat release data will be collected and calculated based on this reduced sample size to provide information related to fire hazard information.

After the test of one single sample, two datasets can be gathered from the load cell and pressure regulator. In terms of the pressure regulator, the real-time compressed air pressure value with respect to the time can be collected and converted mathematically to the input loading level. Another dataset derived from the load cell can provide the real-time force loading value of the sample coupons as the load cell and laminate were loaded at the same axial line simultaneously. The time-to-failure value was determined from the data sets of the load cell as the sensor showed a loading force value before failure and displayed around zero loading values after the sample breaks.

Each sample was tested triplet as its least number of tests to get the average value and standard variation of each type of sample. Results were recorded after being verified to be within the confidence level of 95%.

5.4. Determination of experimental parameters

As shown in Figure 5.4, the stress-strain curves of the laminates in ambient conditions were determined using a universal testing frame. The ultimate tensile strength was used to determine the corresponding stress level and compress air needed to exert on the composite coupon while it is subjected to heat and fire damage. The calculation of the pressure value for the supplied compressed air was

based on the cross-section area of the sample coupon and the bore size of the pneumatic cylinder.

In the real application of structural polymer composites, the percentage of materials' theoretical strength that can be safely used depends on several factors, such as application fields, safety factors, environmental conditions, and the nature of the loads, as pointed out by some references[1]. Besides, the special environmental factor of composite is studied in this work, such as laminate being set on fire while undergoing continuous thermal degradation and delamination. Hence, it would be more meaningful for us to verify the protective effects of this coating even when the composite is subjected to a low level of static axial loadings. On the one hand, the coupon will fail immediately with or without fire under a stress level of 100%. On the other hand, a low-stress level may yield a long failure time. Taking the selection of testing parameters for coupons from chapter 3, three stress levels (35%, 25%, 10%) were chosen to measure the fire structural integrity of polymer composites when subject to axial loading conditions, as shown in Figure 5.4 (a). The in-plane shear response of laminate with a +45/-45 layup is shown in Figure 5.4 (b). The load that reaches the offset shear strength of laminate was chosen to demonstrate composites' matrix-dominated failure under fire in the following tests.

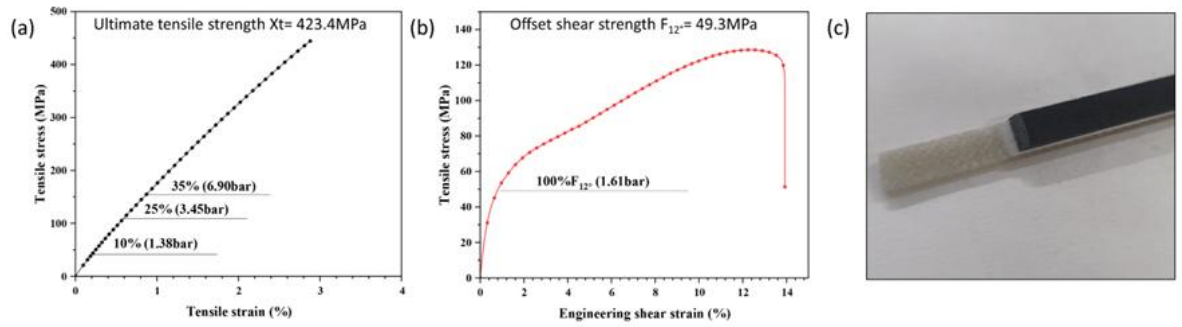

Figure 5.4: (a, b) Symbolic stress-strain curves for determinations of tensile strength and shear strength S12 for the laminates. (c) Digital photo of the machined sample coupons with a bilayer coating layer.

In terms of external heat conditions applied on laminates, a heat flux of 50 kW/m^2 was chosen for screening and trial. This heat flux value was chosen due to its wide use in terms of screening fire hazards when using a cone calorimeter. Under this heat flux, polymer materials tested under a cone calorimeter undergo a forced flaming condition that mimics scenarios of developing or developing fires.[147] It is worthwhile to mention that this bench scale test enables the choices of different

heat flux values to mimic various external fire severity conditions when polymer composites encounter fire hazards.

5.5. Coating protection against axial loading failure in fire

When the load is applied in the axial direction of reinforcement fibers, the composites undergo a fiber-dominated mechanical failure, whether in ambient or fire conditions. The results of time-to-failure for $GFRP_{[0/90]}$ with and without protective coating are shown in Figure 5.5 (a). With a higher stress level applied to the composite coupons, a shorter failure time was found, as expected. The higher stress level applied to the sample may promote crack growth and propagation from the fragile char, accelerating the decomposition of the virgin region below the fire zone, thus contributing to a faster failure time[55]. As shown in Figure 5.5 (b, c), the failure of composite coupon with axial loading acted seemingly like a dry fabric under tensile load failure due to the burning away of the resin matrix.

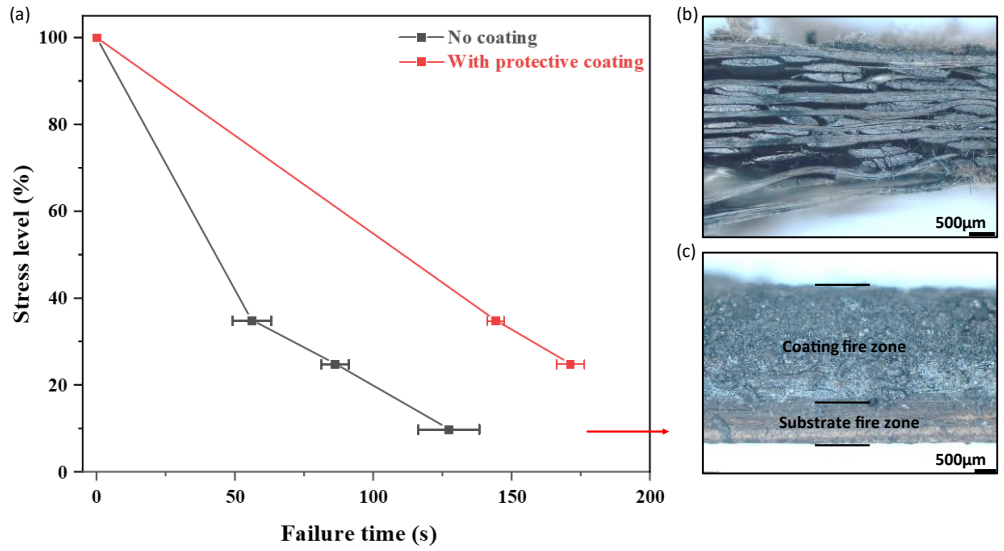

Figure 5.5: (a) Time-to-failure versus stress level curves for composite coupons with [0°/90°]2T layup. (b) Optical images of pristine $GFRP_{[0/90]}$ with no coating after the test. (c) Optical images of coated laminate when subject to fire and load of 10% of tensile strength.

After applying a fire-protective coating on the laminate coupons, the failure time for all three stress levels was prolonged by more than 190%, which indicates a highly efficient protective effect in Table 5.1. During the burning of coated GFRP, the surface coating layer was ignited first, with the formation of an intumescent char layer upon the virgin zone of the polymer composites[136]. With the decomposition of the polymer matrix being delayed, as shown in our previous

work[146], its roles as stress transfer and protection of fiber from fire damage were kept for a longer period compared to coupons that had no protective coating. For a stress level of 10% with respect to the ultimate tensile stress at ambient temperature, the failure time was delayed to a much later time of more than 10 minutes, during which the test had to be stopped and recorded with no specific failure time. As shown in Figure 5.5 (b, c), the coating layer produced an intumescent charring layer with a thickness of nearly three times the laminate origin thickness, protecting the matrix from fastened degradation and cracking caused by burning damage.

Table 5.1: Time-to-failure values for GFRP $_{[0/90]}$ coupons with and without coatings.

Stress level (%)	Time-to-failure (s)	
	No coating	With protective coating
35	56±7	144±3
25	86±5	171±5
10	127±11	>600

5.6. Flame retardant additives protection effect against axial loading failure in fire

Testing parameters for the laminates with additives of APP and CNH were determined based on the mechanical properties of the plane axial tensile strength tested in section 4.9. Due to the limited number of samples, only 25% of the original tensile strength was chosen as a failure load for testing the coupon under simultaneous load. The failure time of the loaded specimens was measured and presented in Figure 5.6. The modification of the materials increases the time-to-failure by more than 16% regarding the samples with only commercial FRs, demonstrating a better performance in fire mechanical properties by introducing these novel fillers.

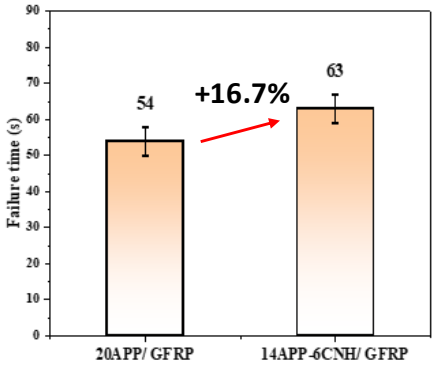

Figure 5.6: Bar chart for the results of failure time of 20APP/GFRP and 14APP-6CNH/GFRP under 50 kW/m^2 and 25% of failure stress loading.

Nevertheless, compared to the flame retardants added into the polymeric coating on the surface of the laminate, the protective effect was shown to be much lower when modifying the polymer matrix. Although the glass fiber stacking pattern was the same for both types of FRPs materials, the polymer matrix is not the same in terms of composition. Hence, to an extent, it can be suggested that fire protective coating methodology served as a superior approach for preventing the mechanical loss of FRPs during fire damage.

5.7. Coating protection against off-axial loading failure in fire

The failure time for GFRPs with +45/-45° was much lower compared to composite with 0°/90° orientation, as shown in Figure 5.7 (a). This was expected to be mainly due to the nature of coupons with +45/-45° off-axial loading, which would undergo a matrix-dominated failure. The thermoset-based polymer matrix has a glass transition temperature (T_g) around 90℃, which indicates it would deform under an even lower temperature upon heating and force loading. With the matrix softening and deforming and the off-axis reinforcement fiber showing no force-loading function, the sample coupons quickly underwent mechanical failure due to the lower matrix strength.

As shown in Figure 5.7 (a), after the fire-protective polymeric coating was applied on the substrate of FRPs, the survival time for FRPs of a static in-plane shear load was increased to 37s, which demonstrated the coating protection effect even in an off-axial loading scenario. The +45/-45° layup coupons with protective coating after failure displayed with polymer matrix burned out nearly completely, as shown in Figure 5.7 (b, c). Even with a protective coating on the substrate of GFRP, the failure time resided in a much shorter span compared to 0°/90° orientation because

a protective coating cannot alter the matrix-dominated failure nature of the sample coupons.

Figure 5.7: (a) Time-to-failure for the composite subject to fire and off-axial loading. (b, c) Digital images of pristine GFRP [+45/-45] with no coating after the test.

The improvements in the failure time by introducing fire protective coating on the FRPs were directly demonstrated by our novel bench scale test for the first time, which provides valuable insights in the early materials design stage.

5.8. Heat release behavior under the new configuration

As reported by our former study, this polymeric coating provided a protective effect in terms of flame retardancy and retention of post-fire in-plane axial tensile strength. The bilayer coating has a top intumescent layer that reacts chemically under heat and fire to expand several hundred percent of its original thickness. This top layer eventually converted into a highly porous carbonaceous layer, limiting thermal and mass transfer into the fire zone through the thickness direction. Between the laminate substrate and the top layer, there was an insulative layer that was chemically transformed into a ceramic-like layer during the thermal process. This ceramifiable layer acted in the lateral stage of the combustion process as a thermally insulative zone, prolonging the thermal transfer and temperature buildup of the composite laminate substrate.

To understand heat release information for the new testing configuration, non-coated laminates with different area sizes, as shown in Figure 5.8 (a), were measured under the CCT test using normal testing procedures without the mechanical testing machine. The laminates wrapped in an aluminum paper tray were tested under 50kW/m^2 without using the retainer frame. An ignition sparkle was applied as usual. In the software setting, the area value was changed to the real area size value before testing with a sample interval of 1s. Due to the weight

balance not being used and the decreased sample size, the results of only the heat release rate were analyzed in this study.

5.8.1. The trend between PHRR value with the sample area

As can be seen in Figure 5.8 (b), the heat release behavior of laminate with an area of 100cm² showed a two-peak pattern. The two-peak pattern of the heat release rate (HRR) curve indicates that laminate displayed a thick charring at the former stage of burning. During the combustion process, the char forms above the pyrolysis zone in an anaerobic decomposition process after the ignition starts. The thermal transfer happened ideally only through the thickness direction from the pyrolysis zone to the virgin zone, which has not reached its decomposition starting temperature in a dynamic process with both thermal transfer and mass loss.[148] Later, the crack of this char layer led to the loss of the blocking effect of thermal and mass transfer, leading to the second peak at the lateral stage of the curve.

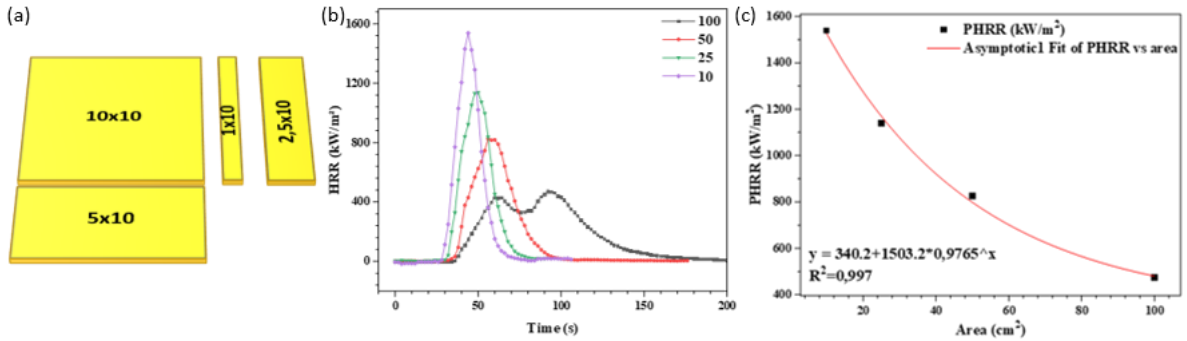

Figure 5.8: (a) Different sizes of samples tested under CCT. (b) Heat release curve with respect to time and (c) linear fitting of PHRR value versus area size of sample coupons.

Nevertheless, as the area size decreased to a smaller value, the curve pattern transformed from a two-peak type into a single-peak type with a visible shoulder, indicating the protective effect from the char was diminished. This was possibly due to the edge-burning effect enhanced by the smaller sample size, as indicated by former research.[137, 149] In the meantime, the peak heat release rate (PHRR) value was also increased to 400% when the area size was decreased to 10% of the standard sample size. There may be an exponential relationship between sample area and PHRR value, as shown by the fitting results from Figure 5.8 (c) for this type of thermoset composite coupon without protective coatings, indicating the edge burning effects rising greatly with decreased sample area size.

5.8.2. Influence of fire protective coating on the heat release

When testing in the new configuration of a small area size, as can be seen in Figure 5.9 (b), the pristine GFRP without coating showed a much sharper peak with a shoulder compared with Figure 5.9 (a), mainly due to the aforementioned edge burning effect. The PHRR value in the new configuration test was relatively lower compared to that tested in Figure 5.9 (a), which was possibly due to the mass loss due to the eruptive nature during the failure process of the composite coupon. For coupons coated with a protective coating, the sample showed a lower. Nevertheless, due to the thermal transfer from the edge of the laminate disrupting the ideal heat transfer through the thickness, the protective effect from the char layer was diminished, and thermal transfer to the virgin zone thereby displayed a plateau with a much shorter duration in Figure 5.9 (b). Later, with the damage of protective char, the second peak with a higher PHRR value emerged even though the protective effect of this charring-type polymeric coating was exemplified as the PHRR value decreased both by more than 30% and significantly decreased the decomposition speed with extended combustion time.

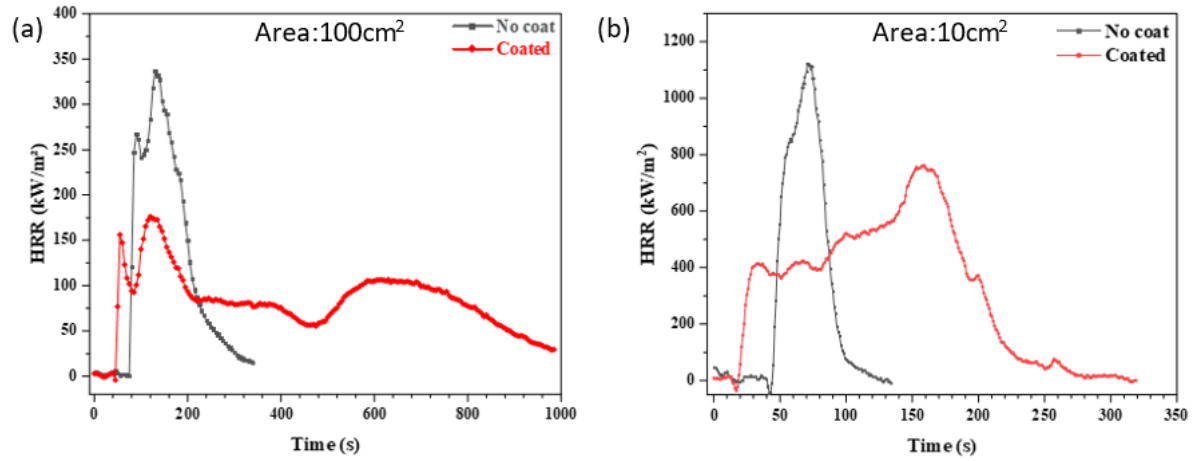

Figure 5.9: (a) Heat release rate curve with respect to time at a normal sample size of 100cm2. (b) Heat release rate curve with respect to time measured using the bench scale machine with a sample size of 10cm^2.

By comparing the heat release behavior between two sample sizes, the protective effects of polymeric coating can still be demonstrated in this new testing configuration for this type of thermoset polymer composite.

The core part of most types of CCT was constructed under similar principles by employing the truncated cone shape heater controlled by the geometric design of heating coils and resistance heating. In most tests, the measurement was done in a horizontal configuration under a well-ventilated atmosphere, too. Hence, this

accessory to the cone calorimeter can be easily adapted into different CCTs, with small changes being made regarding most of the structural supporting section. One potential limitation or constraint of this machine can be its lack of understanding of the usage of this heat release results to predict larger-scale fire performance, which needs further investigations. Another constraint may be its usage for testing polymer composites with thermoplastic matrix, especially those that possess a low melting point, as this type of polymer will melt and become thermally mobile in a very early stage of measurement.

5.9. Conclusions

In this work, a bench scale instrument that can be mounted on CCT was designed, discussed, and manufactured to offer a coupon level test for screening the structural survivability of fires of FRPs. The design of grips, working mechanism, test procedures, and sample preparation were discussed in detail. The influence of the fire-protective polymeric coating on the fire structural survivability for glass fiber-reinforced polymer composite was first directly demonstrated by a tailor-made instrument mounted on a calorimeter using a test on coupon levels. When samples were simultaneously under fire damage and mechanical load, the failure time of the protected laminate coupon was delayed by more than 190% compared to coupons without any protective polymeric coating layer. By employing this machine, which may be universally adapted to various types of CCT, the materials design and selection process can be much more facilitated for fire-safe FRPs.

6. Biomass-based fabric surface coating for natural fabric/epoxy composite

6.1. Introduction

The quest for an environmentally benign approach in chemical engineering has promoted the use of biomass-based FRs in the development of fire-safe polymer composites.[150, 151] Combined with a biobased polymer matrix, the use of biomass-based FRs in fireproofing plant fiber FRPs provides an even more eco-friendly approach, which enhances the life cycling worthiness of plant fiber FRPs for polymer composite industries.[152]

Many phosphorous[153, 154] or boron-based FRs such as APP[94], boric acid[95], organic phosphonate ester[96], etc., have been reported for flame-retardant treatment of plant fiber and its polymer composites recently. However, the use of fossil fuel-based FRs may be improved by replacing them with biomass-based FRs with equivalent or better efficacy. Besides, the multi-step LbL approach is a complicated and time-consuming process that stifles the development of fire-safe PFRPs.

The PEC, which constitutes oppositely charged macromolecules, can interchange between solution or solid state by tailoring the pH, concentration, and extra salt additive in the system.[98, 155] Taken advantage of this phenomenon, a facile process by PEC-based two-step coating using phosphorus or boron compounds has been demonstrated widely in the flame retardant treatment of textiles for natural and synthetic fabrics.[156, 157] Rodriguez et al.[158] demonstrated a two-step process for flax fabric treated by PEI and sodium hexametaphosphate (PSP). The treated flax fabric showed self-extinguishing behavior with a decrease in PHRR by 30%, while no biomass-based FRs were used. Phytic acid, being one of the few naturally derived phosphorus-containing FRs candidates, has shown some promising results when used as a constituent with chitosan for biomass-based PEC as additives[159, 160] or coating on fabrics.[161] Nevertheless, to the best of our knowledge, few reports have demonstrated the potential of biomass-based PEC coating on plant fiber-based fiber reinforcement for the development of fireproofing PFRPs.

In this chapter, a biomass-based PEC coating treatment on woven flax fabric was done using phytic acid and chitosan in a facile two-step impregnation and buffer

curing process. Laminate was produced by vacuum infusion process using the biobased FRs-treated flax fabric and biobased epoxy resin as the polymer matrix. The flammability of the flax fabric itself and the polymer composite were screened. The combustion behavior of the laminate was also examined. Finally, investigations of the flame-retardant coating on the gas and condense phase were conducted with a proposed mechanism for the elaboration of the behavior change from the flame-retardant behavior of coating on fabric only to the polymer composites.

6.2. Samples preparation

6.2.1. Preparation of PEC-based aqueous solution

Various formulations of phytic acid/chitosan polyelectrolyte solution were prepared to verify the optimal viscosity while trying to maintain a high phosphorus content in the PEC solution, as shown in Table 6.1. Finally, the PEC solution was decided with 20wt% of phytic acid and 1wt% of chitosan. Here is the detailed preparation step for the PEC solution. 20wt% of Phytic acid was prepared by diluting 50% Phytic acid (PA) with deionized water. Chitosan-based aqueous solution was prepared by adding it portion-wise into deionized water under mechanical stirring. After that, the phytic acid aqueous solution was added slowly into the chitosan aqueous solution under mechanical stirring to form a uniform and translucent solution formed as a chitosan/phytic acid polyelectrolyte solution named PEC. A few hydrochloric acids were added to the mixture to promote the formation of a translucent miscible solution.

Table 6.1: Formulation of PEC aqueous solution with various concentrations of PA and CH.

Formulations	Phytic acid (wt%)	Chitosan (wt%)	Observed viscosity	Note
20PA1CH	20	1	Medium	Suitable for dip coating
10PA1CH	10	1	Low	Phosphorous content low
20PA2CH	20	2	High	Not suitable for dip coating

6.2.2. cDip coating of flax fabric by PEC solution

The procedure for a few steps of dip-coatings of flax fabric is shown in Figure 6.1. First, pristine flax fabric was cleaned using deionized water under an ultrasonic

bath for 0.5 hours and dried under 70℃ for 1 hour. Then, washed flax fabric named PFL was soaked into the PEC solution bath for 15 minutes before being squeezed and absorbed excessive solution by a roller press. After that, the PEC-soaked flax fabric was then transferred to a 0.1M acetic acid buffer bath for deposition on the flax filament. A roller press was used again to remove excessive acetic acid solution, and the fabric was rinsed by and squeezed to get modified falx fabric named PEC@FL and dried at 70℃ for 6 hours. Weight gain was calculated to be around 12wt%.

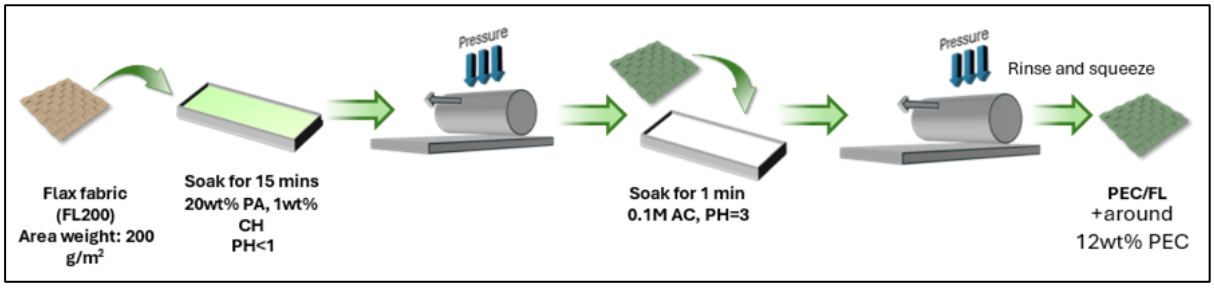

Figure 6.1: Schematic illustration for the dip coating, roller press, and buffer curing process for preparing the PEC-coated flax fabric (PEC@FL).

6.2.3. Preparation of flax fabric-reinforced epoxy composite

The polymer composite was prepared by a widely used vacuum infusion process. 4 layers of either pristine flax fabric or PEC-coated flax fabric were used respectively to form symmetrical laminates. A commercial partly biobased epoxy resin was used with an amine type of curing agent. VARI method was used to fabricate the laminate similar to the works in the above chapters. Process details, curing schedule, and cutting are the same as in section 3.2.1. Finally, a laminate with ~2.2 mm thickness and 28% volume ratio, which may be due to the low compaction pressure of VARI method and porous nature of plant fiber.

6.3. Validation of PEC coating on flax fabric

As can be seen in Figure 6.2, the pristine flax fabric showed a twisted yarn morphology with a diameter of around 500 microns. The single flax fiber has a diameter of around 30~60 microns. After the PEC coating on the flax fiber, the surface morphology showed a conformal PEC-based organic coating layer on both the surface and conjunctions of the multiple single fibers, with some debris film derived from the excessive coating deposition. The EDS map shown in Figure 6.2 (c) also demonstrated the presence of phosphorus elements on the surface of flax

fiber yarns, indicating the presence of phosphorus-based compounds deposited on the surface.

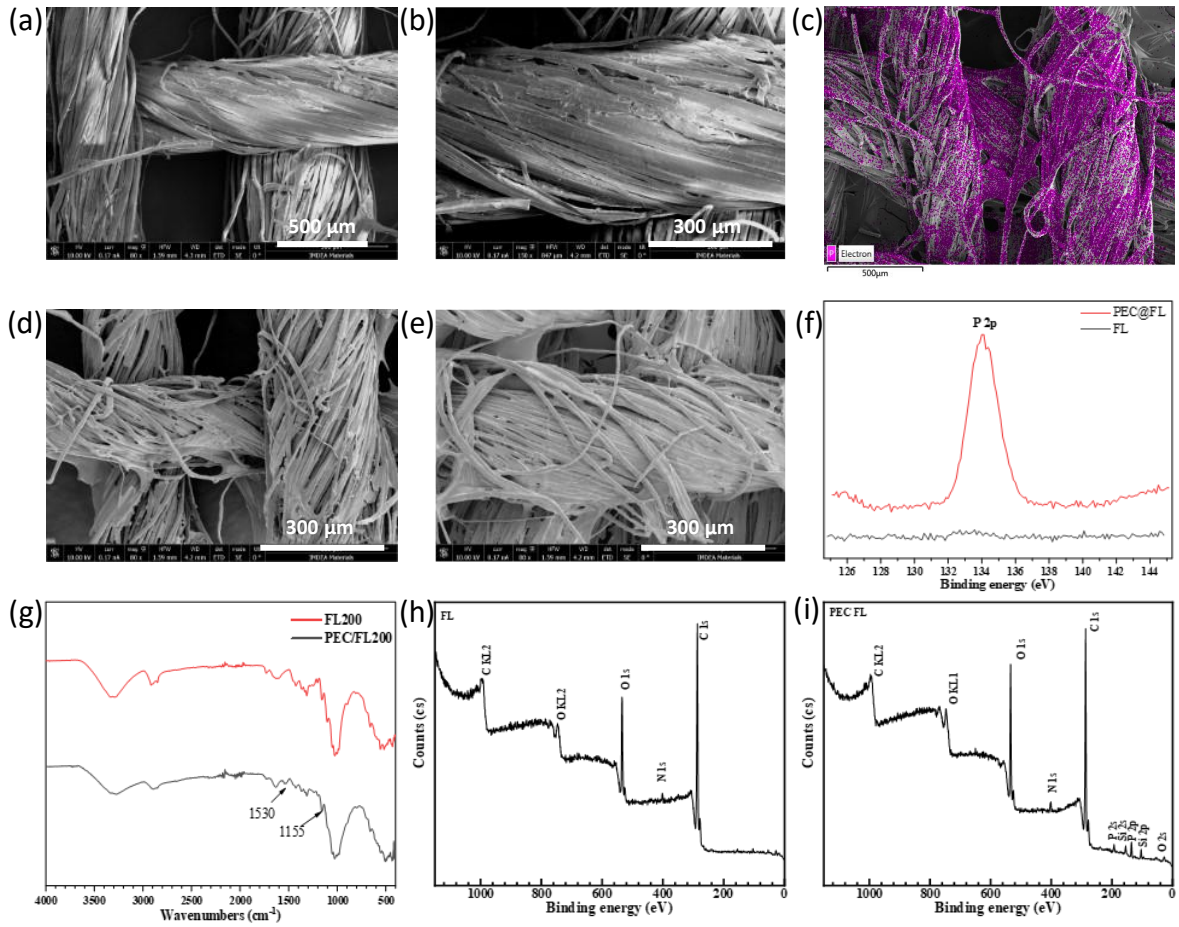

Figure 6.2: Surface morphology of pristine flax fabric FL (a, b) and PEC@FL flax fabric (d, e). EDS images for P elements of PEC@FL (c). High-resolution curve of P2p spectrum for both FL and PEC@FL (f). (g) FTIR curves for flax fabric before and after PEC coating, XPS full survey spectrum for flax fabric before (h) and after (i) PEC coating.

FTIR spectra were obtained to compare the surface composition of FL and PEC@FL. As can be seen from Figure 6.2 (g), a few new peaks around 1530 cm^{-1} and 1155 cm^{-1} were formed, which may indicate the stretching vibration of the O-P-O bond and P=O.[159] Due to the large presence of flax fabric-based cellulose composition, even after the coating, the signals of new peaks were still relatively weak. XPS results showed that a new peak of P_{2p} formed after the PEC coating on the flax fabric in the high-resolution spectrum curve. These new peaks formation around P_{2s} and P_{2p} were also visible in the full survey of the XPS spectrum, as shown in Figure 6.2 (b, c). Hence, in conclusion, it can be said that the PEC coating layer was successfully deposited on the surface of flax fiber using a facile method with only a few steps.

6.4. Flammability of flax fabrics

6.4.1. Vertical burning tests of flax fabrics

The self-extinguishing properties of flax fabric before and after coating treatment were screened with vertical burning tests. As can be seen in Figure 6.3 (a, b), the pristine flax fabric burned out with no residue left, displaying high flammability and low self-extinguishing properties. After applying P, N coating deposition on the flax fiber yarns, the PEC@FL fabric showed self-extinguishing properties with a much less damage length after flame-out. The introduction of biobased flame-retardant deposition on the fiber surface formed a charring layer, as can be seen in Figure 6.3 (b), which may prevent the spreading of fire and fuel supply. However, it is worth noting that the self-extinguishing behavior of reinforcement fabric cannot only represent the burning behavior of the laminate, as the fabric is only one constituent of the polymer composite systems.

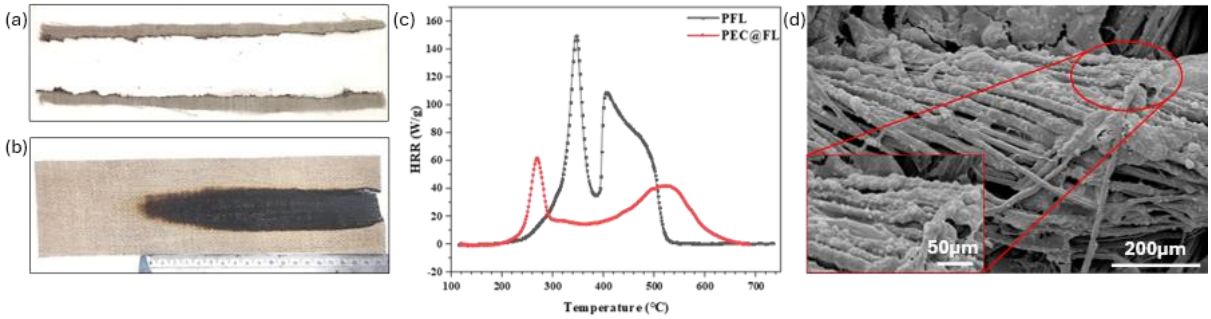

Figure 6.3: Digital pictures after vertical flame burning tests for PFL (a) and PEC@FL (b). Heat release rate versus temperature curves for both fabrics under PCFC tests (c). SEM image of PEC@FL residue after the vertical burning test.

6.4.2. Combustion Heat release for flax fabrics

The MCC measurement provided a facile way to measure the heat release rate and capacity of the flax fabrics with a minimal sample weight. As can be seen in Figure 6.3 (b) and Table 6.2, flax fabrics before and after PEC deposition both showed a two-peak pattern curve under anaerobic decomposition in the pyrolizer and complete oxidation combustion at the combustor chamber. After the deposition of PEC on flax yarns, the peak heat release rate (Peak HRR) was decreased from 160 W/g for pure flax fabric PFL to 62 g/W for that of PEC-treated flax fabric (PEC@FL), indicating a strong suppression effect on the release of combustible volatiles. In addition, the HRC and total heat release (total HR) were decreased respectively by 18% and 42% compared to those pristine fabrics.

Table 6.2: PCFC results of untreated and PEC-coated flax fabric.

Samples	Wt. gain (%)	HRC (J/g-K)	Peak HRR (W/g)	T_p (°C)	Total HR (KJ/g)
PFL	0	156	150	346	15.9
PEC@FL	12	128	62 (-58.6%)	270	9.3 (-42%)

The temperature of peak heat release rate (T_p) shifted to an earlier and lower value for PEC-coated fabric compared to that of no coating applied. This was also observed in the TGA test, as shown in Figure 6.4 (c). This may be attributed to the catalyzing effect derived from phosphate compounds, which promote the dehydration and crosslinking of cellulose and char formation.[162, 163] This formation of char shields the fiber yarns from burning completely, thereby showing self-extinguishing behavior.

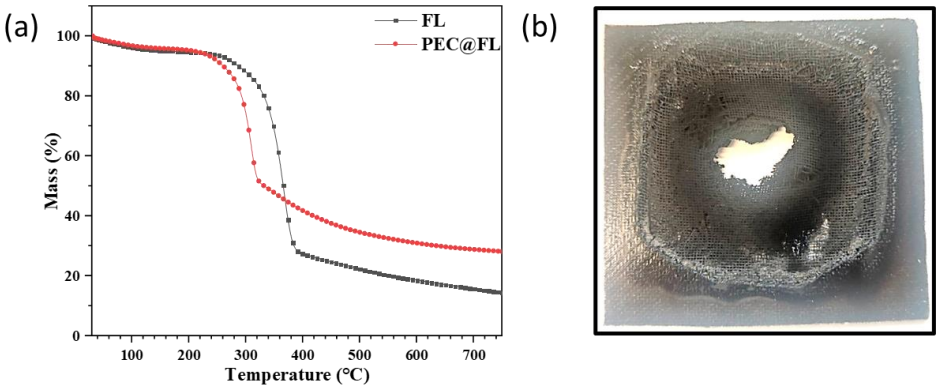

Figure 6.4: (a) Mass loss curves for fabric before and after treatment. (b) digital image of Pure FL/EP after torch fire burn-through tests.

6.5. Combustion behavior of polymer laminates

CCT test was employed to measure the heat release behavior of flax fabric reinforced epoxy composites under horizontal configuration with 50 kW/m2 external heat flux radiation. As shown in Figure 6.5 and Table 6.3, the Pure FL/EP exhibited a single peak pattern curve for heat release rate versus time with a very subtle shoulder before the curve peak. This suggested that the Pure FL/EP displayed mainly a thermally thin type of sample under burning with very limited charring capability, which may be contributed by the flax fabric's limited charring capabilities.[164] At the end of the test, nearly no residue was left for Pure FL/EP as both two constituents, fiber and epoxy resin, showed nearly no residue when measured in TGA tests.

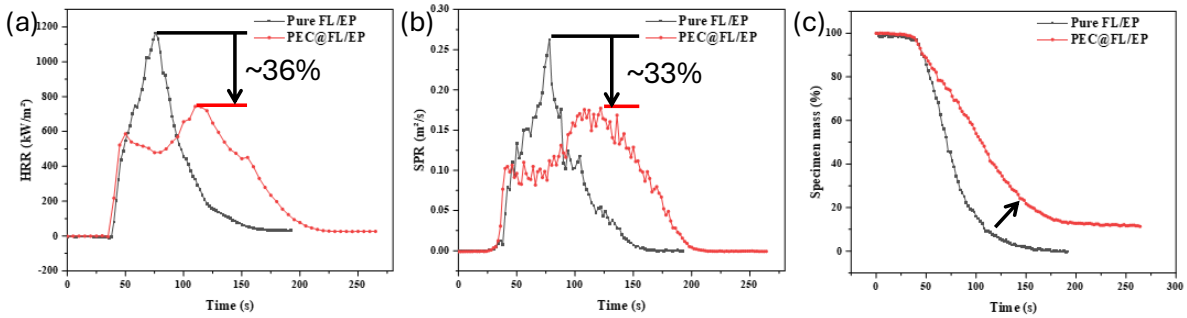

Figure 6.5: Cone calorimeter results for both laminates using flax fabric with and without PEC coating for heat release rate (a), smoke production rate (b), and specimen mass loss temporal curves (c).

CCT test was employed to measure the heat release behavior of flax fabric reinforced epoxy composites under horizontal configuration with 50 kW/m^2 external heat flux radiation. As shown in Figure 6.5 and Table 6.3, the Pure FL/EP exhibited a single peak pattern curve for heat release rate versus time with a very subtle shoulder before the curve peak. This suggested that the Pure FL/EP displayed mainly a thermally thin type of sample under burning with very limited charring capability, which may be contributed by the flax fabric's limited charring capabilities.[147] At the end of the test, nearly no residue was left for Pure FL/EP as both two constituents, fiber and epoxy resin, showed nearly no residue when measured in TGA tests.

Table 6.3: CCT test results under horizontal configuration and 50 kW/m^2 irradiation.

Sample	TTI (s)	PHRR (kW/m^2)	THR (MJ/m^2)	PSRR (m^2/s)	Residue (%)	Mean EHC (MJ/Kg)	FIGRA (kW/sm^2)	MARHE (kW/m^2)
Pure FL/EP	36	1167	56.5	0.26	0	22.2	15.4	446
PEC@FL/EP	33	744	77.1	0.18	11.3	22.3	6.8	420

After the deposition of the PEC-based flame-retardant coating layer of flax fibers, the polymer composites using PEC@FL fabric showed a drastic change in terms of heat release curve patterns from one single peak of Pure FL/EP to two peaks pattern curve for modified polymer composites. The heat release rate (HRR) curve of PEC@FL/EP demonstrated a thick charring behavior with an additional peak at the end of the test, which may be due to the thermal oxidation of cracked chars.

In terms of PHRR value, a decrease of more than 35% reduction in PHRR was achieved for PEC-modified flax fabric reinforced laminate compared to that for

composite with pristine flax fabrics. The fire growth rate index (FIGRA) value is defined as the derivative value of the PHRR value with the time-to-PHRR, as can be calculated from the CCT results.[165, 166] The FIGRA value was decreased from 15.4 to 6.8, as shown in Table 2. This suggested that the fire propagation speed may be much delayed and slowed. In the meantime, the mean effective heat of combustion (EHC) was almost PEC@FL/EP and Pure FL/EP, which may indicate that the coating had limited capability for gas phase behavior.[167]

Smoke release and mass loss can also be recorded throughout the CCT tests, as some results of this are shown in Figure 6.5 (b, c). The peak smoke production rate (PSRR) value was also decreased by more than 30% for modified laminates compared to that of Pure FL/EP, indicating a suppression of smoke release potentials. The mass loss behavior under the forced flaming scenario demonstrated a decreased slope value, indicating the presence of flame-retardant coating delayed thermal decomposition rate in the through-thickness direction. The decreased mass loss rate lowered fuel generation and combustion in the gas phase, which correlates with the decreasing heat release rate in Figure 6.3 (a). In addition, the higher residue value after the CCT test also suggested high charring capabilities for the modified laminate.

6.6. Fire insulation tests

Resistance to fire is one of the important properties of fire-safe polymeric materials in various applications. Compared to carbon, glass, and basalt fibers as reinforcement for polymer composites, natural fibers reinforced polymer composites possessed a much vulnerable capability for resistance to fire penetration and avoiding burn-through.[53] In this study, we implemented a lab-scale torch fire burn-through test to try to preliminary measure the properties of two laminates by mimicking a strong jet-like fire impingement through the thickness direction, as shown in Figure 6.6 (a). Due to the auto switch function of the thermography camera, there were around 10s of measurement value jumping during the test. Torch fire was applied on one side of the laminate with edge protection by calcium silicate board to ensure through-the-thickness direction damage and thermal transfer. A thermographic camera recorded the temperature distribution of the backside.

In Figure 6.6 (d), the temperature for the central point of the back side (T_B) was plotted against time, which demonstrated fire insulation properties through the

thickness. For the Pure FL/EP, the temperature versus time curve displayed a steep slope value with temperature radically rising from the start of fire impingement and reaching almost 300℃ in less than 20 seconds. At the 20s of torch fire impingement, the temperature distribution on the back side of both laminates was shown in Figure 6.6 (b, c), which displayed a drastic difference between Pure FL/EP and PEC@FL/EP. The time to burn-through failure for Pure FL/EP was 30 seconds, indicating a poor fire resistance capability for laminates without flame retardant treatment on flax fabric, as shown in Figure 6.6 (e).

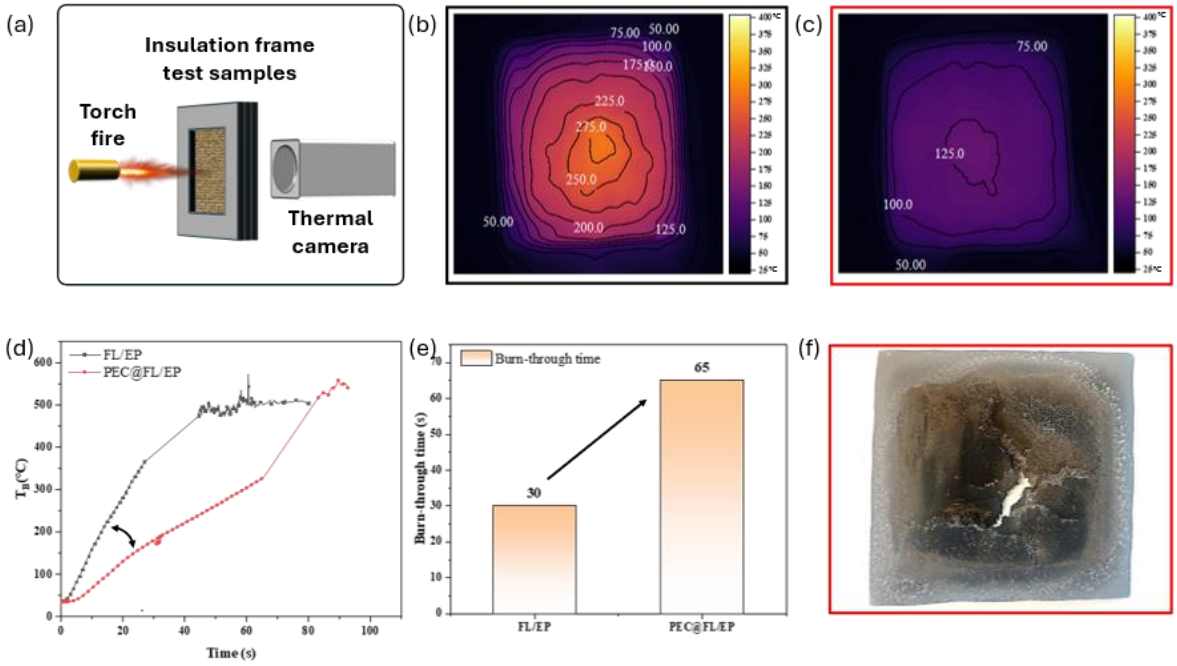

Figure 6.6: (a) schematic illustration for the torch fire burn-through test results. (b, c) Temperature distribution for the back side of the tested laminate at the time of 20 seconds of flame impingement. (d) Temperature versus time curve for the central point on the back side of laminates. (e) Bar chart of the burn-through time for both laminates. (f) Digital images of PEC@FL/EP laminate after burn-through tests.

Nevertheless, after the PEC flame-retardant deposition on the reinforcement fabric surface, the time to burn-through failure was increased by more than 100% to 65 seconds. The T_B-time curve also demonstrated a much lower slope value, indicating the strong delaying effect for thermal transfer through the thickness directions for modified laminate. Digital images of both Pure FL/EP and PEC@FL/EP are shown in Figure 6.4 (b) and Figure 6.6 (f). For Pure EL/EP, a loose, brittle char morphology with fabric-shaped microstructure was left after fire damage at the central area around the failure crack. This was partly due to the nearly no charring capability of the resin matrix or the limited charring capability of the flax fabric. However, the PEC@FL/EP composite showed a much more

compact char morphology without fiber-like microstructure around the burn-through crack area. The change in fire insulation, burn-through time, and char morphology after the test all indicated a possibility of enhancing the protection against fire damage for polymer composite with flax-based natural fiber reinforcements.

6.7. Dynamic mechanical analysis measurement

As continuous fiber-reinforced polymer composites, the dynamic mechanical properties of natural fiber polymer composites under elevated temperatures are also crucial for their application. As shown in Figure 6.7 (a, b), the DMA results demonstrated that there is little interference after the PEC coating on the reinforcement fabric. The temperature for the glass transition temperature (peak of Tan δ) was very close. The storage modulus at 30℃ of PEC@FL/EP was relatively higher than that of Pure FL/EP. This indicated the flame-retardant coating on reinforcement fabric showed little interference in terms of thermos-mechanical properties.

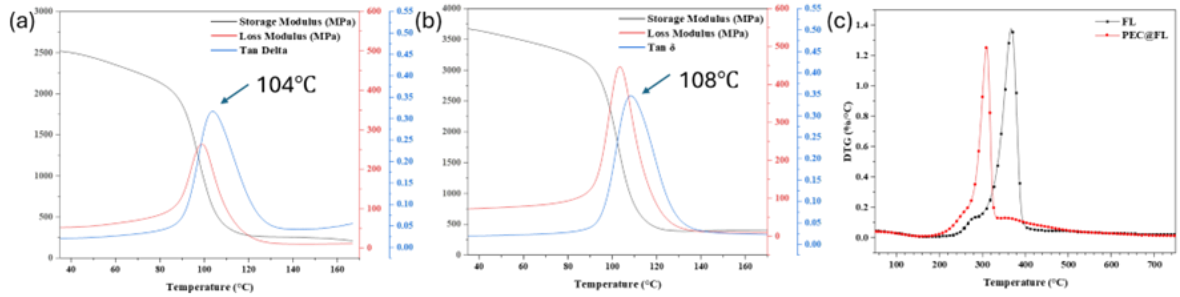

Figure 6.7: Dynamic mechanical properties curves for Pure FL/EP(a) and PEC@FL/EP(b). DTG curves for thermal stability test of flax fabrics.

6.8. Thermal stability of flax fabrics

As shown in Figure 6.7 (c) and Figure S2 (a), the DTG_{max} of PEC@FL is lower than that of FL fabric without any treatment, indicating the decomposition speed was accelerated with the introduction of the PEC complex. Phytic acid is a phosphorus acid-based compound, which has been suggested by various reports on the catalytic decomposition function, thereby lowering DTG_{max} value to around 300℃. On the other hand, the residue value of PEC@FL showed a huge increase of almost 100% compared to that of pristine fabric after decomposition in the N_2 atmosphere. The polymer matrix used in composite possesses a DTGmax value of around 350℃ with

nearly no charring capability, as shown in our former work[168]. The thermal stability of the whole composite material is assumed to be changed due to the introduction of phytic acid and chitosan complex compounds on the surface of reinforcement fabric, which may play a role in the decomposition process of materials.

6.9. Residue morphology

Figure 6.7 (a, d) shows the digital images of char residue after CCT tests for two types of laminates. The Pure FL/EP had very few residues left after the forced flaming test, which is expected due to the limited charring capabilities of the composites without FRs. In terms of PEC@FL/EP, the sample after flame-out demonstrated a thick charring layer, indicating a strong charring capability. This drastic change in charring behavior also corresponds to the recorded mass loss curve in Figure 6.5 (c) in the cone calorimeter test.

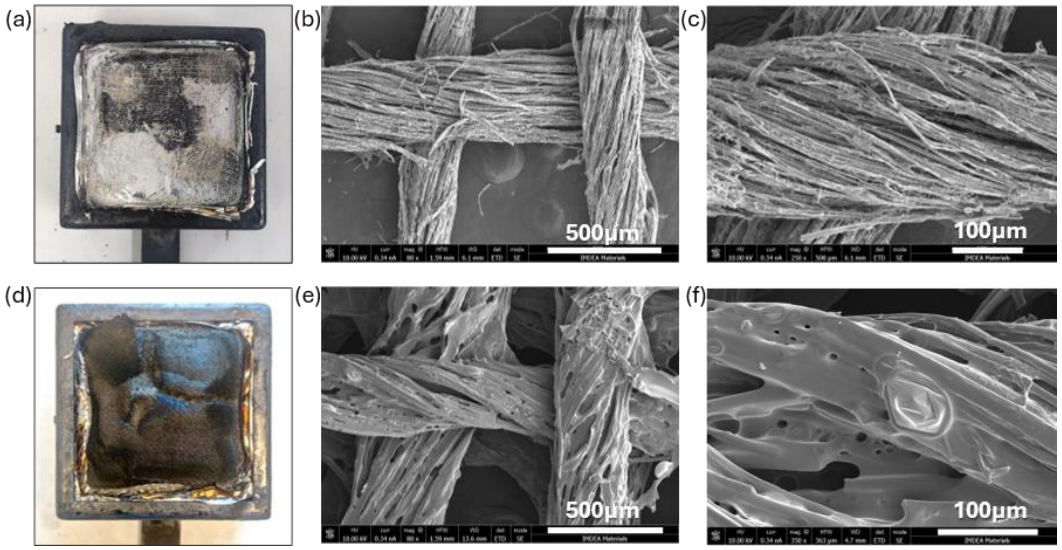

Figure 6.8: Digital photos of char micromorphology after CCT test for Pure FL/EP (a) and PEC@FL/EP (b). SEM images of char residue morphology for Pure FL/EP (b, c) and PEC@FL/EP (e, f).

Residue morphology after the CCT test was screened under the SEM test, as shown in Figure 6.8 (b, c, e, f). In terms of residue morphology for Pure FL/EP after the CCT test, the char left a multi-single fiber-like micromorphology for each layer of flax fabric. The enlarged photo shown in Figure 6.8 (c) suggests that the char from Pure FL/EP is brittle and loose, which may fail to form a char barrier effect. In contrast, the char morphology from PEC@FL/EP in Figure 6.8 (e, f) displayed a yarn-like morphology with a much more compact structure derived from each layer

of flax fabrics. With multiple layers of residue from flax fabrics forming a compact char barrier, this char residue was assumed to stifle the thermal and mass transfer of combustible fuels during combustion in CCT tests.

6.10. Vapor phase analysis during laminate decomposition

As shown in Figure 6.9, the gas phase flame retardant behavior was investigated by implementing the TGA-FTIR test in a nitrogen atmosphere to mimic the anaerobic decomposition and detect released combustible fuels during the combustion process.[114]

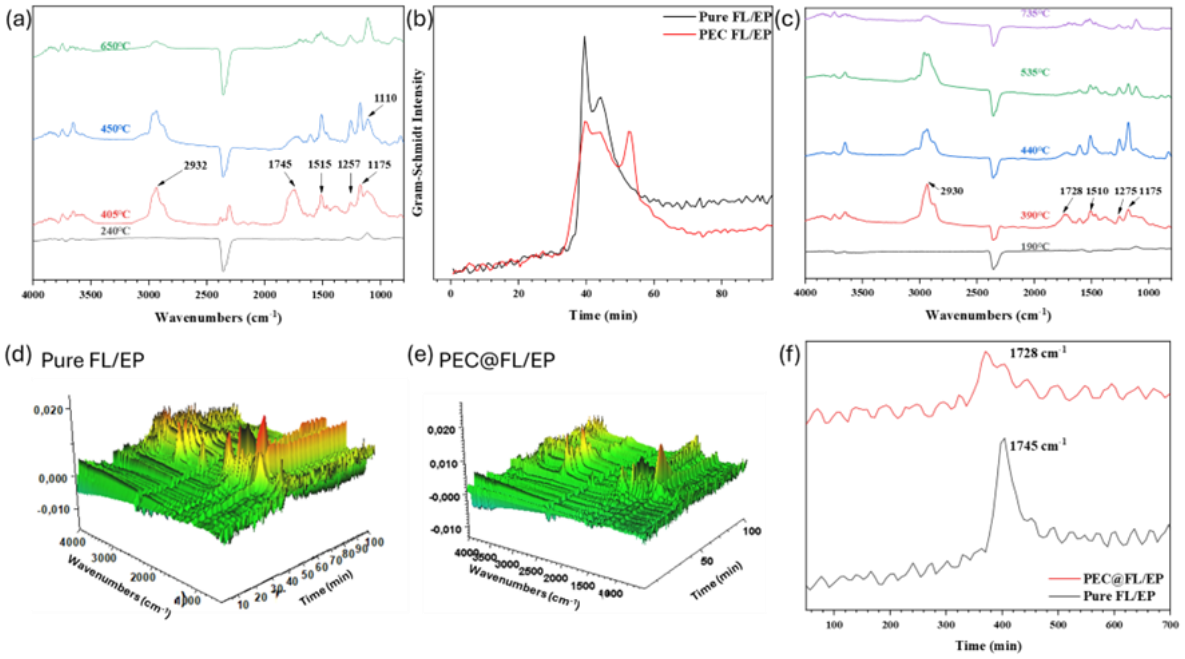

Figure 6.9: FTIR curves of gaseous products released from Pure FL/EP (a) and PEC@FL/EP at different temperatures (a, c). Gram-Schmidt IR intensity of gaseous release products from two laminates(b). 3D construction map of the relationship between temperature, wavenumbers, and intensity of Pure FL/EP (d) and PEC@FL/EP(e). Intensity profiles versus temperature for peak at around 1740 cm-1 for two laminates.

In Figure 6.9 (b), the Gram-Schmidt intensity of PEC@FL/EP was decreased compared to that of Pure FL/EP, which was also shown in the 3D map of Figure 6.9 (d, e). When mapping the FTIR curves of volatile compounds emitted during the decomposition of the two laminates before and after the DTGmax, the result curves are shown in Figure 6.9 (a, c). The intensity around 1730 cm^{-1} was decreased for PEC@FL/EP compared to that of Pure FL/EP alongside the rise of temperature in Figure 6.9 (f), which corresponded to volatiles containing carbonyl bond.[169] The intensity for peaks around 3000 cm^{-1} and 1510 cm^{-1} corresponded to the aromatics and aliphatic C-H bonds were like for both samples.[170] The peak around 1110 cm-

[1] may correspond to the C-O stretching vibration in ester groups. As can be seen, most peaks existed in two laminates. The results from the TGA-FTIR test and the mean EHC values for two laminates indicated limited gas phase behavior for the biomass-based flame-retardant coating.

6.11. Proposed flame-retardant mechanism

After several investigations into both the condense phase and gas phase and the fire hazard results measured from the cone calorimeter, the flame-retardant behavior of this biomass-based coating on reinforcement fabric for the combustion behavior of laminate was proposed. As can be seen in Figure 6.3 (d), for the flax fiber-based natural fabric reinforcement alone, the phytic acid and chitosan-based PEC coating layer catalyzed the dehydration and crosslinking reactions of cellulose, hemicellulose, or lignin compositions and promoted the char formations upon thermal degradation and fire damage. The formation of a microscale intumescent effect on the fiber yarns stifles the thermal transfer into the fibers inside the coatings layer, thereby showing self-extinguishing behavior during the VBT test.

However, the self-extinguishing behavior of the fabric reinforcement itself does not transfer its efficient flame retardancy into the final natural fiber-reinforced thermoset polymer composite. In terms of the monolithic laminate, the fiber reinforcement weight ratio is around 40~45%, with no flame-retardant additives in the resin matrix in our processing method. The PEC-based coating on the natural fiber yarns formed part of the interface between the fiber reinforcement and resin matrix. During the combustion of laminate, the phytic acid/chitosan-based PEC coating promotes mainly each layer of natural fiber to form a compact char structure, as shown in Figure 6.8 (e, f). With multiple layers of this char structure stacking up to stifle fire damage and thermal transfer through the thickness direction, the laminates demonstrated lower PHRR results and FIGRA values as well as longer time for torch fire burn-through, as shown in Table 6.2 and Figure 6.6.

6.12. Conclusions

In this work, a facile, few-step coating process based on biomass-based flame-retardant coating was designed and deposited the flax fiber reinforced bio-epoxy resin, forming highly environmentally benign polymer composite materials with all components used being mostly biobased materials. The aqueous bio-mass

coating solution based on phytic acid/chitosan was developed and tailored to adapt to the widely used pad-dry process. The PEC-coated flax fabric demonstrated self-extinguishing behavior with micro intumescent char forming on the fiber yarns. The laminate using this PEC-coated flax fabric and bio-based epoxy resin demonstrated the capability of lowering the fire hazards compared to that of Pure FL/EP as the peak heat/smoke release rate, mass loss rate, and fire propagation were lowered. The resistance to torch fire burn through was also improved after coating deposition. The flame-retardant behavior changed from natural fabric to polymer composites. In conclusion, this biomass-based coating strategy demonstrated the potential of biobased flame-retardant coating for natural fiber-reinforced biobased thermoset composites.

7. Conclusions and future work

7.1. Conclusions

In this thesis, different flame-retardant approaches for FRPs were employed to develop fiber-reinforced thermoset polymer composites with fireproofing properties. This includes *i)* the bilayer epoxy resin-based polymeric coating on the substrate of glass fiber-reinforced vinyl ester resins. *ii)* the design and synthesis of cobalt-based nanohybrid to be used as a synergist for APP-filled glass fiber-reinforced epoxy composite. *iii)* A bench-scale mechanical testing instrument was designed and manufactured to verify and compare the protective effects on the flame-retardant approaches to FRPs between fire-protective surface finishing and flame retardants additives. *iv)* the development of a biomass-based flame-retardant coating on the surface of flax fiber for the development of fire-safe natural fiber/epoxy composite. Lower reaction-fire properties, as well as higher thermal/fire insulation, were pursued through the development of fireproofing FRPs.

The main conclusions are summarized as follows:

1) Using fire-protective surface finishing, the bilayer epoxy resin-based polymeric coating was developed by introducing an intumescent layer on the outer surface and an insulation layer between the outer coating layer and the laminate by using blade coating and potentially roller coating methods. The polymeric coating imparted a reduction of PHRR and TSP of 50% and 65%, respectively, in terms of heat and smoke release. The thermal/fire insulation test also displayed the superior bilayer coated laminate displayed a non-fire burn-through as well as kept temperature at 300°C for more than 12 minutes. The post-fire in-plane axial tensile properties also preserved more than 85% of its original value before fire damage. Hence, in this work, we demonstrated the comprehensive performance of fire protective coating for fireproofing FRPs. This demonstrated the fire-protective effect of surface protective finishing with minimal influence on the processability and mechanical strength of the laminate. However, due to the introduction of additional surface finishing, the THR was increased in terms of fire hazards. In addition, due to the increase in sample thickness, additional weights were added.

2) By modifying the polymer matrix, a cobalt-based nanohybrid (CNH) was designed, synthesized, and used as a synergist for both epoxy resin and APP-filled

glass fiber-reinforced epoxy composites. The CNH successfully demonstrated superior flame retardancy when partially substituted APP for the biobased epoxy resin in terms of LOI, UL94, and CCT tests. The PHRR was brought down by 74% after the incorporation of the optimal ratio of APP and CNH for epoxy resin. However, this reduction of PHRR was only around 35% for glass fiber-reinforced epoxy composites. This was elaborated by the suppressing effect of charring induced by the incorporation of glass fiber. Nevertheless, the partial substitution of APP by CNH enhanced the in-plane axial tensile properties of laminate compared to the one with only APP as the only additive. This indicated the limitations of the modification of the polymer matrix. It not only tends to decrease the mechanical strength of laminate, but also, the condensed phase effect of flame retardant would be suppressed, which lowers flame retardant efficiency.

3) In order to evaluate and compare the protective effects of different flame-retardant approaches for developing fireproofing composites, A bench scale testing machine was designed and manufactured. The protective coating demonstrated an increase of 190% in failure time compared to 17% for that of adding flame retardant additives. Although different materials were employed in the two compare sets, the main fiber reinforcement and layup of glass fiber woven fabric are the same. Hence, this may indicate the superior protective performance of the flame-retardant polymeric coating. The protective effects of coating on laminate when under off-axial was also demonstrated. Heat release behavior under this new sample size and holding configuration was also discussed.

4) Employing the fiber surface functionalization strategy, a biomass-based flame-retardant coating was designed and applied on the surface of flax fiber to form a novel fiber surface functional sizing. The intumescent coating imparts self-extinguishing effects to the coated fabric, with PHRR lowered by around 58%. The laminated with the fire protective surface sizing showed lowered fire hazards by lowering PHRR and PSP by 36% and 33%. The protective effect of heat/fire insulation was also shown in the torch fire burn-through test, which demonstrated an increase of 200% for burn-through time. This showed the potential of fiber surface functionalization strategy, especially in the use of easily flammable natural fiber as reinforcement. However, the possible influence on the prolonging of mechanical failure of laminate under fire damage needs to be future explored in the future with better fiber reinforcement layup design and processing method.

Based on current research progress, the obtained results demonstrated the importance of investigating the heat/fire insulation and mechanical properties of

laminate after and under fire when developing fireproofing FRPs. In addition, the thesis presented a new method to screen the protective effects of flame-retardant strategy on FRPs in terms of prolonging plane loading mechanical failure under fire damage at bench scale with a coupon level sample.

Lastly, this thesis also demonstrated the advantages and disadvantages of employing different flame-retardant strategies, which provides important information for bridging the material aspects of FRPs design from a coupon level toward the component level and even beyond.

7.2. Future work

While this research has provided valuable insights into flame retarded fiber-reinforced polymer composites, it is important to recognize its limitations and need for future work.

7.2.1. Flame retardant strategies on carbon-fiber reinforced polymer

In terms of materials, only glass fiber and natural fiber with lower strength and modulus than carbon fiber was used. The scope of the thesis mainly uses thermally insulative fibers. The highly thermal conductive carbon fiber brings distinct thermal degradation and fire behavior. In addition, the low resin content of CFRPs, which imparts high strength, also demonstrated the challenge of imparting flame retardancy without influencing the mechanical properties. What's more, although it is a noncombustible material, carbon fiber has also been reported to suffer from thermo-oxidative damage at high temperatures, such as in the combustion scenario. This would bring different challenges to flame retardant strategy.

To impart flame retardancy without deteriorating mechanical strength and prevent earlier mechanical failure, a novel fire-protective coating should be employed on the substrate of CFRPs with high efficacy and low dry film thickness. Silicon resin-based flame-retardant bilayer coating technology should be used in this specific scenario. In the intumescent layer, the silicon resin can toke part in the reinforcement of porous reside mechanical properties with other functional additives. In the insulation layer, the degradation product of silicon resin should toke part in the certification process. The silicon resin should be carefully selected to fulfill properties like viscosity or curing behavior toward the processing methods, such as the spray method, providing greater technological potential for the application of fire-protective coating on CFRPs for structural applications.

7.2.2. New generation bench-scale fire mechanical testing machine

In terms of methodology for screening mechanical failure of FRPs under fire for the development of fire protective material and method, the sample size is small compared to real-life applications, which may limit the generalizability of the results. The machine used a pneumatic driving system, which did not provide enough loading force for future research on CFRPs. In addition, currently, only a heat flux of 50 kW/m^2 is used, providing heat/fire damage that is not high enough for fire structural engineering.

Future improvements need to be made to develop the next generation of bench-scale testing machines. First, the hydraulic driving system can be designed and implemented to fulfill the loading requirements of CFRPs. Second, higher heat flux can be implemented by manipulating the cone heater with power control. In this manner, the influence of heat flux level on the mechanical failure of FRPs under fire damage can be investigated. Third, the correlation of new heat flux results for protected and non-protected FRPs can be investigated in a more comprehensive manner to provide bridging of heat release behavior data between the new sample size and normal cone size sample. Finally, in order to create less disruption to the normal operation of the cone calorimeter, a standalone device with moveable wheels embedded should be designed in the next generation of the machine. More automatic control units should be used instead of manual ones to increase efficiency.

List of publications, patents, and conferences

1) The listed papers have been published during the PhD study

A. First author (5)

[1] **Xiang Ao**, Junchen Xiao, Gloria Guerrero Muñoz, Carlos González*, De-Yi Wang*, Protective Coating Performance for Structural Integrity of Polymer Composites in Fire: Novel Bench Scale Instrument Design and Coupon Level Test. Composites Science and Technology, 257 (2024) 110830. https://doi.org/10.1016/j.compscitech.2024.110830

[2] **Xiang Ao**, Robert Crouse, Carlos González, De-Yi Wang*, Impact of nanohybrid on the performance of non-reinforced biocomposites and glass-fiber reinforced biocomposites: Synthesis, mechanical properties, and fire behavior, Construction and Building Materials 436 (2024) 136922. https://doi.org/10.1016/j.conbuildmat.2024.136922

[3] **Xiang Ao**, Junchen Xiao, Jose Hobson, Jimena de la Vega, Guangzhong Yin, María Luisa Puertas Cuadron, Antonio Esteban Cubillo, Carlos González, De-Yi Wang*, Bilayer coating strategy for glass fiber reinforced polymer composites toward superior fire safety and post-fire mechanical properties, Composites Communications 44 (2023) 101763. https://doi.org/10.1016/j.coco.2023.101763

[4] **Xiang Ao**, Antonio Vázquez-López, Davide Mocerino, Carlos González, De-Yi Wang*, Flame retardancy and fire mechanical properties for natural fiber/polymer composite: A review, Composites Part B: Engineering 268 (2024) 111069. https://doi.org/10.1016/j.compositesb.2023.111069

[5] **Xiang Ao**, Robert Crouse, Gloria Guerrero Muñoz, De-Yi Wang*, A Facile, Biomass-Based Coating for Flax Fabric Toward Plant Fiber Reinforced Biobased Epoxy Composite with Enhanced Fire Safety. Polymer Degradation and Stability, Under review.

B. Co-authored publications (18)

[1] Meihui Zhou, **Xiang Ao**, Monsur Islam, Yuyao Liu, Silvia González Prolongo, De-Yi Wang*, Bio-based epoxy vitrimer with inherent excellent flame retardance and recyclability via molecular design, International Journal of Biological Macromolecules 262(Pt 1) (2024) 129363. https://doi.org/10.1016/j.ijbiomac.2024.129363

[2] Guang-Zhong Yin*, Alba Marta López, Ignacio Collado, Antonio Vázquez-López, **Xiang Ao**, Jose Hobson, Silvia G. Prolongo, De-Yi Wang*, MXene Multi-Functionalization of Polyrotaxane based PCMs and the Applications in Electronic Devices Thermal Management, Nano Materials Science (2024). https://doi.org/10.1016/j.nanoms.2023.12.004

[3] Jie Xu, Xiangrong Liu, Li Wang, Yingkun Zhu, **Xiang Ao**, Fanhui Guo, Zhipeng Xie, Feng Liang, De - Yi Wang*, Jianjun Wu*, Designing of carbon nanohorn - based heterostructure for improved mechanical properties, flame retardancy, and hydrophobicity of composite aerogels, Journal of Polymer Science n/a(n/a) (2024). https://doi.org/10.1002/pol.20240355

[4] Jie Xu, **Xiang Ao**, Jimena de la Vega, Fanhui Guo, Zhipeng Xie, Feng Liang, De-Yi Wang*, Jianjun Wu*, Poly(vinyl alcohol) Composite Aerogel toward Lightweight, Remarkable Flame Retardancy, and Thermal Insulation Properties by Incorporating Carbon Nanohorns and Phytic Acid, ACS Applied Polymer Materials 6(14) (2024) 8027-8039. https://doi.org/10.1021/acsapm.4c00729

[5] Guang-Zhong Yin, Xiao-Mei Yang, Alba Marta López, **Xiang Ao**, Mei-Ting Wang, Javier García Molleja, De-Yi Wang*, PLA aerogel as a universal support for the typical organic phase change energy storage materials, Journal of Energy Storage 73 (2023) 108869. https://doi.org/10.1016/j.est.2023.108869

[6] Antonio Vazquez-Lopez, Jose Sanchez Del Rio Saez, Jimena de la Vega, **Xiang Ao**, De-Yi Wang*, All-Fabric Triboelectric Nanogenerator (AF-TENG) Smart Face Mask: Remote Long-Rate Breathing Monitoring and Apnea Alarm, ACS Sensors 8(4) (2023) 1684-1692. https://doi.org/10.1021/acssensors.2c02825

[7] Antonio Vázquez-López, **Xiang Ao**, José Sánchez del Río Saez, De-Yi Wang*, Triboelectric nanogenerator (TENG) enhanced air filtering and face masks: Recent advances, Nano Energy 114 (2023) 108635. https://doi.org/10.1016/j.nanoen.2023.108635

[8] Xiaolu Li, José Sánchez del Río Sáez, Antonio Vázquez-López, **Xiang Ao**, Raquel Sánchez Díaz, De-Yi Wang*, Eco-friendly functional cellulose paper as a fire alarming via wireless warning transmission for indoor fireproofing, Industrial Crops and Products 200 (2023) 116805. https://doi.org/10.1016/j.indcrop.2023.116805

[9] Xiaolu Li, Jose Sanchez Del Rio Saez, Shuanglan Du, Raquel Sanchez Diaz, **Xiang Ao**, De-Yi Wang*, Bio-based chitosan-based film as a bifunctional fire-

warning and humidity sensor, International Journal of Biological Macromolecules 253(Pt 3) (2023) 126466. https://doi.org/10.1016/j.ijbiomac.2023.126466

[10] Jing Zhang, **Xiang Ao**, Xiuqin Zhang, Rui Wang, Xu Jin, Wen Ye, Baoyun Xu, De-Yi Wang*, Construction of Nanomaterials Based on Molybdenum Disulfide Decorated onto a Metal–Organic Framework (UiO-66) to Improve the Fire Retardancy of Epoxy, ACS Applied Nano Materials 5(12) (2022) 17731-17740. https://doi.org/10.1021/acsanm.2c03691

[11] Abdulmalik Yusuf, José Sánchez del Río, **Xiang Ao**, Ignacio Astarloa Olaizola, De-Yi Wang*, Potential energy-assisted coupling of phase change materials with triboelectric nanogenerator enabling a thermally triggered, smart, and self-powered IoT thermal and fire hazard sensor: Design, fabrication, and applications, Nano Energy 103 (2022) 107790. https://doi.org/10.1016/j.nanoen.2022.107790

[12] Guang-Zhong Yin, Alba Marta López, Xiao-Mei Yang, **Xiang Ao**, Jose Hobson, De-Yi Wang*, Polyrotaxane based leakage-proof and injectable phase change materials with high melting enthalpy and adjustable transition temperature, Chemical Engineering Journal 444 (2022) 136421. https://doi.org/10.1016/j.cej.2022.136421

[13] José Sánchez del Río*, Abdulmalik Yusuf, **Xiang Ao**, Ignacio Astarloa Olaizola, Lucía Urbelz López-Puertas, María Yolanda Ballesteros, Romano Giannetti, Vanesa Martínez, José Luis Jiménez, José Benito Bravo Monge, Xiaosui Chen, De-Yi Wang*, High-resolution TENGS for earthquakes ground motion detection, Nano Energy 102 (2022) 107666. https://doi.org/10.1016/j.nanoen.2022.107666

[14] Xiaolu Li, José Sánchez del Río Saez, **Xiang Ao**, Abdulmalik Yusuf, De-Yi Wang*, Highly-sensitive fire alarm system based on cellulose paper with low-temperature response and wireless signal conversion, Chemical Engineering Journal 431 (2022) 134108. https://doi.org/10.1016/j.cej.2021.134108

[15] Xiaolu Li, José Sánchez del Río Saez, **Xiang Ao**, Antonio Vázquez-López, Xiaoli Xu, Baoyun Xu, De-Yi Wang*, Smart Low-temperature responsive fire alarm based on MXene/Graphene oxide film with wireless transmission: remote real-time luminosity detection, Colloids and Surfaces A: Physicochemical and Engineering Aspects (2022). https://doi.org/10.1016/j.colsurfa.2022.129641

[16] Xiaolu Li, José Sánchez del Río Saez, **Xiang Ao**, Baoyun Xu, De-Yi Wang*, Tailored P/Si-decorated graphene oxide-based fire sensor for sensitive detection at

low-temperature via local and remote wireless transmission, Construction and Building Materials 349 (2022). https://doi.org/10.1016/j.conbuildmat.2022.128600

[17] Jose Hobson, Guangzhong Yin, Xiaoli Yu, X. Zhou, Silvia Gonzalez Prolongo, **Xiang Ao**, De-Yi Wang*, Synergistic Effect of Cerium Oxide for Improving the Fire-Retardant, Mechanical and Ultraviolet-Blocking Properties of EVA/Magnesium Hydroxide Composites, Materials 15(17) (2022) 5867. https://doi.org/10.3390/ma15175867

[18] Wenliang Feng, Jing Zhang, Abdulmalik Yusuf, **Xiang Ao**, Dongfeng Shi, Vinodkumar Etacheri*, De-Yi Wang*, Quasi-solid-state sodium-ion hybrid capacitors enabled by UiO-66@PVDF-HFP multifunctional separators: Selective charge transfer and high fire safety, Chemical Engineering Journal 427 (2022) 130919. https://doi.org/10.1016/j.cej.2021.130919

2) The listed patents have been granted during the PhD study

[1] De-Yi Xiang, Xiang Ao. Dispositivo de Prueba Mecánica Acoplable a Un Calorímetro De Cono, ES1308130U [P]. 2024.

[2] José Sánchez del Río Sáez, De-Yi Wang, David Patrizi García, Xiang Ao, Alejandro Ureña Fernández, María Sánchez Martínez, Xoan Xosé Fernández Sanchez-Romate, Dispositivo de monitorización de la respiración, ES2935558 [P]. 2024.

[3] José Sánchez del Río Sáez, Tomás Sánchez Villaluenga, Alberto Brunete González, De-Yi Wang, Jie Xu, Xiang Ao, Dispositivo portable y comunicado de detección de impactos y monitorización del estado del usuario que lo porta, y sistema que lo comprende, ES2958227 [P]. 2024.

3) Presentation and poster in conferences during the PhD study:

[1] **Xiang Ao**, Carlos González, De-Yi Wang*. Bilayer Coating with Coupled Intumescent and Creamification Effects Toward High Fire Safety and Fire Structural Survivability of Fiber-Reinforced Polymer Composites. **Poster presentation** in European Meeting on Fire Retardant Polymeric Materials, 26 – 29 June 2023, Zurich, Switzerland.

[2] **Xiang Ao**, Carlos González, De-Yi Wang*. Bilayer Coating with Coupled Intumescent and Creamification Effects Toward High Fire Safety and Fire

Structural Survivability of Fiber-Reinforced Polymer Composites. **Poster presentation** at International Conference on Eco-Friendly Additives and Materials (ECOFRAM 2024), 22 – 23 May 2024, Valencia, Spain.

References

[1] E.J. Barbero, Introduction to composite materials design, CRC Press2010. https://doi.org/10.1201/9781315296494.
[2] H. Dodiuk, Handbook of thermoset plastics, William Andrew2014. https://doi.org/10.1016/C2019-0-03750-8.
[3] D.V. Rosato, D.V. Rosato, Reinforced plastics handbook, Elsevier2004. https://doi.org/10.1016/B978-1-85617-450-3.X5000-2.
[4] K. Daehn, R. Basuhi, J. Gregory, M. Berlinger, V. Somjit, E.A. Olivetti, Innovations to decarbonize materials industries, Nature Reviews Materials 7(4) (2021) 275-294. https://doi.org/10.1038/s41578-021-00376-y
[5] V.G. Zuin, K. Kummerer, Chemistry and materials science for a sustainable circular polymeric economy, Nat Rev Mater 7(2) (2022) 76-78. https://doi.org/10.1038/s41578-022-00415-2
[6] G. Hayes, M. Laurel, D. MacKinnon, T. Zhao, H.A. Houck, C.R. Becer, Polymers without Petrochemicals: Sustainable Routes to Conventional Monomers, Chemical Reviews 123(5) (2023) 2609-2734. https://doi.org/10.1021/acs.chemrev.2c00354
[7] R.M. Cywar, N.A. Rorrer, C.B. Hoyt, G.T. Beckham, E.Y.X. Chen, Bio-based polymers with performance-advantaged properties, Nature Reviews Materials 7(2) (2021) 83-103. https://doi.org/10.1038/s41578-021-00363-3
[8] M. Li, Y.Q. Pu, V.M. Thomas, C.G. Yoo, S. Ozcan, Y.L. Deng, K. Nelson, A.J. Ragauskas, Recent advancements of plant-based natural fiber-reinforced composites and their applications, Composites Part B-Engineering 200 (2020). https://doi.org/10.1016/j.compositesb.2020.108254
[9] W. Woigk, C.A. Fuentes, J. Rion, D. Hegemann, A.W. van Vuure, C. Dransfeld, K. Masania, Interface properties and their effect on the mechanical performance of flax fibre thermoplastic composites, Composites Part A: Applied Science and Manufacturing 122 (2019) 8-17. https://doi.org/10.1016/j.compositesa.2019.04.015
[10] W. Brouwer, Natural fibre composites: where can flax compete with glass?, Sampe Journal 36(6) (2000) 18-23.
[11] R. Kozlowski, M. Wladyka-Przybylak, Flammability and fire resistance of composites reinforced by natural fibers, Polymers for Advanced Technologies 19(6) (2008) 446-453. https://doi.org/10.1002/pat.1135
[12] W. Obande, C.M. Ó Brádaigh, D. Ray, Continuous fibre-reinforced thermoplastic acrylic-matrix composites prepared by liquid resin infusion – A review, Composites Part B: Engineering 215 (2021) 108771. https://doi.org/10.1016/j.compositesb.2021.108771
[13] J. Green, Mechanisms for flame retardancy and smoke suppression-a review, Journal of Fire Sciences 14(6) (1996) 426-442. https://doi.org/10.1177/073490419601400602
[14] F. Laoutid, L. Bonnaud, M. Alexandre, J.M. Lopez-Cuesta, P. Dubois, New prospects in flame retardant polymer materials: From fundamentals to nanocomposites, Materials Science and Engineering: R: Reports 63(3) (2009) 100-125. https://doi.org/10.1016/j.mser.2008.09.002

[15] S.T. Lazar, T.J. Kolibaba, J.C. Grunlan, Flame-retardant surface treatments, Nature Reviews Materials 5(4) (2020) 259-275. https://doi.org/10.1038/s41578-019-0164-6
[16] M.E. Mngomezulu, M.J. John, V. Jacobs, A.S. Luyt, Review on flammability of biofibres and biocomposites, Carbohydrate Polymers 111 (2014) 149-82. https://doi.org/10.1016/j.carbpol.2014.03.071
[17] G. Sanchez-Olivares, S. Rabe, R. Perez-Chavez, F. Calderas, B. Schartel, Industrial-waste agave fibres in flame-retarded thermoplastic starch biocomposites, Composites Part B: Engineering 177 (2019) 107370. https://doi.org/10.1016/j.compositesb.2019.107370
[18] M. Kim, J. Choe, Development of the fire retardant glass fabric/carbonized phenolic composite, Composite Structures 148 (2016) 191-197. https://doi.org/10.1016/j.compstruct.2016.04.003
[19] C.I. Idumah, A. Hassan, Emerging trends in flame retardancy of biofibers, biopolymers, biocomposites, and bionanocomposites, Reviews in Chemical Engineering 32(1) (2016) 115-148. https://doi.org/10.1515/revce-2015-0017
[20] R. Sonnier, A. Taguet, L. Ferry, J.-M. Lopez-Cuesta, Flame Retardancy of Natural Fibers Reinforced Composites, Towards Bio-based Flame Retardant Polymers, Springer International Publishing2018, pp. 73-98 https://doi.org/10.1007/978-3-319-67083-6_3.
[21] Y.M. Ghazzawi, A.F. Osorio, M.T. Heitzmann, Fire performance of continuous glass fibre reinforced polycarbonate composites: the effect of fibre architecture on the fire properties of polycarbonate composites, Journal of Composite Materials 53(12) (2019) 1705-1715. https://doi.org/10.1177/0021998318808052
[22] L. Atabek Savas, A. Mutlu, A.S. Dike, U. Tayfun, M. Dogan, Effect of carbon fiber amount and length on flame retardant and mechanical properties of intumescent polypropylene composites, Journal of Composite Materials 52(4) (2018) 519-530. https://doi.org/10.1177/0021998317710
[23] Y.M. Ghazzawi, A.F. Osorio, M.T. Heitzmann, The effect of fibre length and fibre type on the fire performance of thermoplastic composites: The behaviour of polycarbonate as an example of a charring matrix, Construction and Building Materials 234 (2020) 117889. https://doi.org/10.1016/j.conbuildmat.2019.117889
[24] S. Eibl, D. Swanson, Influence of out - of - plane fiber orientation on reaction - to - fire properties of carbon fiber reinforced polymer matrix composites, Fire and Materials 42(2) (2017) 234-243. https://doi.org/10.1002/fam.2484
[25] K. Grigoriou, A.P. Mouritz, Influence of ply stacking pattern on the structural properties of quasi-isotropic carbon-epoxy laminates in fire, Composites Part A: Applied Science and Manufacturing 99 (2017) 113-120. https://doi.org/10.1016/j.compositesa.2017.04.008
[26] L. Zhang, H. Wang, J. Zhang, Y. Tian, J. Li, X. Chen, Experimental study on the influence of different laying methods on the thermomechanical properties of carbon fiber/epoxy hybrid composite, Materials Research Express 7(2) (2020) 025601. https://doi.org/10.1088/2053-1591/ab6d29
[27] G. Camino, L. Costa, M.L. Di Cortemiglia, Overview of fire retardant mechanisms, Polymer Degradation and Stability 33(2) (1991) 131-154. https://doi.org/10.1016/0141-3910(91)90014-I

[28] Y.J. Xu, L.Y. Qu, Y. Liu, P. Zhu, An overview of alginates as flame-retardant materials: Pyrolysis behaviors, flame retardancy, and applications, Carbohydrate Polymers 260 (2021) 117827. https://doi.org/10.1016/j.carbpol.2021.117827
[29] X. Wang, E.N. Kalali, J.-T. Wan, D.-Y. Wang, Carbon-family materials for flame retardant polymeric materials, Progress in Polymer Science 69 (2017) 22-46. https://doi.org/10.1016/j.progpolymsci.2017.02.001
[30] L. Zhang, Z. Li, D.-Y. Wang, Polydopamine-assisted strategies for preparation of fire-safe polymeric materials: A review, European Polymer Journal 138 (2020) 109973. https://doi.org/10.1016/j.eurpolymj.2020.109973
[31] A.P. Mouritz, A.G. Gibson, Fire properties of polymer composite materials, Springer Science & Business Media2007. https://doi.org/10.1007/978-1-4020-5356-6.
[32] A.P. Mouritz, Post-fire flexural properties of fibre-reinforced polyester, epoxy and phenolic composites, Journal of Materials Science 37(7) (2002) 1377-1386. https://doi.org/10.1023/a:1014520628915
[33] M. Bazli, M. Abolfazli, Mechanical Properties of Fibre Reinforced Polymers under Elevated Temperatures: An Overview, Polymers (Basel) 12(11) (2020) 2600. https://doi.org/10.3390/polym12112600
[34] C. Katsoulis, B.K. Kandola, P. Myler, E. Kandare, Post-fire flexural performance of epoxy-nanocomposite matrix glass fibre composites containing conventional flame retardants, Composites Part A: Applied Science and Manufacturing 43(8) (2012) 1389-1399. https://doi.org/10.1016/j.compositesa.2012.03.009
[35] C. Zhu, J. Li, M. Clement, X. Yi, C. Rudd, X. Liu, The effect of intumescent mat on post-fire performance of carbon fibre reinforced composites, Journal of Fire Sciences 37(3) (2019) 257-272. https://doi.org/10.1177/0734904119849395
[36] H. Li, E. Kandare, S. Li, Y. Wang, B.K. Kandola, P. Myler, A.R. Horrocks, Integrated thermal, micro- and macro-mechanical modelling of post-fire flexural behaviour of flame-retarded glass/epoxy composites, Computational Materials Science 59 (2012) 22-32. https://doi.org/10.1016/j.commatsci.2012.02.026
[37] F.K. Özmen, M.E. Üreyen, A.S. Koparal, Cleaner production of flame-retardant-glass reinforced epoxy resin composite for aviation and reducing smoke toxicity, Journal of Cleaner Production 276 (2020) 124065. https://doi.org/10.1016/j.jclepro.2020.124065
[38] A. Moriyama, T. Hasegawa, C. Nagaya, K. Hamada, T. Himaki, M. Murakami, M. Horie, J. Takahashi, H. Iwahashi, H. Moritomi, Assessment of harmfulness and biological effect of carbon fiber dust generated during new carbon fiber recycling method, Journal of Hazardous Materials 378 (2019) 120777. https://doi.org/10.1016/j.jhazmat.2019.120777
[39] L. Greiner, M. Döring, S. Eibl, Prevention of the formation of respirable fibers in carbon fiber reinforced epoxy resins during combustion by phosphorus or silicon containing flame retardants, Polymer Degradation and Stability 185 (2021) 109497. https://doi.org/10.1016/j.polymdegradstab.2021.109497
[40] S. Eibl, Potential for the formation of respirable fibers in carbon fiber reinforced plastic materials after combustion, Fire and Materials 41(7) (2017) 808-816. https://doi.org/10.1002/fam.2423

[41] A.P. Mouritz, S. Feih, E. Kandare, Z. Mathys, A.G. Gibson, P.E. Des Jardin, S.W. Case, B.Y. Lattimer, Review of fire structural modelling of polymer composites, Composites Part A: Applied Science and Manufacturing 40(12) (2009) 1800-1814. https://doi.org/10.1016/j.compositesa.2009.09.001
[42] B. Vieille, A. Alia, A. Coppalle, L. Lin, In situ tensile behavior of hybrid carbon and glass fibers reinforced PEEK laminates: Isothermal or fire testing conditions, Composites Part B: Engineering 262 (2023) 110807. https://doi.org/10.1016/j.compositesb.2023.110807
[43] B. Vieille, A. Coppalle, L. Le Pluart, E. Schuhler, A. Chaudhary, B. Rijal, A. Alia, N. Delpouve, Kerosene flame behaviour of C/PEKK composite laminates: Influence of exposure time and laminates lay-up on residual mechanical properties, Composites Part B: Engineering 222 (2021). https://doi.org/10.1016/j.compositesb.2021.109046
[44] T.S. Bhat, V.S. Chevali, A.P. Mouritz, FIRE STRUCTURAL PERFORMANCE OF FLAX FIBRE REINFORCED LAMINATES, 20th International Conference on Composite Materials (ICCM), Aalborg Univ Press, Copenhagen, DENMARK, 2015.
[45] T. Bhat, V. Chevali, X. Liu, S. Feih, A.P. Mouritz, Fire structural resistance of basalt fibre composite, Composites Part A: Applied Science and Manufacturing 71 (2015) 107-115. https://doi.org/10.1016/j.compositesa.2015.01.006
[46] J. Sim, C. Park, D.Y. Moon, Characteristics of basalt fiber as a strengthening material for concrete structures, Composites Part B: Engineering 36(6-7) (2005) 504-512. https://doi.org/10.1016/j.compositesb.2005.02.002
[47] B.W. Liu, H.B. Zhao, Y.Z. Wang, Advanced Flame-Retardant Methods for Polymeric Materials, Advanced Materials 34(46) (2022) e2107905. https://doi.org/10.1002/adma.202107905
[48] W. He, P. Song, B. Yu, Z. Fang, H. Wang, Flame retardant polymeric nanocomposites through the combination of nanomaterials and conventional flame retardants, Progress in Materials Science 114 (2020) 100687. https://doi.org/10.1016/j.pmatsci.2020.100687
[49] B.K. Kandola, F. Magnoni, J.R. Ebdon, Flame retardants for epoxy resins: Application - related challenges and solutions, Journal of Vinyl and Additive Technology (2022). https://doi.org/10.1002/vnl.21890
[50] L. Zhang, Z. Li, Q.-Q. Bi, L.-Y. Jiang, X.-D. Zhang, E. Tang, X.-M. Cao, H.-F. Li, J. Hobson, D.-Y. Wang, Strong yet tough epoxy with superior fire suppression enabled by bio-based phosphaphenanthrene towards in-situ formed Diels-Alder network, Composites Part B: Engineering 251 (2023) 110490. https://doi.org/10.1016/j.compositesb.2022.110490
[51] Y. Hou, Z. Xu, R. An, H. Zheng, W. Hu, K. Zhou, Recent progress in black phosphorus nanosheets for improving the fire safety of polymer nanocomposites, Composites Part B: Engineering 249 (2023) 110404. https://doi.org/10.1016/j.compositesb.2022.110404
[52] S. Araby, B. Philips, Q. Meng, J. Ma, T. Laoui, C.H. Wang, Recent advances in carbon-based nanomaterials for flame retardant polymers and composites, Composites Part B: Engineering 212 (2021) 108675. https://doi.org/10.1016/j.compositesb.2021.108675
[53] X. Ao, A. Vázquez-López, D. Mocerino, C. González, D.-Y. Wang, Flame retardancy and fire mechanical properties for natural fiber/polymer composite: A

review, Composites Part B: Engineering 268 (2024) 111069. https://doi.org/10.1016/j.compositesb.2023.111069
[54] Á. Pomázi, A. Toldy, Multifunctional Gelcoats for Fiber Reinforced Composites, Coatings 9(3) (2019) 173. https://doi.org/10.3390/coatings9030173
[55] E. Kandare, B.K. Kandola, P. Myler, Evaluating the influence of varied fire-retardant surface coatings on post-heat flexural properties of glass/epoxy composites, Fire Safety Journal 58 (2013) 112-120. https://doi.org/10.1016/j.firesaf.2013.01.009
[56] B.K. Kandola, W. Bhatti, E. Kandare, A comparative study on the efficacy of varied surface coatings in fireproofing glass/epoxy composites, Polymer Degradation and Stability 97(11) (2012) 2418-2427. https://doi.org/10.1016/j.polymdegradstab.2012.07.023
[57] B.K. Kandola, L. Krishnan, J.R. Ebdon, Blends of unsaturated polyester and phenolic resins for application as fire-resistant matrices in fibre-reinforced composites: Effects of added flame retardants, Polymer Degradation and Stability 106 (2014) 129-137. https://doi.org/10.1016/j.polymdegradstab.2013.12.021
[58] Á. Pomázi, M. Krecz, A. Toldy, Thermal behaviour and fire and mechanical performance of carbon fibre-reinforced epoxy composites coated with flame-retardant epoxy gelcoats, Journal of Thermal Analysis and Calorimetry 148(7) (2023) 2685-2702. https://doi.org/10.1007/s10973-022-11710-z
[59] Á. Pomázi, M. Krecz, A. Toldy, The effect of the combined application of solid- and gas-phase flame retardants in epoxy gelcoats on the thermal stability, fire performance and adhesion of coated carbon fibre–reinforced epoxy composites, Journal of Thermal Analysis and Calorimetry (2022). https://doi.org/10.1007/s10973-022-11770-1
[60] P. Luangtriratana, B.K. Kandola, P. Myler, Ceramic particulate thermal barrier surface coatings for glass fibre-reinforced epoxy composites, Materials & Design 68 (2015) 232-244. https://doi.org/10.1016/j.matdes.2014.11.057
[61] P. Luangtriratana, B.K. Kandola, J.R. Ebdon, UV-polymerisable, phosphorus-containing, flame-retardant surface coatings for glass fibre-reinforced epoxy composites, Progress in Organic Coatings 78 (2015) 73-82. https://doi.org/10.1016/j.porgcoat.2014.10.004
[62] K. Williams, J.R. Ebdon, B.K. Kandola, Intumescent fire - retardant coatings for plastics based on poly(vinylphosphonic acid): Improving water resistance with comonomers, Journal of Applied Polymer Science 137(1) (2019). https://doi.org/10.1002/app.47601
[63] S. Bourbigot, B. Gardelle, S. Duquesne, Intumescent silicone-based coatings for the fire protection of carbon fiber reinforced composites, Fire Safety Science 11 (2014) 781-793. https://doi.org/10.3801/IAFSS.FSS.11-781
[64] E. Kandare, C. Chukwudolue, B.K. Kandola, The use of fire - retardant intumescent mats for fire and heat protection of glass fibre - reinforced polyester composites: Thermal barrier properties, Fire and Materials 34(1) (2009) 21-38. https://doi.org/10.1002/fam.1000
[65] E. Kandare, P. Luangtriratana, B.K. Kandola, Fire reaction properties of flax/epoxy laminates and their balsa-core sandwich composites with or without fire protection, Composites Part B: Engineering 56 (2014) 602-610. https://doi.org/10.1016/j.compositesb.2013.08.090

[66] J. Li, C. Zhu, Z. Zhao, P. Khalili, M. Clement, J. Tong, X. Liu, X. Yi, Fire properties of carbon fiber reinforced polymer improved by coating nonwoven flame retardant mat for aerospace application, Journal of Applied Polymer Science 136(30) (2019) 47801. https://doi.org/10.1002/app.47801
[67] F.-Q. Zhang, Y.-Z. Zhao, Y.-J. Xu, Y. Liu, P. Zhu, Flame retardation of vinyl ester resins and their glass fiber reinforced composites via liquid DOPO-containing 1-vinylimidazole salts, Composites Part B: Engineering 234 (2022) 109697. https://doi.org/10.1016/j.compositesb.2022.109697
[68] T. Liu, J. Peng, J. Liu, X. Hao, C. Guo, R. Ou, Z. Liu, Q. Wang, Fully recyclable, flame-retardant and high-performance carbon fiber composites based on vanillin-terminated cyclophosphazene polyimine thermosets, Composites Part B: Engineering 224 (2021) 109188. https://doi.org/10.1016/j.compositesb.2021.109188
[69] Y. Xiao, X. Mu, B. Wang, W. Hu, J. Wang, F. Zhou, C. Ma, Y. Hu, L. Song, A novel phosphorous-containing polymeric compatibilizer: Effective reinforcement and flame retardancy in glass fiber reinforced polyamide 6 composites, Composites Part B: Engineering 205 (2021) 108536. https://doi.org/10.1016/j.compositesb.2020.108536
[70] M.M. Velencoso, A. Battig, J.C. Markwart, B. Schartel, F.R. Wurm, Molecular Firefighting-How Modern Phosphorus Chemistry Can Help Solve the Challenge of Flame Retardancy, Angewandte Chemie. International Edition in English 57(33) (2018) 10450-10467. https://doi.org/10.1002/anie.201711735
[71] R.M. Perez, J.K.W. Sandler, V. Altstädt, T. Hoffmann, D. Pospiech, M. Ciesielski, M. Döring, Effect of DOP-based compounds on fire retardancy, thermal stability, and mechanical properties of DGEBA cured with 4,4′ -DDS, Journal of Materials Science 41(2) (2006) 341-353. https://doi.org/10.1007/s10853-005-2720-2
[72] B. Perret, B. Schartel, K. Stöß, M. Ciesielski, J. Diederichs, M. Döring, J. Krämer, V. Altstädt, Novel DOPO-based flame retardants in high-performance carbon fibre epoxy composites for aviation, European Polymer Journal 47(5) (2011) 1081-1089. https://doi.org/10.1016/j.eurpolymj.2011.02.008
[73] B. Schartel, A.I. Balabanovich, U. Braun, U. Knoll, J. Artner, M. Ciesielski, M. Döring, R. Perez, J.K.W. Sandler, V. Altstädt, T. Hoffmann, D. Pospiech, Pyrolysis of epoxy resins and fire behavior of epoxy resin composites flame-retarded with 9,10-dihydro-9-oxa-10-phosphaphenanthrene-10-oxide additives, Journal of Applied Polymer Science 104(4) (2007) 2260-2269. https://doi.org/10.1002/app.25660
[74] B. Perret, B. Schartel, K. Stöß, M. Ciesielski, J. Diederichs, M. Döring, J. Krämer, V. Altstädt, A New Halogen-Free Flame Retardant Based on 9,10-Dihydro-9-oxa-10-phosphaphenanthrene-10-oxide for Epoxy Resins and their Carbon Fiber Composites for the Automotive and Aviation Industries, Macromolecular Materials and Engineering 296(1) (2011) 14-30. https://doi.org/10.1002/mame.201000242
[75] C. Campana, R. Leger, R. Sonnier, P. Ienny, L. Ferry, Effect of Hygrothermal Ageing on the Mechanical and Fire Properties of a Flame Retardant Flax Fiber/Epoxy Composite, Polymers (Basel) 14(19) (2022) 20. https://doi.org/10.3390/polym14193962
[76] Z. Wei, Z. Yang, Z. Chen, T. Yu, Q. Li, W. Yang, Y. Li, Bio-inspired dopamine-functionalized silica nanoparticles via self-polymerization to simultaneously

enhance thermal stability, fire safety and dynamic mechanical properties of PFRP composites, Journal of Thermal Analysis and Calorimetry 148(5) (2022) 1935-1948. https://doi.org/10.1007/s10973-022-11857-9
[77] X. Zhang, J. Wu, Z. Qin, Y.-T. Pan, Z. Geng, X. Wu, W. Zhang, R. Yang, Intrinsic flame-retardant vinyl ester resin and its fiberglass-reinforced composite with excellent comprehensive properties by structural design, Polymer Degradation and Stability 218 (2023) 110561. https://doi.org/10.1016/j.polymdegradstab.2023.110561
[78] C. Thiyagu, U. NarendraKumar, Effect of ammonium polyphosphate on fire - retardant, mechanical, and vibrational analysis of epoxy/glass/ramie hybrid composite, Polymer Composites 44(1) (2022) 621-631. https://doi.org/10.1002/pc.27123
[79] E.V. Bachtiar, K. Kurkowiak, L. Yan, B. Kasal, T. Kolb, Thermal Stability, Fire Performance, and Mechanical Properties of Natural Fibre Fabric-Reinforced Polymer Composites with Different Fire Retardants, Polymers (Basel) 11(4) (2019) 16. https://doi.org/10.3390/polym11040699
[80] M. Ejaz, M.M. Azad, A.u.R. Shah, S.K. Afaq, J.-i. Song, Synergistic effect of aluminum trihydrate and zirconium hydroxide nanoparticles on mechanical properties, flammability, and thermal degradation of polyester/jute fiber composite, Cellulose 29(3) (2022) 1775-1790. https://doi.org/10.1007/s10570-022-04417-9
[81] A. Pomazi, A. Toldy, Particle Distribution of Solid Flame Retardants in Infusion Moulded Composites, Polymers (Basel) 9(7) (2017). https://doi.org/10.3390/polym9070250
[82] A. Toldy, Á. Pomázi, B. Szolnoki, The effect of manufacturing technologies on the flame retardancy of carbon fibre reinforced epoxy resin composites, Polymer Degradation and Stability 174 (2020) 109094. https://doi.org/10.1016/j.polymdegradstab.2020.109094
[83] L. Boccarusso, L. Carrino, M. Durante, A. Formisano, A. Langella, F. Memola Capece Minutolo, Hemp fabric/epoxy composites manufactured by infusion process: Improvement of fire properties promoted by ammonium polyphosphate, Composites Part B: Engineering 89 (2016) 117-126. https://doi.org/10.1016/j.compositesb.2015.10.045
[84] A. Bifulco, J. Chen, A. Sekar, W.W. Klingler, A. Gooneie, S. Gaan, Recycling of flame retardant polymers: Current technologies and future perspectives, Journal of Materials Science & Technology (2024). https://doi.org/10.1016/j.jmst.2024.02.039
[85] P.-X. Tian, Y.-D. Li, Y. Weng, Z. Hu, J.-B. Zeng, Reprocessable, chemically recyclable, and flame-retardant biobased epoxy vitrimers, European Polymer Journal (2023) 112078. https://doi.org/10.1016/j.eurpolymj.2023.112078
[86] P.-X. Tian, Y.-D. Li, Z. Hu, J.-B. Zeng, Flame-retardant epoxy vitrimers with high strength and high-Tg for recyclable carbon fiber-reinforced composites, Composites Communications 47 (2024) 101870. https://doi.org/10.1016/j.coco.2024.101870
[87] P.-X. Tian, Y.-D. Li, Z. Hu, J.-B. Zeng, Fire-resistant and high-performance epoxy vitrimers for fully recyclable carbon fiber-reinforced composites, Materials Today Chemistry 36 (2024) 101965. https://doi.org/10.1016/j.mtchem.2024.101965

[88] W. Gieparda, S. Rojewski, S. Wüstenhagen, A. Kicinska-Jakubowska, A. Krombholz, Chemical modification of natural fibres to epoxy laminate for lightweight constructions, Composites Part A: Applied Science and Manufacturing 140 (2021) 10. https://doi.org/10.1016/j.compositesa.2020.106171
[89] L. Zhang, Y. Ou, D.Y. Wang, Surface functionalization of carbon fabric towards high-performance epoxy composites via enhanced fiber–matrix interfacial strength and intergrowth charring behavior, Express Polymer Letters 15(6) (2021) 503-514. https://doi.org/10.3144/expresspolymlett.2021.43
[90] F. Chu, X. Yu, Y. Hou, X. Mu, L. Song, W. Hu, A facile strategy to simultaneously improve the mechanical and fire safety properties of ramie fabric-reinforced unsaturated polyester resin composites, Composites Part A: Applied Science and Manufacturing 115 (2018) 264-273. https://doi.org/10.1016/j.compositesa.2018.10.006
[91] J. Taibi, S. Rouif, J.-L. Clément, B. Ameduri, R. Sonnier, B. Otazaghine, Flame retardancy of flax fibers by pre-irradiation grafting of a phosphonate monomer, Industrial Crops and Products 176 (2022) 114334. https://doi.org/10.1016/j.indcrop.2021.114334
[92] R. Sonnier, B. Otazaghine, A. Viretto, G. Apolinario, P. Ienny, Improving the flame retardancy of flax fabrics by radiation grafting of phosphorus compounds, European Polymer Journal 68 (2015) 313-325. https://doi.org/10.1016/j.eurpolymj.2015.05.005
[93] X.-H. Shi, Y.-J. Xu, J.-W. Long, Q. Zhao, X.-M. Ding, L. Chen, Y.-Z. Wang, Layer-by-layer assembled flame-retardant architecture toward high-performance carbon fiber composite, Chemical Engineering Journal 353 (2018) 550-558. https://doi.org/10.1016/j.cej.2018.07.146
[94] X.-C. Jiang, P. Li, Y. Liu, Y.-W. Yan, P. Zhu, Preparation and properties of APP flame-retardant ramie fabric reinforced epoxy resin composites, Industrial Crops and Products 197 (2023) 116611. https://doi.org/10.1016/j.indcrop.2023.116611
[95] W. Guo, E.N. Kalali, X. Wang, W. Xing, P. Zhang, L. Song, Y. Hu, Processing bulk natural bamboo into a strong and flame-retardant composite material, Industrial Crops and Products 138 (2019) 111478. https://doi.org/10.1016/j.indcrop.2019.111478
[96] P. Khalili, B. Blinzler, R. Kadar, R. Bisschop, M. Forsth, P. Blomqvist, Flammability, Smoke, Mechanical Behaviours and Morphology of Flame Retarded Natural Fibre/Elium((R)) Composite, Materials (Basel) 12(17) (2019) 2648. https://doi.org/10.3390/ma12172648
[97] X. Song, F. Song, X.-M. Ding, J.-M. Wu, X.-H. Wang, F. Wang, R. Feng, X.-L. Wang, Y.-Z. Wang, Construction of bio-based ramie fabric/epoxy resin composites with high flame retardant and mechanical performances, Industrial Crops and Products 194 (2023) 116281. https://doi.org/https://doi.org/10.1016/j.indcrop.2023.116281
[98] M. Tirrell, Polyelectrolyte Complexes: Fluid or Solid?, ACS Cent Sci 4(5) (2018) 532-533. https://doi.org/10.1021/acscentsci.8b00284
[99] V.S. Meka, M.K.G. Sing, M.R. Pichika, S.R. Nali, V.R.M. Kolapalli, P. Kesharwani, A comprehensive review on polyelectrolyte complexes, Drug

Discovery Today 22(11) (2017) 1697-1706. https://doi.org/10.1016/j.drudis.2017.06.008
[100] X.-H. Shi, L. Chen, B.-W. Liu, J.-W. Long, Y.-J. Xu, Y.-Z. Wang, Carbon Fibers Decorated by Polyelectrolyte Complexes Toward Their Epoxy Resin Composites with High Fire Safety, Chinese Journal of Polymer Science 36(12) (2018) 1375-1384. https://doi.org/10.1007/s10118-018-2164-1
[101] X.-H. Shi, L. Chen, Q. Zhao, J.-W. Long, Y.-M. Li, Y.-Z. Wang, Epoxy resin composites reinforced and fire-retarded by surficially-treated carbon fibers via a tunable and facile process, Composites Science and Technology 187 (2020) 107945. https://doi.org/10.1016/j.compscitech.2019.107945
[102] V. Kodur, S. Venkatachari, V.A. Matsagar, S.B. Singh, Test Methods for Characterizing the Properties of Fiber-Reinforced Polymer Composites at Elevated Temperatures, Polymers (Basel) 14(9) (2022) 24. https://doi.org/10.3390/polym14091734
[103] M. Rashid, K. Chetehouna, A. Cablé, N. Gascoin, Analysing Flammability Characteristics of Green Biocomposites: An Overview, Fire Technology 57(1) (2020) 31-67. https://doi.org/10.1007/s10694-020-01001-0
[104] E. Kandare, A.K. Chukwunonso, B.K. Kandola, The effect of fire - retardant additives and a surface insulative fabric on fire performance and mechanical property retention of polyester composites, Fire and Materials 35(3) (2011) 143-155. https://doi.org/10.1002/fam.1039
[105] L. Krishnan, B.K. Kandola, J.R. Ebdon, The Effects of Some Phosphorus-Containing Fire Retardants on the Properties of Glass Fibre-Reinforced Composite Laminates Made from Blends of Unsaturated Polyester and Phenolic Resins, Journal of Composites Science 5(10) (2021) 258. https://doi.org/10.3390/jcs5100258
[106] C. Zhu, S. Li, J. Li, M. Clement, C. Rudd, X. Yi, X. Liu, Fire performance of sandwich composites with intumescent mat protection: Evolving thermal insulation, post-fire performance and rail industry testing, Fire Safety Journal 116 (2020) 103205. https://doi.org/10.1016/j.firesaf.2020.103205
[107] A.P. Mouritz, Z. Mathys, Post-fire mechanical properties of marine polymer composites, Composite Structures 47(1) (1999) 643-653. https://doi.org/10.1016/S0263-8223(00)00043-X
[108] A.P. Mouritz, Z. Mathys, Post-fire mechanical properties of glass-reinforced polyester composites, Composites Science and Technology 61(4) (2001) 475-490. https://doi.org/10.1016/S0266-3538(00)00204-9
[109] A. Anjang, V.S. Chevali, B.Y. Lattimer, S.W. Case, S. Feih, A.P. Mouritz, Post-fire mechanical properties of sandwich composite structures, Composite Structures 132 (2015) 1019-1028. https://doi.org/10.1016/j.compstruct.2015.07.009
[110] A. Anjang, A.P. Mouritz, S. Feih, Influence of fibre orientation on the tensile performance of sandwich composites in fire, Composites Part A: Applied Science and Manufacturing 100 (2017) 342-351. https://doi.org/10.1016/j.compositesa.2017.05.028
[111] T. Loh, Fire Response of Light-weight Structural Materials Under Complex Loads, RMIT University, 2018.
[112] E. Kandare, G.J. Griffin, S. Feih, A.G. Gibson, B.Y. Lattimer, A.P. Mouritz, Fire structural modelling of fibre–polymer laminates protected with an

intumescent coating, Composites Part A: Applied Science and Manufacturing 43(5) (2012) 793-802. https://doi.org/10.1016/j.compositesa.2011.05.012
[113] M. Maqsood, G. Seide, Biodegradable Flame Retardants for Biodegradable Polymer, Biomolecules 10(7) (2020) 1038. https://doi.org/10.3390/biom10071038
[114] H. Vahabi, Analysis of Flame Retardancy in Polymer Science, Elsevier2022. https://doi.org/10.1016/C2020-0-01599-9.
[115] V. Babrauskas, Ignition handbook: principles and applications to fire safety engineering, fire investigation, risk management and forensic science, Fire Science Publishers2003.
[116] Y.-M. Li, S.-L. Hu, D.-Y. Wang, Polymer-based ceramifiable composites for flame retardant applications: A review, Composites Communications 21 (2020) 100405. https://doi.org/10.1016/j.coco.2020.100405
[117] Y. Ou, C. González, J.J. Vilatela, Interlaminar toughening in structural carbon fiber/epoxy composites interleaved with carbon nanotube veils, Composites Part A: Applied Science and Manufacturing 124 (2019). https://doi.org/10.1016/j.compositesa.2019.105477
[118] R.G. Puri, A.S. Khanna, Intumescent coatings: A review on recent progress, Journal of Coatings Technology and Research 14(1) (2016) 1-20. https://doi.org/10.1007/s11998-016-9815-3
[119] P. Acuña, J. Zhang, G.-Z. Yin, X.-Q. Liu, D.-Y. Wang, Bio-based rigid polyurethane foam from castor oil with excellent flame retardancy and high insulation capacity via cooperation with carbon-based materials, Journal of Materials Science 56(3) (2020) 2684-2701. https://doi.org/10.1007/s10853-020-05125-0
[120] Y.-M. Li, C. Deng, Z.-Y. Zhao, L.-X. Han, P. Lu, Y.-Z. Wang, Carbon fiber-based polymer composite via ceramization toward excellent electromagnetic interference shielding performance and high temperature resistance, Composites Part A: Applied Science and Manufacturing 131 (2020). https://doi.org/10.1016/j.compositesa.2020.105769
[121] L. Wang, J. Wang, L. Zheng, Z. Li, L. Wu, X. Wang, Superelastic, Anticorrosive, and Flame-Resistant Nitrogen-Containing Resorcinol Formaldehyde/Graphene Oxide Composite Aerogels, ACS Sustainable Chemistry & Engineering 7(12) (2019) 10873-10879. https://doi.org/10.1021/acssuschemeng.9b01735
[122] L. Wang, S. Wu, X. Dong, R. Wang, L. Zhang, J. Wang, J. Zhong, L. Wu, X. Wang, A pre-constructed graphene–ammonium polyphosphate aerogel (GAPPA) for efficiently enhancing the mechanical and fire-safety performances of polymers, Journal of Materials Chemistry A 6(10) (2018) 4449-4457. https://doi.org/10.1039/c8ta00736e
[123] P. Acuña, X. Lin, M.S. Calvo, Z. Shao, N. Pérez, F. Villafañe, M.Á. Rodríguez-Pérez, D.-Y. Wang, Synergistic effect of expandable graphite and phenylphosphonic-aniline salt on flame retardancy of rigid polyurethane foam, Polymer Degradation and Stability 179 (2020). https://doi.org/10.1016/j.polymdegradstab.2020.109274
[124] L. Zhang, J. Zhang, D.-Y. Wang, Hierarchical layered double hydroxide nanosheets/phosphorus-containing organosilane functionalized hollow glass microsphere towards high performance epoxy composite: Enhanced interfacial

adhesion and bottom-up charring behavior, Polymer 210 (2020) 123018. https://doi.org/10.1016/j.polymer.2020.123018
[125] A.B. Morgan, Non-halogenated flame retardant handbook, John Wiley & Sons2021. https://doi.org/10.1002/9781118939239.
[126] T. Chu, Y. Lu, B. Hou, P. Jafari, Z. Zhou, H. Peng, S. Huo, P. Song, The application of ammonium polyphosphate in unsaturated polyester resins: A mini review, Polymer Degradation and Stability 225 (2024) 110796. https://doi.org/10.1016/j.polymdegradstab.2024.110796
[127] Z.-B. Shao, X. Song, T.-C. Wang, J. Cui, W. Ye, B. Xu, D.-Y. Wang, Facile Fabrication of organic zirconium/inorganic phosphorus complex for super-efficiently flame-retardant epoxy resin, Composites Communications 36 (2022) 101360. https://doi.org/10.1016/j.coco.2022.101360
[128] K. Song, Y.-T. Pan, J. Zhang, P. Song, J. He, D.-Y. Wang, R. Yang, Metal–Organic Frameworks–Based Flame-Retardant System for Epoxy Resin: A Review and Prospect, Chemical Engineering Journal 468 (2023) 143653. https://doi.org/10.1016/j.cej.2023.143653
[129] J. Zhang, Z. Li, X.L. Qi, D.Y. Wang, Recent Progress on Metal-Organic Framework and Its Derivatives as Novel Fire Retardants to Polymeric Materials, Nanomicro Lett 12(1) (2020) 173. https://doi.org/10.1007/s40820-020-00497-z
[130] J. Lin, K. Wang, J. Li, D. Yang, Y. Zhu, X. Wang, Growing metal–organic framework nanoparticles on short carbon fibers to improve flame retardancy, smoke suppression and mechanical properties of the flame retardant epoxy composites, Journal of Materials Science 56(36) (2021) 19899-19914. https://doi.org/10.1007/s10853-021-06507-8
[131] V. Unnikrishnan, O. Zabihi, Q. Li, M. Ahmadi, M.R.G. Ferdowsi, T. Kannangara, P. Blanchard, A. Kiziltas, P. Joseph, M. Naebe, Multifunctional PA6 composites using waste glass fiber and green metal organic framework/graphene hybrids, Polymer Composites 43(9) (2022) 5877-5893. https://doi.org/10.1002/pc.27002
[132] R. Samiee, S. Montazeri, B. Ramezanzadeh, M. Mahdavian, Ce-MOF nanorods/aluminum hydroxide (AlTH) synergism effect on the fire-retardancy/smoke-release and thermo-mechanical properties of a novel thermoplastic acrylic intumescent composite coating, Chemical Engineering Journal 428 (2022) 132533. https://doi.org/10.1016/j.cej.2021.132533
[133] Y.T. Pan, L. Zhang, X. Zhao, D.Y. Wang, Interfacial engineering of renewable metal organic framework derived honeycomb-like nanoporous aluminum hydroxide with tunable porosity, Chem Sci 8(5) (2017) 3399-3409. https://doi.org/10.1039/c6sc05695d
[134] B. Schartel, T.R. Hull, Development of fire - retarded materials — Interpretation of cone calorimeter data, Fire and Materials 31(5) (2007) 327-354. https://doi.org/10.1002/fam.949
[135] Y. Hu, X. Wang, Flame Retardant Polymeric Materials: A Handbook, CRC Press2019. https://doi.org/10.1201/b22345.
[136] J. Alongi, Z. Han, S. Bourbigot, Intumescence: Tradition versus novelty. A comprehensive review, Progress in Polymer Science 51 (2015) 28-73. https://doi.org/10.1016/j.progpolymsci.2015.04.010

[137] A. Sandinge, P. Blomqvist, M. Rahm, A modified specimen holder for cone calorimeter testing of composite materials to reduce influence from specimen edges, Fire and Materials 46(1) (2021) 80-94. https://doi.org/10.1002/fam.2949
[138] B. Perret, B. Schartel, K. Stöß, M. Ciesielski, J. Diederichs, M. Döring, J. Krämer, V. Altstädt, A New Halogen - Free Flame Retardant Based on 9,10 - Dihydro - 9 - oxa - 10 - phosphaphenanthrene - 10 - oxide for Epoxy Resins and their Carbon Fiber Composites for the Automotive and Aviation Industries, Macromolecular Materials and Engineering 296(1) (2010) 14-30. https://doi.org/10.1002/mame.201000242
[139] C. Lukas, Communication: Measurement of heat flux in the cone calorimeter, Fire and Materials 19(2) (2004) 97-98. https://doi.org/10.1002/fam.810190208
[140] V. Babrauskas, Development of the cone calorimeter—A bench - scale heat release rate apparatus based on oxygen consumption, Fire and Materials 8(2) (2004) 81-95. https://doi.org/10.1002/fam.810080206
[141] Y.-T. Pan, X. Wang, Z. Li, D.-Y. Wang, A facile approach towards large-scale synthesis of hierarchically nanoporous SnO2@Fe2O3 0D/1D hybrid and its effect on flammability, thermal stability and mechanical property of flexible poly(vinyl chloride), Composites Part B: Engineering 110 (2017) 46-55. https://doi.org/10.1016/j.compositesb.2016.11.009
[142] R. Chapple, C. Chivas-Joly, J.C. Roux, L. Dumazert, L. Ferry, J.M. Lopez-Cuesta, E.L. Erskine, B.K. Kandola, Characterization of aerosolized particles in effluents from carbon fibre composites incorporating nanomaterials during simultaneous fire and impact, NanoImpact 29 (2023) 100446. https://doi.org/10.1016/j.impact.2022.100446
[143] R. Chapple, B.K. Kandola, P. Myler, L. Ferry, J.M. Lopez - Cuesta, C. Chivas - Joly, E.L. Erskine, The effect of simultaneous heat/fire and impact on carbon fibril and particle release from carbon fiber - reinforced composites, Polymer Composites 42(11) (2021) 6127-6145. https://doi.org/10.1002/pc.26290
[144] Y. Sun, X.L. Shi, Y.L. Yang, G. Suo, L. Zhang, S. Lu, Z.G. Chen, Biomass - Derived Carbon for High - Performance Batteries: From Structure to Properties, Advanced Functional Materials 32(24) (2022) 2201584. https://doi.org/10.1002/adfm.202201584
[145] S.D. Thoppul, J. Finegan, R.F. Gibson, Mechanics of mechanically fastened joints in polymer–matrix composite structures – A review, Composites Science and Technology 69(3-4) (2009) 301-329. https://doi.org/10.1016/j.compscitech.2008.09.037
[146] X. Ao, J. Xiao, J. Hobson, J. de la Vega, G. Yin, M.L. Puertas Cuadron, A. Esteban Cubillo, C. González, D.-Y. Wang, Bilayer coating strategy for glass fiber reinforced polymer composites toward superior fire safety and post-fire mechanical properties, Composites Communications 44 (2023) 101763. https://doi.org/10.1016/j.coco.2023.101763
[147] Y. Quan, Z. Zhang, R.N. Tanchak, Q. Wang, A review on cone calorimeter for assessment of flame-retarded polymer composites, Journal of Thermal Analysis and Calorimetry 147(19) (2022) 10209-10234. https://doi.org/10.1007/s10973-022-11279-7

[148] P. Patel, T.R. Hull, A.A. Stec, R.E. Lyon, Influence of physical properties on polymer flammability in the cone calorimeter, Polymers for Advanced Technologies 22(7) (2011) 1100-1107. https://doi.org/10.1002/pat.1943
[149] J. Lindholm, A. Brink, M. Hupa, Influence of decreased sample size on cone calorimeter results, Fire and Materials 36(1) (2011) 63-73. https://doi.org/10.1002/fam.1087
[150] M. Wang, G.-Z. Yin, Y. Yang, W. Fu, J.L. Díaz Palencia, J. Zhao, N. Wang, Y. Jiang, D.-Y. Wang, Bio-based flame retardants to polymers: A review, Advanced Industrial and Engineering Polymer Research 6(2) (2023) 132-155. https://doi.org/10.1016/j.aiepr.2022.07.003
[151] L. Costes, F. Laoutid, S. Brohez, P. Dubois, Bio-based flame retardants: When nature meets fire protection, Materials Science and Engineering: R: Reports 117 (2017) 1-25. https://doi.org/10.1016/j.mser.2017.04.001
[152] A.D. La Rosa, G. Recca, J. Summerscales, A. Latteri, G. Cozzo, G. Cicala, Bio-based versus traditional polymer composites. A life cycle assessment perspective, Journal of Cleaner Production 74 (2014) 135-144. https://doi.org/10.1016/j.jclepro.2014.03.017
[153] M.S. Özer, S. Gaan, Recent developments in phosphorus based flame retardant coatings for textiles: Synthesis, applications and performance, Progress in Organic Coatings 171 (2022) 107027. https://doi.org/10.1016/j.porgcoat.2022.107027
[154] X.-L. Li, X.-H. Shi, M.-J. Chen, Q.-Y. Liu, Y.-M. Li, Z. Li, Y.-H. Huang, D.-Y. Wang, Biomass-based coating from chitosan for cotton fabric with excellent flame retardancy and improved durability, Cellulose 29(9) (2022) 5289-5303. https://doi.org/10.1007/s10570-022-04566-x
[155] Q. Wang, J.B. Schlenoff, The Polyelectrolyte Complex/Coacervate Continuum, Macromolecules 47(9) (2014) 3108-3116. https://doi.org/10.1021/ma500500q
[156] D.L. Smith, N.A. Vest, M.O. Convento, M.D. Montemayor, J.C. Grunlan, Buffer induced ionically crosslinked polyelectrolyte treatment for self-extinguishing polyester, npj Materials Degradation 8(1) (2024) 14. https://doi.org/10.1038/s41529-024-00432-2
[157] K.M. Holder, R.J. Smith, J.C. Grunlan, A review of flame retardant nanocoatings prepared using layer-by-layer assembly of polyelectrolytes, Journal of Materials Science 52(22) (2017) 12923-12959. https://doi.org/10.1007/s10853-017-1390-1
[158] D. Rodriguez - Melendez, D.L. Smith, S.G. Fisher, R. Sonnier, H. Vahabi, J.C. Grunlan, Two - Step Polyelectrolyte Complex Coating for Flame Retardant Flax, Macromolecular Materials and Engineering 309(1) (2023). https://doi.org/10.1002/mame.202300229
[159] T. Zhang, H. Yan, L. Shen, Z. Fang, X. Zhang, J. Wang, B. Zhang, A phosphorus-, nitrogen- and carbon-containing polyelectrolyte complex: preparation, characterization and its flame retardant performance on polypropylene, RSC Advances 4(89) (2014) 48285-48292. https://doi.org/10.1039/c4ra09243k
[160] Z. Zhang, X. Li, Z. Ma, H. Ning, D. Zhang, Y. Wang, A facile and green strategy to simultaneously enhance the flame retardant and mechanical properties of poly(vinyl alcohol) by introduction of a bio-based polyelectrolyte complex formed

by chitosan and phytic acid, Dalton Transactions 49(32) (2020) 11226-11237. https://doi.org/10.1039/d0dt02019b
[161] X.-W. Cheng, J.-P. Guan, X.-H. Yang, R.-C. Tang, F. Yao, A bio-resourced phytic acid/chitosan polyelectrolyte complex for the flame retardant treatment of wool fabric, Journal of Cleaner Production 223 (2019) 342-349. https://doi.org/10.1016/j.jclepro.2019.03.157
[162] B.K. Kandola, A.R. Horrocks, Complex char formation in flame-retarded fibre-intumescent combinations—II. Thermal analytical studies, Polymer Degradation and Stability 54(2-3) (1996) 289-303. https://doi.org/10.1016/S0141-3910(96)00054-7
[163] S. Gaan, G. Sun, Effect of phosphorus flame retardants on thermo-oxidative decomposition of cotton, Polymer Degradation and Stability 92(6) (2007) 968-974. https://doi.org/10.1016/j.polymdegradstab.2007.03.009
[164] D. Gysau, Fillers for paints: fundamentals and applications, Vincentz Network GmbH & Co KG2006.
[165] S. Bourbigot, X. Flambard, Heat resistance and flammability of high performance fibres: A review, Fire and Materials 26(4-5) (2002) 155-168. https://doi.org/10.1002/fam.799
[166] A.B. Morgan, M. Bundy, Cone calorimeter analysis of UL - 94 V - rated plastics, Fire and Materials 31(4) (2006) 257-283. https://doi.org/10.1002/fam.937
[167] A.P. Mouritz, Z. Mathys, A.G. Gibson, Heat release of polymer composites in fire, Composites Part A: Applied Science and Manufacturing 37(7) (2006) 1040-1054. https://doi.org/10.1016/j.compositesa.2005.01.030
[168] X. Ao, R. Crouse, C. González, D.-Y. Wang, Impact of nanohybrid on the performance of non-reinforced biocomposites and glass-fiber reinforced biocomposites: Synthesis, mechanical properties, and fire behavior, Construction and Building Materials 436 (2024) 136922. https://doi.org/10.1016/j.conbuildmat.2024.136922
[169] W. Wu Klingler, V. Rougier, Z. Huang, D. Parida, S. Lehner, A. Casutt, D. Rentsch, K.B. Hedlund, G.A. Barandun, V. Michaud, S. Gaan, Recyclable flame retardant phosphonated epoxy based thermosets enabled via a reactive approach, Chemical Engineering Journal 466 (2023) 143051. https://doi.org/10.1016/j.cej.2023.143051
[170] M. Zhang, J. Xiao, W. Tang, Y. He, P. Tan, M. Haranczyk, D.Y. Wang, A Novel Benchmarking Approach to Assess Fire Safety of Liquid Electrolytes in Lithium - Ion Batteries, Advanced Energy Materials n/a(n/a) (2024) 2401241. https://doi.org/10.1002/aenm.202401241